STELLINGEN

I

Bij volle enkelschroefschepen dient bij het ontwerpen van voortstuwers, die aangepast zijn aan de periferiale ongelijkmatigheid van het snelheidsveld, rekening te worden gehouden met de verandering van dit veld door de schroefwerking.

II

De tendens bij het ontwerpen van grote tankers om naar extreem lage lengte-breedte verhoudingen te gaan, is zowel uit economisch oogpunt als uit oogpunt van de kostprijs van het schip niet aan te bevelen.

III

Doordat de koersstabiliteit van een schip door het toepassen van een bulb in het algemeen ongunstig beïnvloed wordt, dient overwogen te worden of de winst in snelheid opweegt tegen het verlies in tijd door de grotere weg die het schip moet afleggen.

IV

Bij het bepalen van de cavitatie-inceptie grenzen in een watertunnel, verdient het uit oogpunt van reproduceerbaarheid van de metingen de voorkeur uit te gaan van het verdwijnpunt van cavitatie.

V

De lengte van de stopweg van een schip wordt niet door het beschikbare vermogen bepaald, maar door de bestuurbaarheid van het schip tijdens de stopmanoeuvre.

VI

Het technisch onderhoud dat het menselijk organisme nodig heeft voor een goed functioneren, maakt dit organisme in toenemende mate tot een probleem bij de ontwikkeling van de ruimtevaart.

VII

Door toepassing van tegengesteld draaiende schroeven bij schepen mag niet verwacht worden dat door het geringere rotatieverlies in de stroming een besparing in vermogen te verwachten is, zoals gesuggereerd wordt door Hadler[1] en Lindgren e.a.[2]

[1] J. B. HADLER: 'Contra-rotating propeller propulsion. A state-of-the-art report'. New York, Metropolitan Section of SNAME, Dec. 1968, New York.

[2] H. LINDGREN, C. A. JOHNSON and G. DYNE: 'Studies of the application of ducted and contra rotating propellers on merchant ships', 7th Symp. on Naval Hydrodynamics, Rome, Aug. 1968.

Dissertatie M. W. C. OOSTERVELD.
Delft, 25 juni 1970

VIII

In een discussie op een artikel van Kermeen e.a.[3] wijzen Holl en Robertson op de afhankelijkheid van het cavitatiegetal van het getal van Weber. Zij betrekken de lengtemaat hierbij op een karakteristieke lengtemaat van het lichaam. Dit is physisch onjuist. De lengtemaat moet betrokken worden op de beldiameter.

[3] R. W. KERMEEN, J. T. MCGRAW and B. R. PARKIN: 'Mechanism of cavitation inception and the related scale-effects problem'. Trans. ASME, May 1955 pag. 540.

IX

Bij het toepassen van een 'Haselton propeller' bij een onderzeeboot mag verwacht worden, dat slechts bij kleine naaf-schroef diameter verhoudingen door een cyclische spoedverstelling van de bladen aanzienlijke dwarskrachten zijn op te wekken.

X

Het model ter verklaring en berekening van de physische eigenschappen van het menselijke evenwichtssysteem kan slechts een benadering blijven ten gevolge van het adaptatie- en habituatie phenomeen dat genoemd systeem met andere zintuigen gemeen heeft.

XI

Het is tot op heden niet mogelijk gebleken om de erosie bestendigheid van een materiaal te correleren met de mechanische eigenschappen.

XII

De verordening van het Plassenschap Loosdrecht en Omstreken met betrekking tot de maximaal toelaatbare snelheid van motorboten in verband met hinderlijke golfverschijnselen levert in zijn huidige vorm geen bijdrage tot het verminderen van deze verschijnselen.

WAKE ADAPTED DUCTED PROPELLERS

WAKE ADAPTED DUCTED PROPELLERS

PROEFSCHRIFT

TER VERKRIJGING VAN DE GRAAD VAN
DOCTOR IN DE TECHNISCHE WETENSCHAPPEN
AAN DE TECHNISCHE HOGESCHOOL DELFT
OP GEZAG VAN DE RECTOR MAGNIFICUS
DR. IR. C. J. D. M. VERHAGEN, HOOGLERAAR IN DE
AFDELING DER TECHNISCHE NATUURKUNDE
VOOR EEN COMMISSIE UIT DE SENAAT TE VERDEDIGEN
OP DONDERDAG 25 JUNI 1970 TE 14.00 UUR

DOOR

MARINUS WILLEM CORNELIS OOSTERVELD

WERKTUIGKUNDIG INGENIEUR
GEBOREN TE AMSTERDAM

H. VEENMAN & ZONEN N.V. - WAGENINGEN - 1970

Dit proefschrift is goedgekeurd door de promotor Prof. Dr. Ir. J. D. VAN MANEN

Aan mijn ouders
aan mijn vrouw

CONTENTS

1. INTRODUCTION

A ducted propeller consists of a combination of an annular airfoil and an impeller, acting as a propulsion unit. A schematic view of a ducted propeller is given in Fig. 1.

The axial force acting on the impeller of a ducted propeller usually differs from the net thrust of the system. A positive or negative force may act on the nozzle depending on the nozzle shape and the operating condition. Due to the nozzle action the velocity at the impeller plane can be either less than or greater than the velocity at the propeller plane of a conventional screw with the same diameter and speed of advance.

Insight into the shape of the nozzle profile of a ducted propeller can be gained by Fig. 2. Here the flow through different types of ducted propellers is superimposed on the flow through an open propeller. Both the open propeller and the ducted propellers are designed for the same mass flow rate and velocity in the ultimate wake. Consequently the thrust and ideal efficiency of these systems are equal.

The ducted propeller with the accelerating flow type of nozzle is now used extensively in cases where the ship screw is heavily loaded or where the screw is limited in diameter. The accelerating nozzle offers a means of increasing the efficiency of heavily loaded propellers. The nozzle itself produces a positive thrust.

In the case of the decelerating flow type of nozzle, the nozzle is used to increase the static pressure at the impeller. This ducted propeller system is the so called pumpjet. The duct will produce a negative thrust. This nozzle may be used if retardation of propeller cavitation is desired. For naval ships a reduction in noise level can be obtained which may be of importance for tactical reasons.

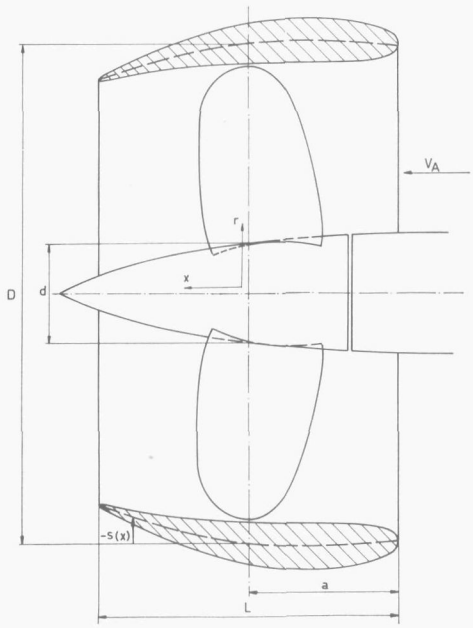

FIG. 1. Ducted propeller.

FIG. 2. General form of streamlines enforced by different nozzle types.

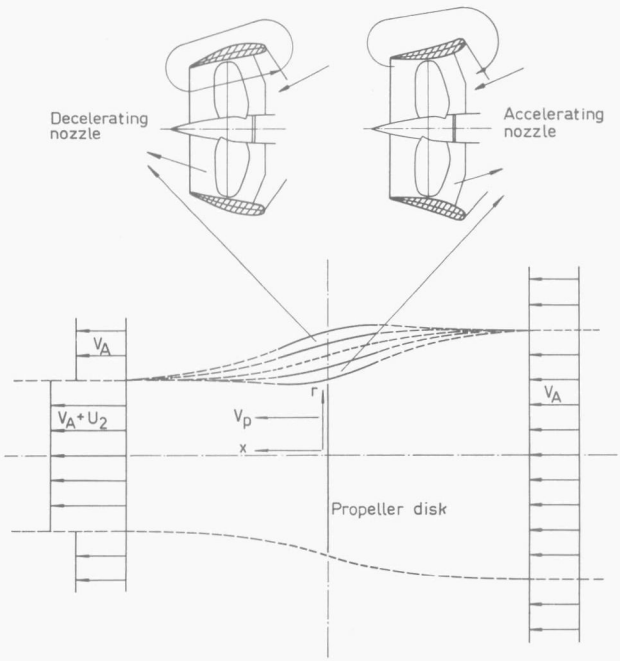

Although the idea of surrounding a propeller by a nozzle is already very old, it has lasted until the early 1930 before the ducted propeller came into practical use. LUISA STIPA (1) and later on KORT (2) experimentally proved the advantages which can be obtained by application of the accelerating nozzle. These investigations clearly show that an increase in efficiency can be obtained by this nozzle at heavy screw loads. Primarily due to the work done by KORT, the application of ducted propellers behind certain ship types (tugs, pushboats, trawlers) has become common practice. This may be the reason that the accelerating ducted propeller is frequently referred to as the 'KORT' nozzle.

Many studies on ducted propellers have been made during the last 40 years. An extensive summary of this work was made by SACKS and BURNELL (3) in 1960. A general review of the more recent theoretical studies on ducted propellers has been given by WEISSINGER and MAASS (4).

Among the theoretical studies on ducted propellers the investigations of HORN and AMTSBERG (5), KÜCHEMAN and WEBER (6) and DICKMANN and WEISSINGER (7) may be mentioned in particular. Especially, the work of DICKMANN and WEISSINGER (7) was the first step to the development of more refined theories on ducted propellers. This paper was the base for the work which has been performed at *Karlsruhe* by DICKMANN, WEISSINGER, WIEDEMER, BOLLHEIMER, BRAKHAGE, MAASS and RAUTMANN. Some of the basic ideas used at *Karlsruhe* were also used by other investigators working at *Therm* (ORDWAY, RITTER, GREENBERG, HOUGH, KASKEL, LO, SLUYTER,

SONNERUP), at *NSRDC* (MORGAN, CASTER, CHAPLIN, VOIGT), at *Viday* (NIELSEN, KRIEBEL, MENDENHALL, SACKS, SPANGLER) and by many others.

Most of the theoretical investigations on ducted propellers were concentrated to a large extent on the linearized theory and on axisymmetrical nozzles in a uniform flow.

A discussion of the adequacy of the different studies is beyond the scope of the work described in the following. The design of a ducted propeller depends on a large number of variables. For the design of an optimum ducted propeller system it is attractive therefore to have a sound theoretical calculation method available supported by carefully selected systematic experiments.

Recently, a comparison of theory and experiment on ducted propellers was given by MORGAN and CASTER (8). Tests on ducted propellers are scarce, however, and most of these tests are restricted to isolated applications.

By far the most extensive systematic experiments on ducted propellers for application on ships have been performed at the *NSMB* by VAN MANEN (9, 10, 12) and VAN MANEN and SUPERINA (11). These investigations concerned nozzles of the accelerating flow type. This work gives valuable advices for the design of optimum ducted propeller systems from the viewpoint of efficiency for ships. A review of this work was given by VAN MANEN and OOSTERVELD (13) in 1966.

Recently, the results of systematic experiments on ducted propellers of the decelerating flow type were given by OOSTERVELD (14).

In the following a general discussion of the design of ducted propellers is given. Besides, some new developments in the field of ship propulsion by special types of ducted propellers will be discussed.

2. GENERAL RELATIONS FOR FLOW AND FORCE ACTION

In the combined arrangement of duct and propeller, the axial force on the impeller differs usually from the net thrust of the system. The force set up on the nozzle will be positive or negative depending on the nozzle shape and the operating condition.

Insight into the working principle of a ducted propeller can be gained by the application of the fundamental momentum relationship. Fig. 3 shows the simplified system, by which the ducted propeller can be replaced.

The total thrust T acting on the fluid due to impeller and nozzle is:

$$T = \rho\,[V_A + U_1]\,\frac{\pi}{4}\,D^2 U_2$$

applying the momentum theorem over the control volume given in Fig. 3. The thrust T_P developed by the impeller can be obtained by calculating the pressure difference across the impeller disk using BERNOULLI's equation:

$$T_P = \rho\,[V_A + U_2]\,\frac{\pi}{4}\,D^2 U_2$$

The kinetic energy E lost in the impeller slipstream is given by:

$$E = \tfrac{1}{2}\,\rho\,[V_A + U_1]\,\frac{\pi}{4}\,D^2 U_2^2$$

Hence the ideal efficiency η_i of the propulsion device is defined by:

$$\eta_i = \frac{V_A T}{V_A T + E} = \frac{2}{1 + \sqrt{1 + \tau C_T}}$$

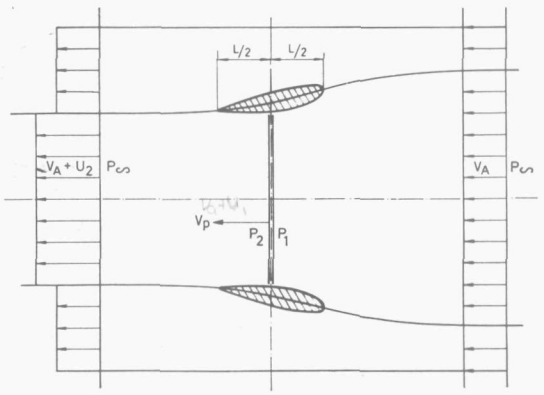

FIG. 3. Control volume used for momentum considerations.

where,

$$C_T = \frac{T}{\frac{1}{2}\rho V_A^2 \frac{\pi}{4} D^2}$$

$$\tau = \frac{T_p}{T}$$

The mean axial velocity at the impeller plane can be written as:

$$\frac{V_P}{V_A} = \frac{V_A + U_1}{V_A} = \frac{C_T}{2\left[-1 + \sqrt{1 + \tau C_T}\right]}$$

The mean axial velocity due to the impeller is:

$$\frac{U_P}{V_A} = \tfrac{1}{2}\left[-1 + \sqrt{1 + \tau C_T}\right]$$

Hence, the mean axial velocity U_N induced by the nozzle at the impeller becomes:

$$\frac{U_N}{V_A} = \frac{1 - \tau}{2\tau}\left[1 + \sqrt{1 + \tau C_T}\right]$$

The mean value of the static pressure at the impeller, P_{mean} can be calculated from

$$P_{mean} = \tfrac{1}{2}\left[P_1 + P_2\right]$$

Hence the mean static pressure coefficient C_{Pmean} can be written as:

$$C_{Pmean} = \frac{P_{mean} - P_\infty}{\frac{1}{2}\rho V_A^2} = 1 + \tfrac{1}{2}\tau C_T - \left[\frac{1 + \sqrt{1 + \tau C_T}}{2\tau}\right]^2$$

The ideal efficiency η_i, the velocity ratio V_P/V_A and the pressure coefficient C_{Pmean} are given as functions of the thrust coefficient C_T and for different values of the thrust

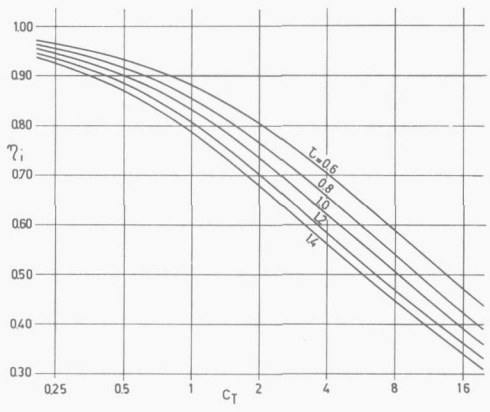

FIG. 4. Ideal efficiency of ducted propeller system.

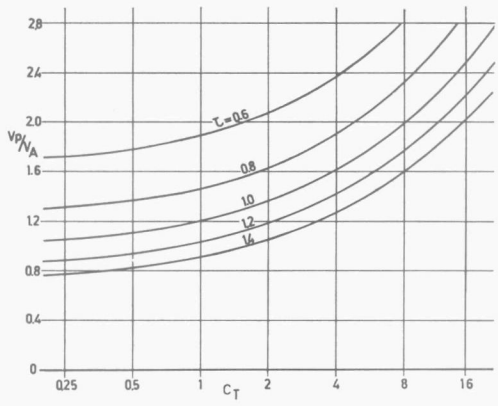

FIG. 5. Mean axial velocity at impeller plane of a ducted propeller.

ratio τ in Figs. 4 through 6. The inflow velocity of the impeller of a ducted propeller can be either less or greater than the inflow velocity of an open propeller under equal conditions. The thrust ratio τ of an open propeller is equal to 1. It can be seen from Fig. 5 that when due to the nozzle action the flow rate through the impeller is increased, a positive axial force or thrust is developed on the nozzle (thus $\tau < 1$). In

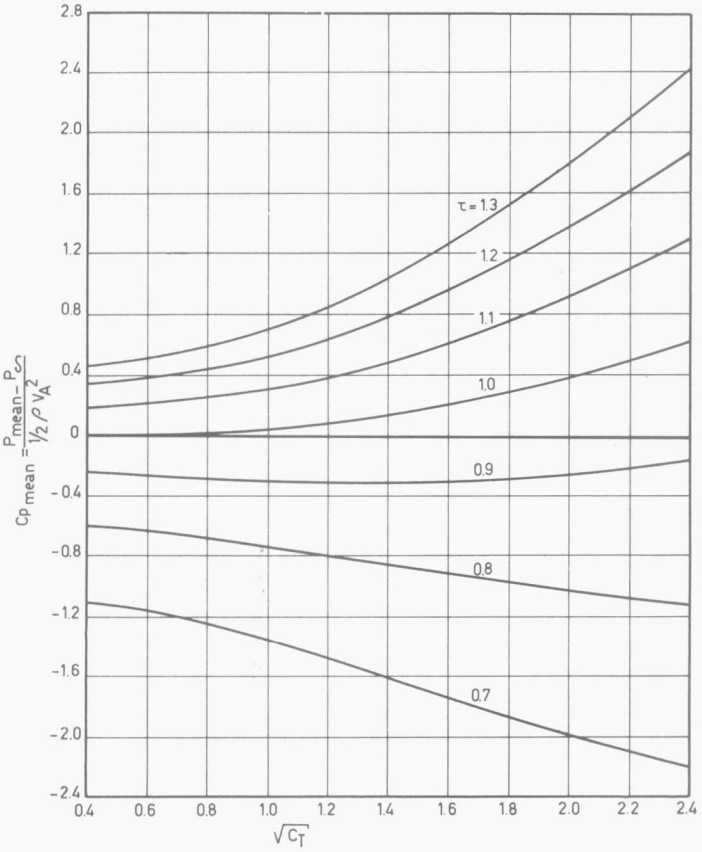

FIG. 6. Mean static pressure at impeller plane of a ducted propeller.

the case of a nozzle which reduces the flow rate through the impeller, a negative axial force is acting on the nozzle (thus $\tau > 1$).

It follows from Fig. 4 that, if the diameter of a ducted propeller system is kept constant, the *ideal efficiency* η_i of the system increases with decreasing values of the impeller thrust-total thrust ratio τ. Thus the ducted propeller with the flow accelerating type of nozzle offers a means of improving the efficiency if compared with an open propeller.

Fig. 6, shows that the static pressure at the impeller increases with increasing values of the thrust ratio τ. 'Ram pressures' at the impeller plane are built up when τ exceeds a value of 1. A reduction of the flow rate by the nozzle results in an increment of the static pressure at the impeller. The increment is attractive from a point of view of retardation of screw *cavitation*. The duct itself, however, will produce a negative thrust. In order to compensate for the increased nozzle drag, the impeller loading must be enlarged. An improvement of the cavitation characteristics of the screw will,

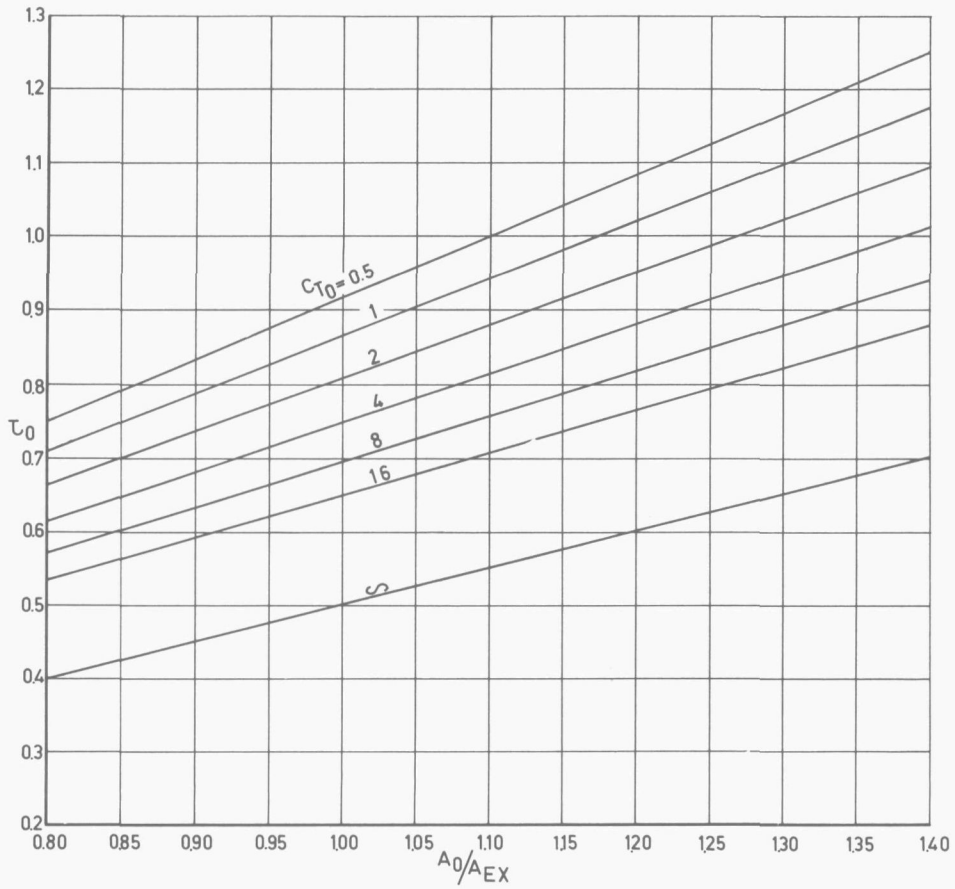

FIG. 7. Relation between impeller disk area-nozzle exit area ratio, thrust coefficient C_T and thrust ratio τ of a ducted propeller.

therefore, only be obtained if the gain in static pressure exceeds the unfavourable effect of the increased screw loading.

It may be concluded from these considerations that the application of a shroud around a propeller can attribute to a higher efficiency or better cavitation characteristics. The elementary theory used so far takes into account only the state of the flow at the impeller and infinitely far upstream and downstream. It does not consider what happens to the flow outside these regions.

To derive a relation between the shape of the nozzle profile and the characteristics of the nozzle-propeller system, the assumption can be made that the wake area A_∞ and the exit area of the nozzle A_{EX} (see Fig. 3) are equal. If the disc area of the impeller is denoted by A_o, the following relation between the impeller disk area-nozzle exit area ratio, the thrust coefficient C_T and the thrust ratio τ holds:

$$\frac{A_o}{A_{EX}} = \frac{2\,[1 + \tau C_T - \sqrt{1 + \tau C_T}]}{C_T}$$

Calculations of the area ratio A_o/A_{EX} have been made and the results are presented in Fig. 7.

For a more refined evaluation of the characteristics of ducted propellers, use can be made of theoretical and experimental methods. In the following, a simplified method has been described based on a vortex theory, which enables the calculation of the characteristics of systematic series of nozzle shapes as well as the more general characteristics of ducted propellers. In addition, the results of open-water tests with systematic series of ducted propellers both with the flow accelerating and with the flow decelerating nozzles are given.

3. CALCULATIONS ON DUCTED PROPELLERS WITH VORTEX THEORY

A large number of theoretical investigations have been conducted on ducted propellers during the past thirty years. An extensive summary of this work was made by SACKS and BURNELL (3) in 1960. Recently a general review on theoretical studies of ducted propellers was given by WEISSINGER and MAASS (4).

The calculations on ducted propellers may be classified into two types:

- the direct problem of ducted propellers in which the geometry of the ducted propeller system is given and the pressure distribution and the force on the duct must be determined.
- the inverse problem of ducted propellers in which a certain combination of impeller forces and duct forces are given and the shape of the nozzle must be determined.

Both the direct and the inverse problem require the solution of a singular integral equation. The present investigation is concerned with the inverse problem although a slightly different approach has been chosen. In this approach the nozzle shape was determined for a given uniform loading of the actuator disk representing the impeller and for a given circulation of the nozzle. This method is very attractive, because the computation is simple. However, it gives only the possibility of determining nozzle shapes which will operate satisfactorily for a given flow condition. This method gives also the possibility of determining the more general characteristics of ducted propellers in an easy way.

The calculations on ducted propellers were based on the following assumptions. The forward velocity of the ducted propeller system was assumed to be sufficiently large, the nozzle loading and the blade loading of the impeller sufficiently low to permit the application of the linearized theory. The effect of the hub shape on the flow field was neglected. Further, the fluid was assumed to be inviscid and incompressible. The ducted propeller system considered consists of an annular airfoil of finite length and of an impeller having an infinite number of blades.

The mathematical model of the ducted propeller configuration can be composed by means of vortex distributions. The impeller was regarded as a uniformly loaded actuator disk set normal to the free stream. It was driven to rotate with an angular velocity ω. Free trailing vortices started from the disk at hub and tip radius. The flow around the nozzle was represented by a sinusoidal bound ring vortex distribution with zero strength at the leading and trailing edges and by a ring vortex distribution with zero strength at the leading edge and equal to the strength of the circumferential component of the helical trailing vortices at the impeller disk. The resulting mathematical model is summarized in Fig. 8.

Assume the vortex strength per unit impeller disk area at the radius of the impeller to be equal to $\gamma(R_1)$, the strength of the different vortex distributions then becomes:

- vortex strength per unit impeller disk area at radius r

$$\gamma(r) = \frac{R_1}{r}\gamma(R_1)$$

– strength per unit area of the trailing vortex sheet starting from the impeller disk at the tip radius

$$\sqrt{1+\mu^2}\cdot\gamma(R_1)$$

– strength per unit area of the trailing vortex sheet starting from the impeller disk at the hub radius

$$\sqrt{1+\mu^2\lambda^2}\cdot\frac{1}{\lambda}\gamma(R_1)$$

– strength per unit area of the bound ring vortex distribution along the nozzle

$$\mu\gamma(R_1)\,\frac{\sin\theta}{2\sqrt{a\,1-a)}} \qquad (\text{for } -aL < x < 0\ )$$

$$\gamma(R_1)\sin\theta \qquad (\text{for } -aL < x < (1-a)\,L)$$

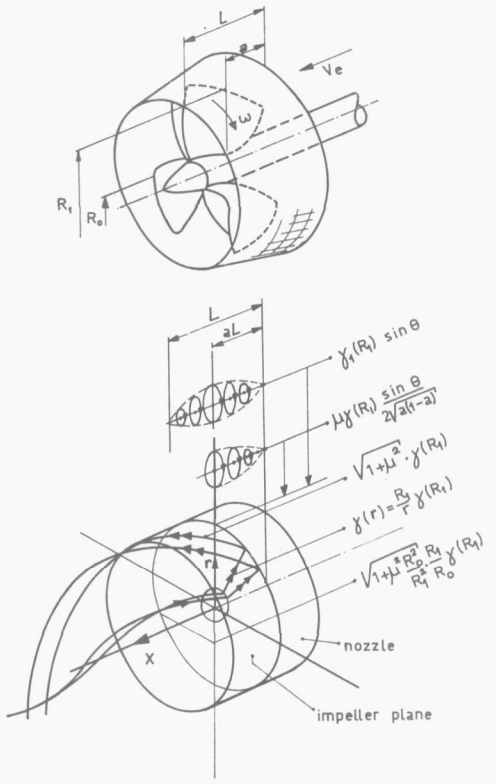

FIG. 8. Representation of ducted propeller by vortex distributions.

where,

$$\mu = \frac{\omega R_1}{V_A};\ \lambda = \frac{R_0}{R_1};\ x + (a - 0.5)\, L = 0.5\, L\cos\theta$$

while the definitions of R_0, R_1, r, x, L, a and so on are given in Fig. 8.

The thickness effect of the nozzle profile on the flow field can be taken into account in the linearized theory by representing the nozzle by a distribution of ring sources and sinks along a cylinder with radius R_1 (see Fig. 8). In the case of very thin nozzle profiles, the strength of the sink and source distributions representing the nozzle profile can be calculated by considering the flow around the profile as two-dimensional. Then the local source strength is equal to the derivative of the profile thickness:

$$g(x) = \frac{dh(x)}{dx}$$

where $h(x)$ denotes the local thickness of the nozzle profile.

The total induced velocities due to the different vortex and source distributions representing the impeller and the nozzle can be calculated according to the law of Biot-Savart if the main dimensions of the system (L/D; a/L; d/D; S/L and the thickness distribution of the nozzle), the advance coefficient of the screw ($J = V_A/nD$), and the loading of the impeller and nozzle are given. The impeller thrust and torque, the thrust on the nozzle and the ideal efficiency of the system can be calculated now for the chosen values of the design parameters. In addition, the shape of the nozzle and the pressure distribution along the nozzle can be computed. The method for the calculation of the ducted propeller characteristics is, in a more detailed way, given in the Appendix.

It is shown in the Appendix, that for the chosen load distributions of impeller and nozzle, the shape of the nozzle is completely determined by the values of the thrust coefficient C_{To}, the thrust ratio τ_o and the main dimensions of the ducted propeller system. Here, the subscript 'o' denotes that a ducted propeller system is considered with an impeller rotating at infinite angular velocity or with an advance coefficient J equal to zero. Then, the tangentially induced velocities and consequently the losses due to the rotation of the fluid are zero. The case that the impeller rotates with an infinite angular velocity coincides with the case that the impeller rotates with finite angular velocity while a stator is used to eliminate the rotational losses. Thus starting from given thrust coefficients C_{To}, thrust ratios τ_o (thus at $J = 0$) and the main dimensions the characteristics of ducted propellers can be calculated. It must be noted that for the thickness distribution of the nozzle profiles of all nozzles given in the following, the NACA four-digit wing section basic thickness form was used. First, the shape of the nozzle profile and the pressure distribution along the nozzle can be derived. Secondly, the thrust coefficient C_T, thrust ratio τ and the ideal efficiency η_i of such a ducted propeller can be calculated over a range of advance coefficients J.

This method of calculation was followed for the determination of the characteristics of systematic series of flow decelerating type nozzles as will be given in section 6. In the following section the theory will be used for the determination of the more general characteristics of ducted propellers.

4. POTENTIALITIES OF NOZZLES

The choice of the shape of the nozzle profile and the nozzle length depends mainly on requirements with respect to efficiency, danger of flow separation on the nozzle, and critical cavitation indexes on nozzle and propeller.

Flow separation occurs if the nozzle is too heavily loaded. If flow separation occurs on the interior or exterior surface of the nozzle, the drag of the nozzle will increase sharply. Moreover, the propeller will be operating in a highly irregular flow if separation occurs on the interior surface of the nozzle. In either case, the efficiency of the system would begin to decrease. Therefore, flow separation on the nozzle surface should be avoided. In order to evaluate, the maximum loading of the nozzle without separation, the flow around the nozzle profile can be assumed to be two-dimensional. By analogy to the two-dimensional airfoil flow, the approximation that flow separation occurs if the lift coefficient, C_L, exceeds a value of 1.0–1.5 can be used. It must be investigated, however, whether this rough approximation gives a reliable criterion for the nozzle loading.

The method described in section 3 for the calculations of nozzle propeller characteristics enables the analysis of the sectional lift coefficient C_L of nozzles under design condition:

$$C_L = \frac{\rho V_A \Gamma L}{\frac{1}{2}\rho V_A^2 L}$$

together with

$$\Gamma = -\frac{1}{L}\int_{-aL}^{(1-a)L} \gamma_1 (R_1) \sin\theta \, dx + \frac{1}{L}\int_{-aL}^{0} \mu\gamma (R_1) \frac{\sin\theta}{2\sqrt{a(1-a)}} dx$$

Analyses of the sectional lift coefficient C_L have been made for nozzles with different thrust ratios τ and different thickness ratios of the nozzle profile S/L. The result is given in Fig. 9, which shows that the loading of the accelerating type of nozzle is strongly restricted by the risk of flow separation on the interior surface of the nozzle. The risk of flow separation on the exterior surface of the decelerating nozzle, however, is small even in the case of large thrust ratios τ.

In order to investigate the effect of nozzle length on overall efficiency, the drag of the nozzle must be calculated. The efficiency of the ducted propeller system may be written as $\eta = \eta_i \eta_{fN}$, where the efficiency factor due to nozzle drag η_{fN} is:

$$\eta_{fN} = \frac{T - D_N}{T} = 1 - \frac{4L}{D} \cdot \frac{C_{DN}}{C_T} \{1 + \tfrac{1}{4}[-1 + \sqrt{1 + \tau C_T}]\}^2$$

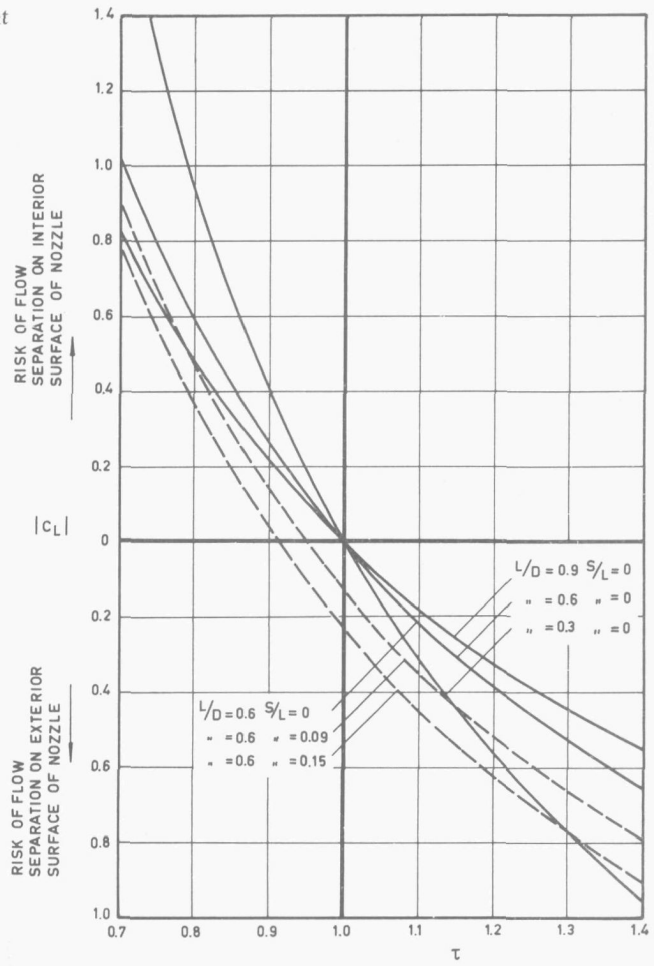

FIG. 9. Sectional lift coefficient of nozzle profile.

where C_{DN} denotes the sectional drag coefficient of the nozzle.

$$C_{DN} = \frac{D_N}{\pi D L\frac{1}{2} \rho V^2}$$

The flow around the nozzle is fully turbulent because the value of the Reynolds number based on the profile length is beyond 10^6. The drag in this region of Reynolds numbers may be expressed by the following empiric relation (15):

$$C_{DN} = 2 C_f \left[1 + 2 \left(\frac{S}{L}\right)^2\right]$$

where C_f is the turbulent skin-friction drag coefficient. Calculations of the efficiency factor η_{fN} have been made. The results are given in Fig. 10 which shows that the efficiency losses due to nozzle drag become substantial if the ducted propeller system is lightly loaded.

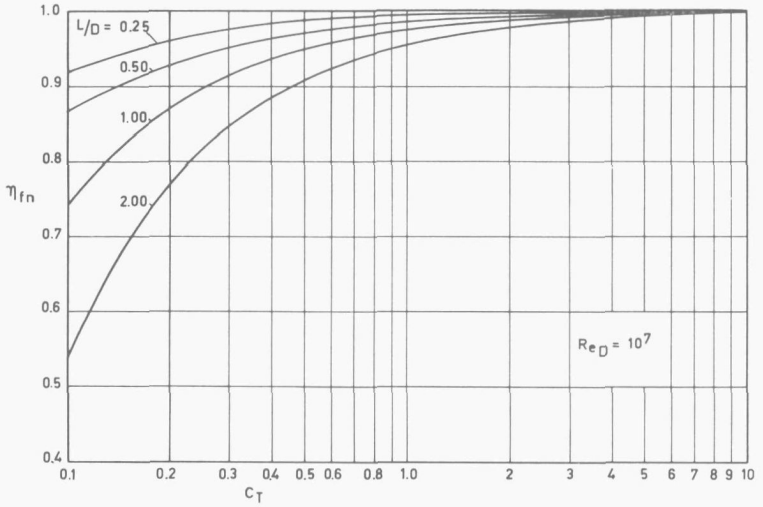

FIG. 10. Efficiency factor due to frictional nozzle drag of ducted propeller.

Investigations of the optimum nozzle shape from the viewpoint of efficiency lead to the conclusion that a maximum contraction of the nozzle should be aimed at. Consequently, the impeller thrust-total thrust ratio τ must be as small as possible. The contraction is limited by the risk of flow separation on the interior surface of the nozzle. If by analogy to the two-dimensional airfoil flow the approximation is used that flow separation occurs if the lift coefficient C_L exceeds a value of 1, then the optimum value of the thrust ratio τ for a given length-diameter ratio L/D of the ducted propeller system can be obtained from Fig. 9. Hence, the optimum ideal efficiency of the ducted propeller can be obtained as a function of the nozzle length-diameter ratio L/D and the thrust coefficient C_T using the results presented in Fig. 10. Analyses of the optimum ideal efficiency and the efficiency losses due to nozzle drag have been made for ducted propellers with different nozzle length-diameter ratios L/D and for a thickness ratio $S/L = 0.15$ of the nozzle profile. The result is given in Fig. 11. From this diagram it can be seen that the use of a nozzle leads to an increase of the efficiency at higher screw loads ($C_T > 1 - 2$). At these screw loadings a nozzle with a length-diameter ratio $L/D = 0.5$–1.0 is advisable. For a shorter nozzle the gain in ideal efficiency will be lower, whereas for a longer nozzle the gain in ideal efficiency will be counter-balanced by the frictional nozzle drag.

The application of the decelerating type of nozzle results in an increment of the pressure at the impeller and a reduction of the pressure at the exterior surface of the nozzle. Consequently, the risk of cavitation on the exterior surface of the decelerating nozzle becomes substantial. The earlier described method for the calculation of the ducted propeller characteristics enables the calculation of the static pressure along the nozzle and at the impeller plane under design condition. The minimum static pressure at the exterior surface of the nozzle and the mean static pressure at the impeller plane

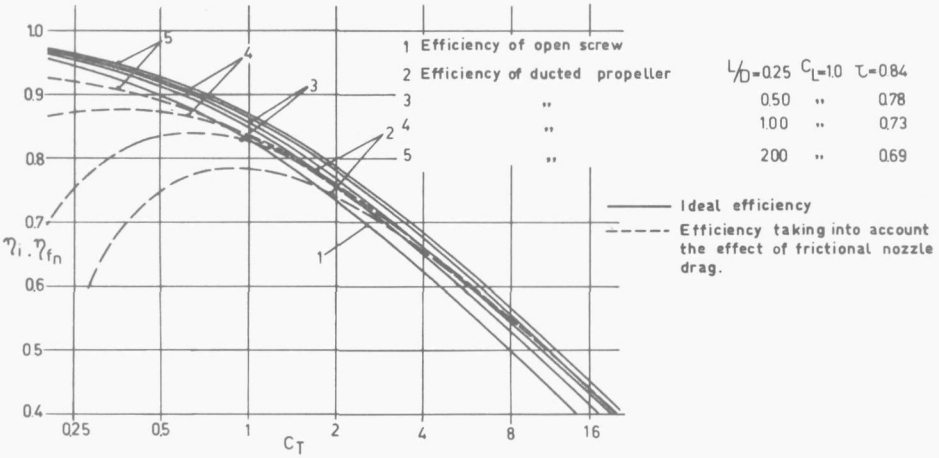

FIG. 11. Optimum ideal efficiency and efficiency losses due to nozzle drag of a ducted propeller system.

are denoted by P_{min} and P_{mean}. The following non-dimensional pressure coefficients are introduced:

$$C_{Pmean} = \frac{P_{mean} - P_\infty}{\frac{1}{2}\rho V_A^2} \qquad C_{Pmin} = \frac{P_{min} - P_\infty}{\frac{1}{2}\rho V_A^2}$$

where P_∞ and $\frac{1}{2}\rho V_A^2$ are the static pressure and the dynamic pressure of the undisturbed stream respectively. Calculations of C_{Pmin} and C_{Pmean} have been made for nozzles with different length-diameter ratios L/D and different maximum thickness ratios S/L. Minimum pressures which may occur at the exterior surface of the decelerating nozzle are given in Fig. 12.

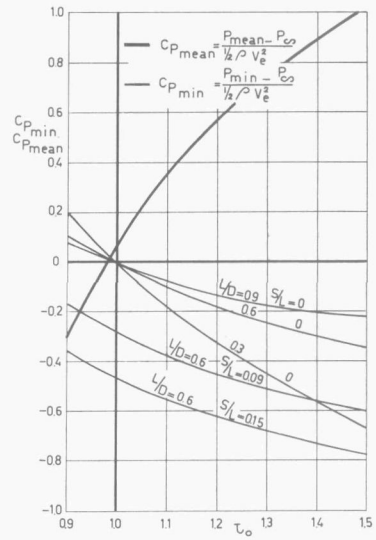

FIG. 12. Minimum static pressure at the exterior surface of decelerating nozzles.

The reduction of the flow rate inside the decelerating type of nozzle, results in an increment of the static pressure at the impeller. This increment is attractive from a point of view of retardation of screw cavitation. The duct itself, however, will produce a negative thrust ($\tau > 1$). In order to compensate for this thrust loss (induced nozzle drag), the screw loading must be increased. An improvement of cavitation properties of the screw will therefore only be obtained if the gain in static pressure at least compensates the unfavourable effect of the increased screw loading.

An approximate method of calculation has been followed here in order to determine whether an improvement of the screw cavitation characteristics can be obtained by application of a nozzle. A comprehensive set of data on the cavitation properties of propellers according to the vortex theory (see Ref. (16)) permits the introduction of the following empirical relation for the minimum pressure on the screw blades:

$$\left[C_{Pmin}\right]_{screw} = \frac{P_{min} - P_\infty}{\frac{1}{2}\rho V_A^2} = -\frac{\pi\,[2.4 + 0.6\,Z]\,C_T}{8\,[A_E/A_o + 0.2]}$$

where the blade area ratio and the number of blades of the screw are denoted by A_E/A_o and Z respectively. The ducted propeller may now be regarded as operating in open-water with an equivalent uniform stream velocity $(V_A + U_N)$, and an equivalent static pressure of the undisturbed stream $(P_\infty + \frac{1}{2}\rho V_A^2 - \frac{1}{2}(V_A + U_N)^2)$. U_N denotes the mean axial velocity at the impeller due to the nozzle action. The relation between U_N, C_T and τ has been calculated with the aid of the momentum theory given before.

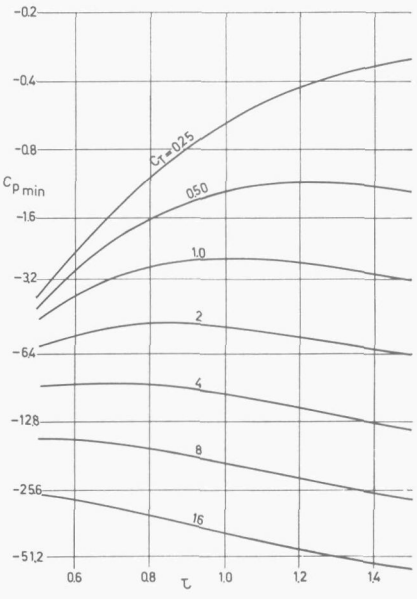

FIG. 13. Minimum static pressure at impeller blades of a ducted propeller.

Hence, the minimum static pressure coefficient on the impeller blades of the ducted propeller may be written as:

$$\left[C_{Pmin}\right]_{ducted\ propeller} = \frac{P_{min} - P_{\infty}}{\frac{1}{2}\rho V_A^2} = -\frac{\pi\,[2.4 + 0.6\,Z]\,\tau C_T}{8\,[A_E/A_0 + 0.2]} + 1 - \left(1 + \frac{U_N}{V_A}\right)^2$$

Analyses of the pressure coefficient C_{Pmin} corresponding to ducted propellers with different thrust coefficients C_T and thrust ratios τ and for $A_E/A_o = 1$ and $Z = 5$ were made. The result is presented in Fig. 13. This diagram shows that, for the particular screw considered ($A_E/A_o = 1$, $Z = 5$) only for low values of C_T, the flow decelerating type of nozzle affects favourably the cavitation properties of the screw. If ducted propellers are considered with larger blade area ratios of the impeller or with more rotor rows or both, the flow decelerating type of nozzle may even for larger values of the thrust coefficient C_T favourably affect the cavitation properties of the screw.

If we compare the results presented in Figs. 12 and 13 then it can be seen that for the particular screw considered the minimum pressures occurring at the impeller blades are much lower than the minimum pressures at the exterior surface of the nozzle even at large thrust ratios τ.

5. THE FLOW ACCELERATING NOZZLE

From the theoretical calculations given in the preceding sections it was concluded that the use of an accelerating nozzle leads to an increase of efficiency at higher screw loads ($C_T > 1$). In addition, at higher screw loadings a long nozzle is advisable, while at light screw loadings a short nozzle should be used. At high screw loads, however, the nozzle must not have a larger L/D ratio than about 1.0. Above this value the loss in efficiency due to the frictional nozzle drag will still be larger than the gain in ideal efficiency which can be obtained by application of a nozzle.

Extensive experimental investigations with screw series in accelerating nozzles have been performed by VAN MANEN (9, 10, 12) and VAN MANEN and SUPERINA (11), in order to supply data for the design of ducted propellers for optimum efficiency.

These tests were carried out with the usual tank apparatus for open-water tests with ducted propellers. Fig. 14 shows the test equipment which is fitted under the carriage running over the basin during the tests. The usual routine of open-water tests was followed; the rpm of the screw was kept constant and by varying the speed of advance the desired value of the advance coefficient J was obtained. The rpm was chosen as high as possible to obtain a high Reynolds number. Speeds above 3 m/sec. could not be investigated on account of the towing carriage.

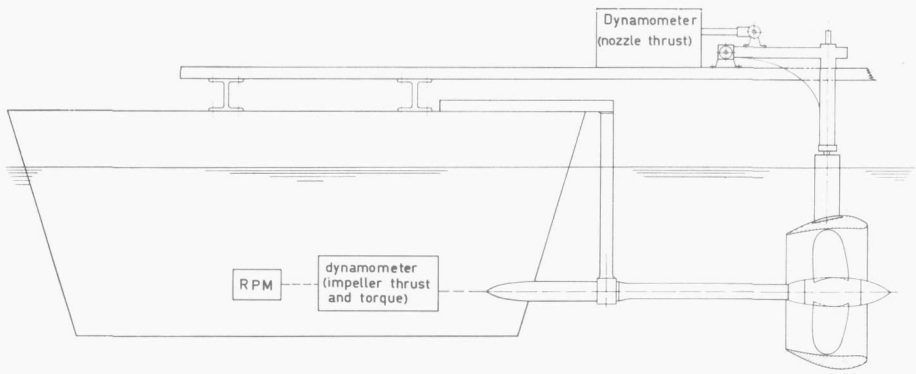

FIG. 14. Test equipment for open-water tests with ducted propellers.

The tests with the different types of accelerating nozzles were first carried out with B-series screws. Later on, however, special screw series for use in nozzles were designed.

The investigations on accelerating nozzles were focussed on the determination of the optimum nozzle shape from the viewpoint of efficiency. Therefore, the influence of variations in camber ratio of the nozzle profile f/L and in the angle between the nose-tail line of the nozzle profile and the propeller shaft α_i on the characteristics, was systematically determined. A review of the tested nozzle shapes is given in Table 1. The dimensions of these nozzles are given in Fig. 15.

FIG. 15. Profiles of nozzles nos. 2 through 8, and 10 and 11.

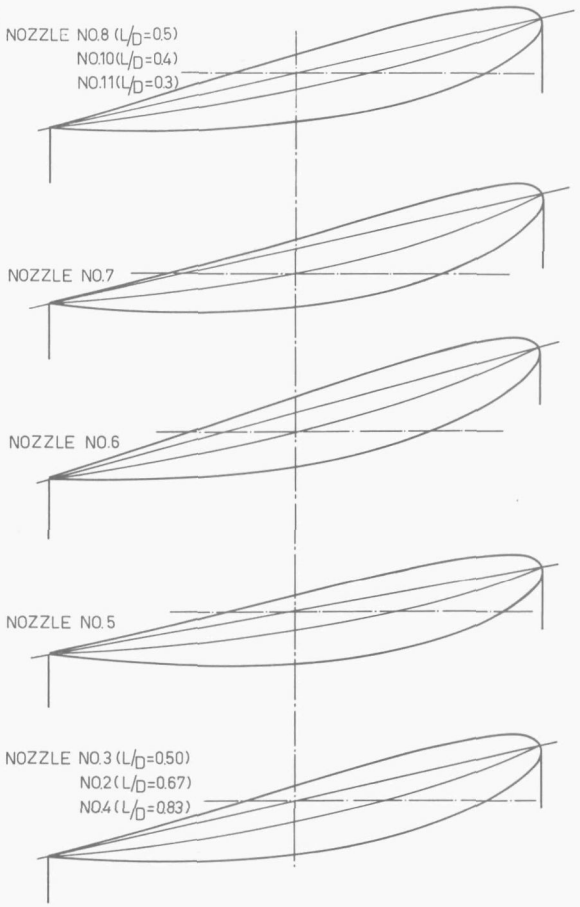

TABLE 1. Particulars of nozzles nos. 2 through 8 and 10 and 11

Nozzle no.	L/D	S/L	f/L	α_i (degr.)	Profile
2	0.67	0.15	0.04	12.7	NACA 4415
3	0.50	0.15	0.04	12.7	NACA 4415
4	0.83	0.15	0.04	12.7	NACA 4415
5	0.50	0.15	0.04	15.2	NACA 4415
6	0.50	0.15	0.04	10.2	NACA 4415
7	0.50	0.15	0.05	12.7	NACA 5415
8	0.50	0.15	0.03	12.7	NACA 3415
10	0.40	0.15	0.05	12.7	NACA 5415
11	0.30	0.15	0.05	12.7	NACA 5415

The test results with nozzle no. 7 in combination with the B 4-55 screw series are given in Fig. 16. For particulars of the B 4-55 screw series see (17), (18). In Fig. 16, the results are plotted in the conventional way with the coefficients:

$$K_T = \frac{T}{\rho\, n^2 D^4} \qquad K_Q = \frac{Q}{\rho\, n^2 D^5}$$

$$K_{TN} = \frac{T_N}{\rho\, n^2 D^4} \qquad \eta_o = \frac{J}{2\pi} \cdot \frac{K_T}{K_Q}$$

as functions of the advance coefficient $J = V_A/nD$ with the pitch ratio P/D of the screw as parameter.

From the results of open-water tests with the nozzle shapes summarized in Table 1, it appears that the smallest optimum diameters and the highest efficiencies are obtained with the lowest impeller thrust-total thrust ratios τ. This is in accordance with the conclusion that a maximum contraction of the nozzle should be aimed at.

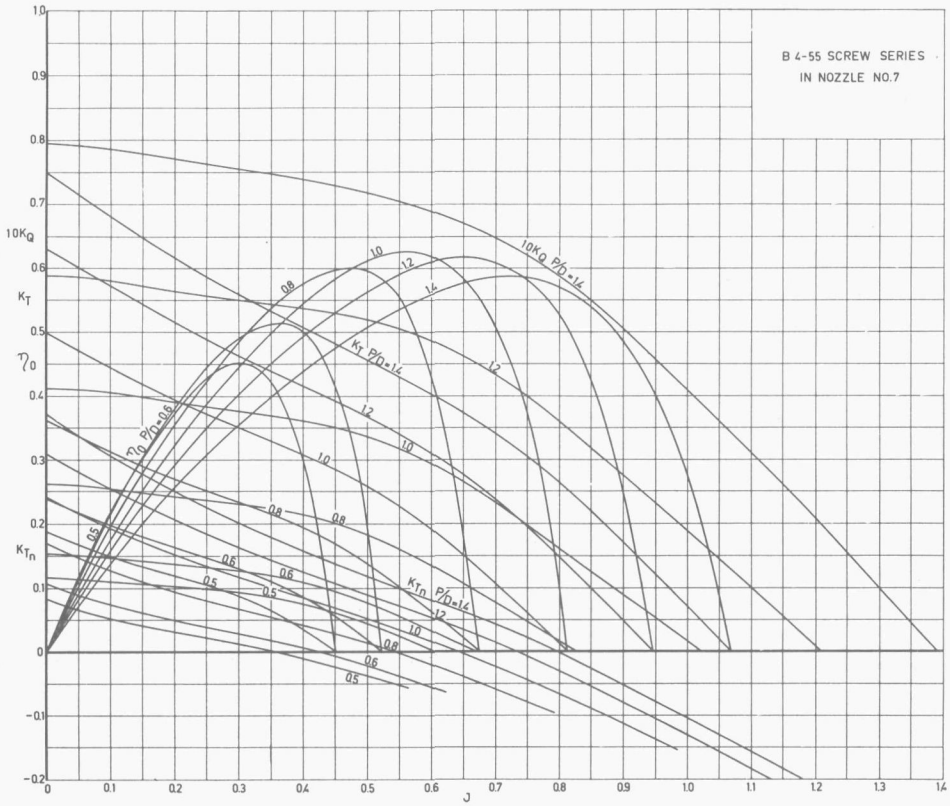

FIG. 16. Open-water test results of nozzle no. 7 with B4–55 screw series.

TABLE 2. Particulars of nozzles nos. 18, 19 and 20

Nozzle no.	L/D	S/L	f/L	α_i (degr.)	Profile
18	0.50	0.15	0.09	10.2	NACA 9415
19	0.50	0.15	0.07	10.2	NACA 7415
20	0.50	0.15	0.05	10.2	NACA 5415

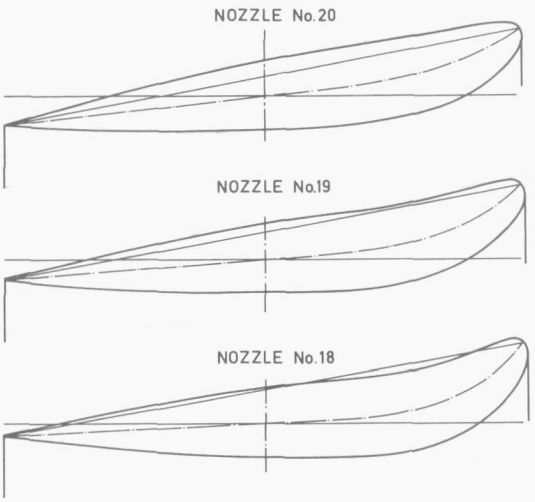

FIG. 17. Profiles of nozzles nos. 18, 19 and 20.

Lately, three new nozzle types were tested which did have some advantages over the types tested before. These nozzle profiles meet the following practical requirements:

1. An axial cylindrical part at the inner side of the nozzle at the location of the screw
2. A diverging part of the nozzle behind the screw
3. A maximum thickness ratio of the nozzle profile of 0.15.

The dimensions of these nozzles are summarized in Table 2. The nozzle profiles are given in Fig. 17. An angle between the nose-tail line of the nozzle profile and the shaft axis α_i of 10.2 degrees has been chosen for these nozzles. The camber ratios of these new nozzle profiles exceed the value of 0.05 so far investigated. The camber ratios for the nozzles no. 18, 19 and 20 were respectively 0.05; 0.07 and 0.09. Only very slight differences in the test results with the B 4-55 screw series in combination with these nozzles were found. The open-water test results of nozzle no. 19 in combination with the B 4-55 screw series are given in Fig. 18.

On the basis of these test results a, from the structural point of view, simple nozzle shape was chosen. This nozzle (nozzle no. 19A) did have, as already mentioned, an axial cylindrical part at the inner side of the nozzle at the location of the screw, the outside of the nozzle profile is made straight and the trailing edge of the nozzle is thicker. Besides, it must be noted that a nozzle with a thick trailing edge will have better qualities when stopping than a nozzle with a sharp trailing edge. The profile of nozzle no. 19A is shown in Fig. 19.

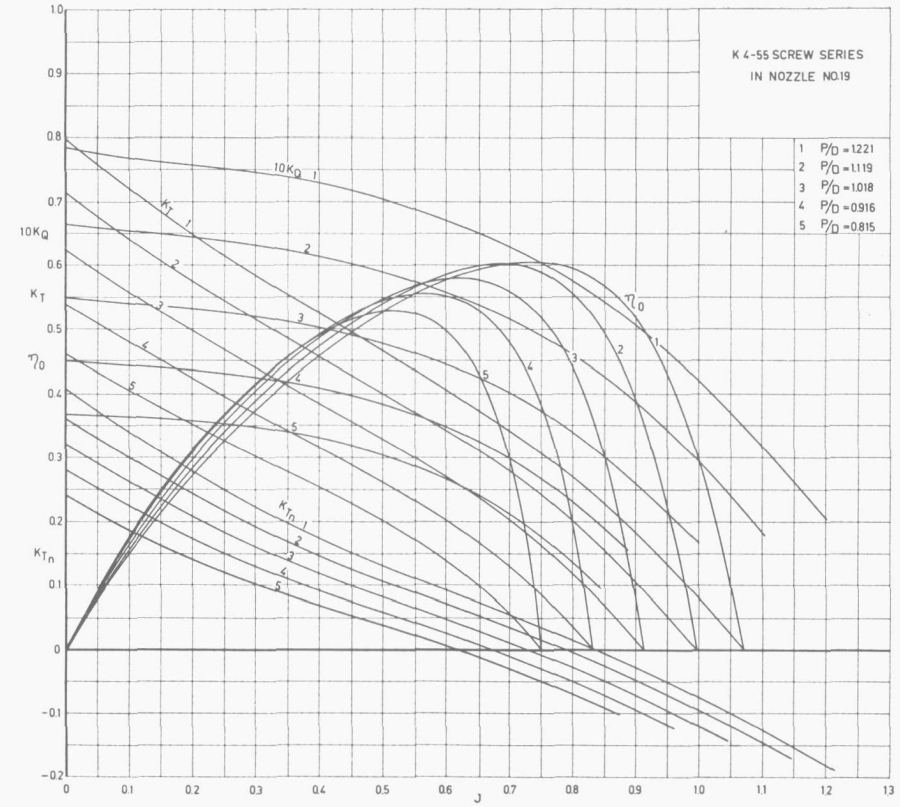

FIG. 18. Open-water test results of nozzle no. 19 with B4–55 screw series.

Most of the tests discussed so far were carried out with the Wageningen B-screw series. However, frequently a screw type with wider blade tips (Kaplan type) than the B-series screw type is preferred since the former is less susceptible to cavitation at the blade tips. Extensive investigations performed at the *NSMB* have led to the design of screw series, having uniform pitch and flat face sections. The main reasons for the choice of this type of pitch distribution and these blade sections are the advantages met when casting this type of screw. The results of the experiments mentioned show that this type of screw did not have drawbacks with respect to efficiency and cavitation. These screw series were designated the Ka-series.

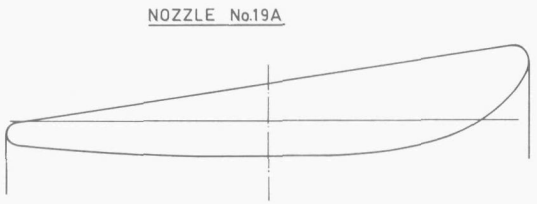

FIG. 19. Profile of nozzle no. 19A.

TABLE 3A. Dimensions of the Ka-screw series

	r/R	0.2	0.3	0.4	0.5	0.6	0.7	0.8	0.9	1.0	
Length of the blade sections in percentages of the maximum length of the blade section at 0.6 R	from centre line to trailing edge	30.21	36.17	41.45	45.99	49.87	52.93	55.04	56.33	56.44	Length of blade section at 0.6 R = $= 1.969 \frac{1}{Z} \cdot \frac{A_E}{A_O}$
	from centre line to leading edge	36.94	40.42	43.74	47.02	50.13	52.93	55.04	56.33	56.44	
	total length	67.15	76.59	85.19	93.01	100.00	105.86	110.08	112.66	122.88	
Max. blade thickness in percentages of the diam.		4.00	3.52	3.00	2.45	1 90	1.38	0.92	0.61	0.50	Maximum thickness at centre of shaft = 0.049 D
Distance of maximum thickness from leading edge in percentages of the length of the sections		34.98	39.76	46.02	49.13	49.98	—	—	—	—	

TABLE 3B. Ordinates of the Ka-screw series

	Distance of the ordinates from the maximum thickness											
	From maximum thickness to trailing edge					From maximum thickness to leading edge						
r/R	100%	80%	60%	40%	20%	20%	40%	60%	80%	90%	95%	100%
					Ordinates for the back							
0.2	—	38.23	63.65	82.40	95.00	97.92	90.83	77.19	55.00	38.75	27.40	—
0.3	—	39.05	66.63	84.14	95.86	97.63	90.06	75.62	53.02	37.87	27.57	—
0.4	—	40.56	66.94	85.69	96.25	97.22	88.89	73.61	50.00	34.72	25.83	—
0.5	—	41.77	68.59	86.42	96.60	96.77	87.10	70.46	45.84	30.22	22.24	—
0.6	—	43.58	68.26	85.89	96.47	96.47	85.89	68.26	43.58	28.59	20.44	—
0.7	—	45.31	69.24	86.33	96.58	96.58	86.33	69.24	45.31	30.79	22.88	—
0.8	—	48.16	70.84	87.04	96.76	96.76	87.04	70.84	48.16	34.39	26.90	—
0.9	—	51.75	72.94	88.09	97.17	97.17	88.09	72.94	51.75	38.87	31.87	—
1.0	—	52.00	73.00	88.00	97.00	97.00	88.00	73.00	52.00	39.25	32.31	—
					Ordinates for the face							
0.2	20.21	7.29	1.77	0.1	—	0.21	1.46	4.37	10.52	16.04	20.62	33.33
0.3	13.85	4.62	1.07	—	—	0.12	0.83	2.72	6.15	8.28	10.30	21.18
0.4	9.17	2.36	0.56	—	—	—	0.42	1.39	2.92	3.89	4.44	13.47
0.5	6.62	0.68	0.17	—	—	—	0.17	0.51	1.02	1.36	1.53	7.81

Note: The percentages of the ordinates relate to the maximum thickness of the corresponding section.

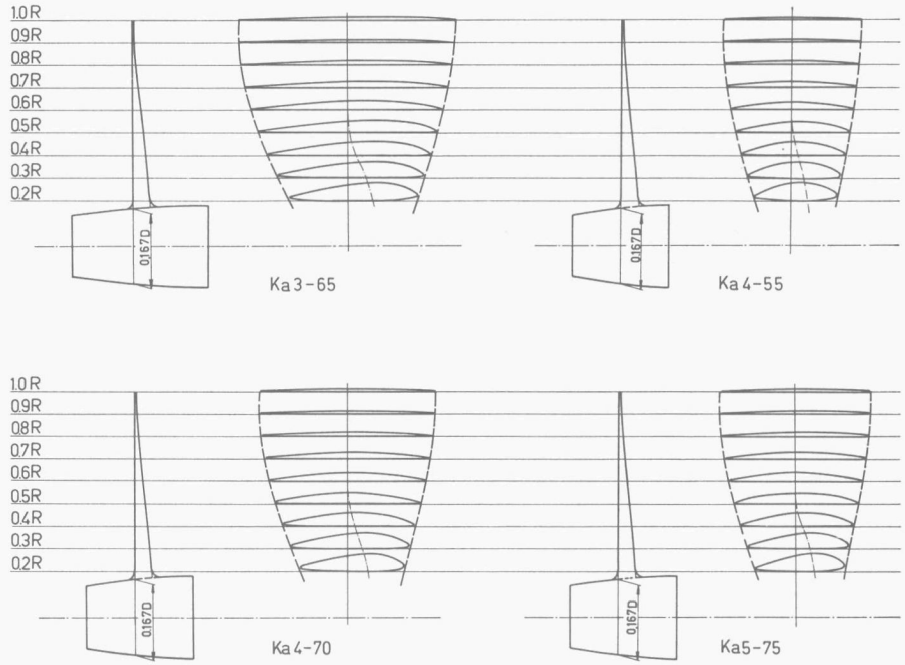

FIG. 20. Particulars of the Ka 3–65; Ka 4–55; Ka 4–70 and Ka 5–75 screw series.

Up till now open-water tests with the Ka 3-65; Ka 4-55; Ka 4-70 and Ka 5-75 screw series in combination with nozzle no. 19A, have been performed. The particulars of these screw models are given in Table 3 and in Fig. 20. The screws were located in the nozzles with a uniform tip clearance of 1 mm (about 0.4 percent of the screw diameter D).

The fairing of the open-water test results was performed with the aid of a CDC 3300 computer by means of a regression analysis. The thrust and torque coefficients K_T, K_{TN} and K_Q were expressed as polynomials of advance coefficient J and pitch ratio P/D:

$$K_T = A_{0,0} + A_{0,1} J + \cdots + A_{0,6} J^6 +$$
$$+ A_{1,0}\left(\frac{P}{D}\right) + A_{1,1}\left(\frac{P}{D}\right) J + \cdots + A_{1,6}\left(\frac{P}{D}\right) J^6 +$$
$$+ A_{2,0}\left(\frac{P}{D}\right)^2 + A_{2,1}\left(\frac{P}{D}\right)^2 J + \cdots + A_{2,6}\left(\frac{P}{D}\right)^2 J^6 +$$
$$\cdots\cdots\cdots\cdots\cdots\cdots\cdots\cdots\cdots\cdots\cdots\cdots$$
$$+ A_{6,0}\left(\frac{P}{D}\right)^6 + A_{6,1}\left(\frac{P}{D}\right)^6 J + \cdots + A_{6,6}\left(\frac{P}{D}\right)^6 J^6$$

$$K_{TN} = B_{0,0} + B_{0,1} J + \cdots + B_{6,6} \left(\frac{P}{D}\right)^6 J^6$$

$$K_Q = C_{0,0} + C_{0,1} J + \cdots + C_{6,6} \left(\frac{P}{D}\right)^6 J^6$$

With the aid of a regression analysis the significant terms of the polynomials and the values of the corresponding coefficients were determined. From this analysis it was found that most of the terms with high powers of J and P/D were insignificant. The results for the Ka 3-65; Ka 4-55; Ka 4-70 and Ka 5-75 screw series in combination with nozzle no. 19A are given in Table 4.

These results can be used directly for solving problems which arise when designing and analyzing ducted screw propellers if a computer is available. Also the results will be given in graphical form. With the aid of a tape-controlled drawing machine the

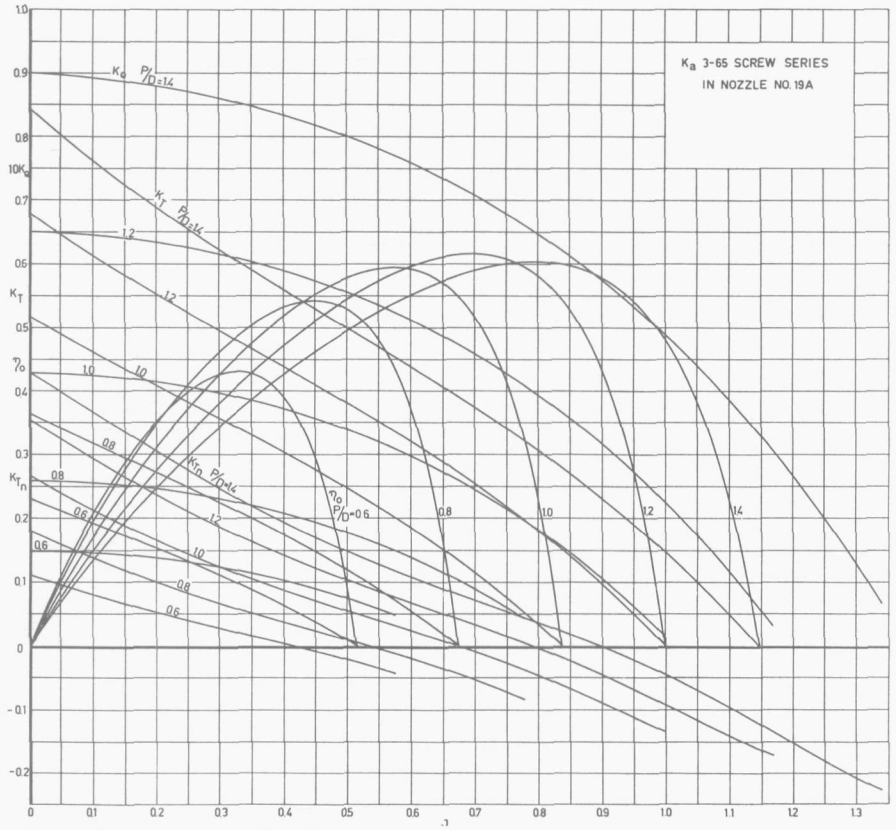

FIG. 21. Open-water test results of Ka 3–65 screw series with nozzle no. 19 A.

TABLE 4. Form of polynomial and coefficients of Ka-screw series in combination with nozzle no. 19A

		Ka 3-65			Ka 4-55		
x	y	Axy	Cxy	Bxy	Axy	Cxy	Bxy
0	0	+0.028100	+0.006260	+0.154000	—0.375000	—0.034700	—0.045100
0	1	—0.143910		+0.115560	—0.203050	+0.018568	
0	2		—0.017942	—0.123761	+0.830306		
0	3	—0.383783			—2.746930		—0.663741
0	4		—0.008089			—0.195582	—0.244626
0	5			—0.741240		+0.317452	
0	6			+0.646894	+0.067548	—0.093739	
1	0			—0.542674	+2.030070	+0.158951	+0.244461
1	1	—0.429709		—0.749643	—0.392301	—0.048433	—0.578464
1	2		—0.016644		—0.611743		+1.116820
1	3				+4.319840	+0.024157	+0.751953
1	4				—0.341290		
1	5					—0.123376	
1	6			—0.162202			—0.08916
2	0	+0.671268		+0.972388	—3.031670	—0.212253	
2	1						—0.146178
2	2	+0.286926		+1.468570			—0.917516
2	3				—2.007860		
2	4						
2	5						
2	6						
3	0	—0.182294	+0.040041	—0.317644	+2.836970	+0.156133	+0.068186
3	1						+0.174041
3	2			—1.084980			+0.102334
3	3				+0.391304		
3	4						
3	5						
3	6			—0.032298			
4	0				—0.994962		
4	1					+0.030740	
4	2					+0.073587	
4	3			+0.199637			
4	4						
4	5						
4	6						
5	0					—0.031826	
5	1			+0.060168	+0.015742	—0.014568	
5	2					—0.109363	
5	3						
5	4					+0.043862	
5	5						
5	6						
6	0		—0.003460		+0.043782	+0.007947	—0.008581
6	1	—0.017378	—0.000674				
6	2		+0.001721			+0.038275	
6	3						
6	4					—0.021971	
6	5						
6	6					+0.000700	
0	7					+0.022850	+0.088319

Ka 4-70			Ka 5-75		
Axy	Cxy	Bxy	Axy	Cxy	Bxy
+0.030550	+0.006735	+0.076594	+0.033000	+0.007210	−0.000813
−0.148687		+0.075223	−0.153463		+0.034885
	−0.016306	−0.061881		−0.014670	
−0.391137		−0.138094	−0.398491		−0.276187
	−0.007244			−0.006398	
		−0.370620			
		+0.323447			
		−0.271337			
−0.432612		−0.687921	−0.435515		−0.626198
	−0.024012	+0.225189		−0.031380	+0.450379
		−0.081101			
+0.667657		+0.666028	+0.664045		+0.359718
	+0.005193	+0.734285	+0.283225	+0.010386	
−0.172529	+0.046605	−0.202467	−0.162764	+0.053169	−0.087289
		−0.542490			
		−0.016149			
	−0.007366			−0.014731	
		+0.099819			
		+0.030084			
	−0.001730				
−0.017293	−0.000337		−0.017208		
	+0.000861	−0.001876			−0.003751

coefficients K_T, K_{TN}, K_Q and η_0 were drawn in the conventional way as a function of J. The diagrams of the Ka 3-65; Ka 4-55; Ka 4-70 and Ka 5-75 screw series in combination with nozzle no. 19A are given in Figs. 21 through 24.

For design purposes various types of more practical diagrams can be derived from the $K_T - K_{TN} - K_Q - J$ diagram. The most widely encountered design problem of screw propellers or ducted propellers for ships is the one where the speed of advance of the screw V_A, the power to be absorbed by the screw P, and the number of revolutions N are given. The diameter D is to be chosen such that the greatest efficiency can be obtained. The problem of the optimum diameter of the system can be solved in an easy way by plotting η_o and J as a function of

$$\frac{K_Q{}^{1/2}}{J^{5/2}} : : \frac{NP^{1/2}}{V_A^{5/2}}$$

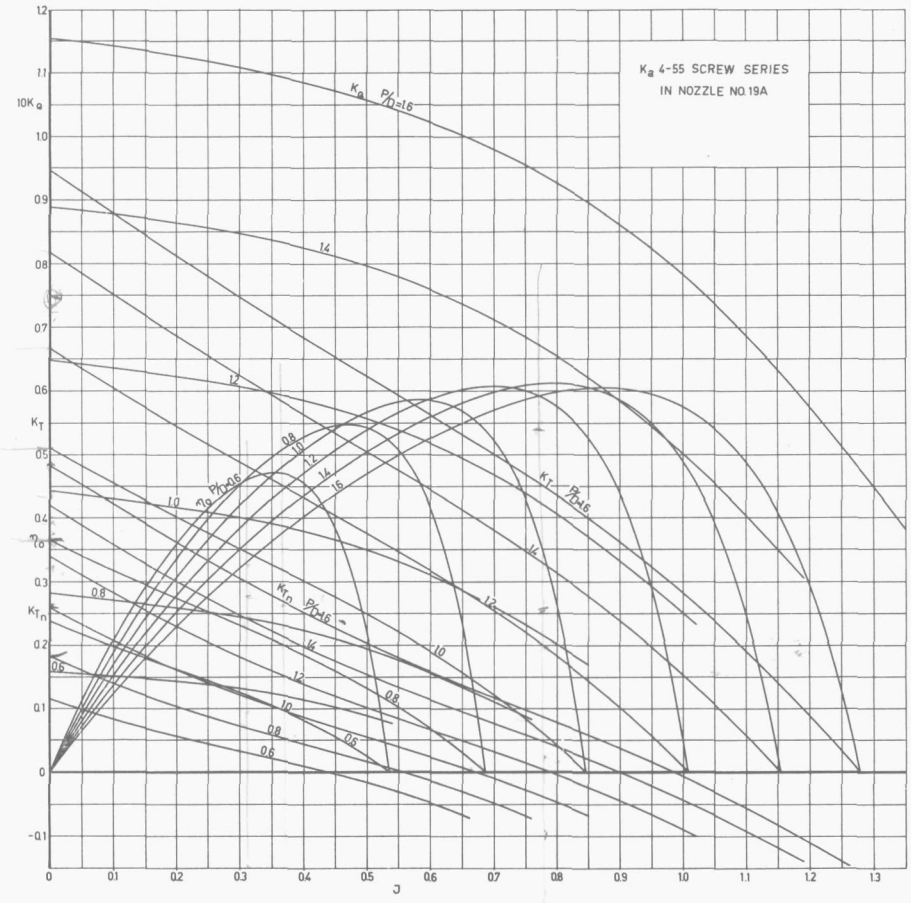

FIG. 22. Open-water test results of Ka 4–55 screw series with nozzle no. 19 A.

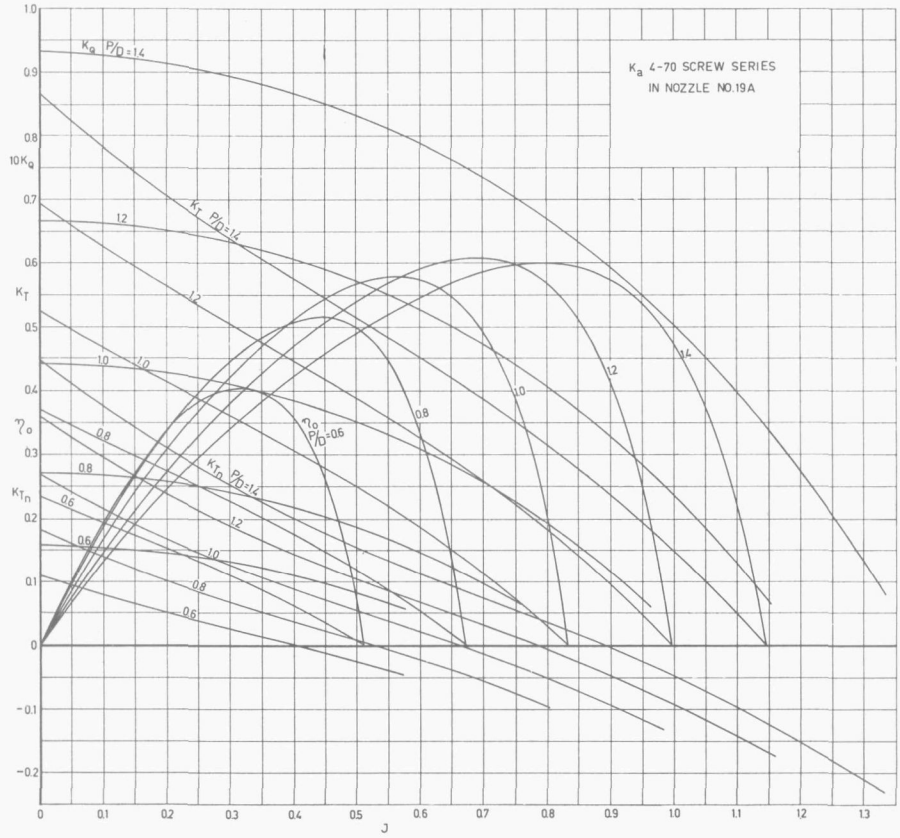

FIG. 23. Open-water test results of Ka 4–70 screw series with nozzle no. 19 A.

The well-known coefficient B_p see (17) and (18) is related to the above dimensionless variable $K_Q^{1/2}/J^{5/2}$ by the equation:

$$B_p = 33.07\, K_Q^{1/2}/J^{5/2} = NP^{1/2}/V_A^{5/2}$$

where

N = number of revolutions per minute

P = power in HP

V_A = speed of advance in knots

In the usual diagram, the design coefficient B_P is the base and a new speed ratio is used. This speed ratio is defined as:

$$\delta = \frac{ND}{V_A} = \frac{101.27}{J}$$

in which

D = screw diameter in feet.

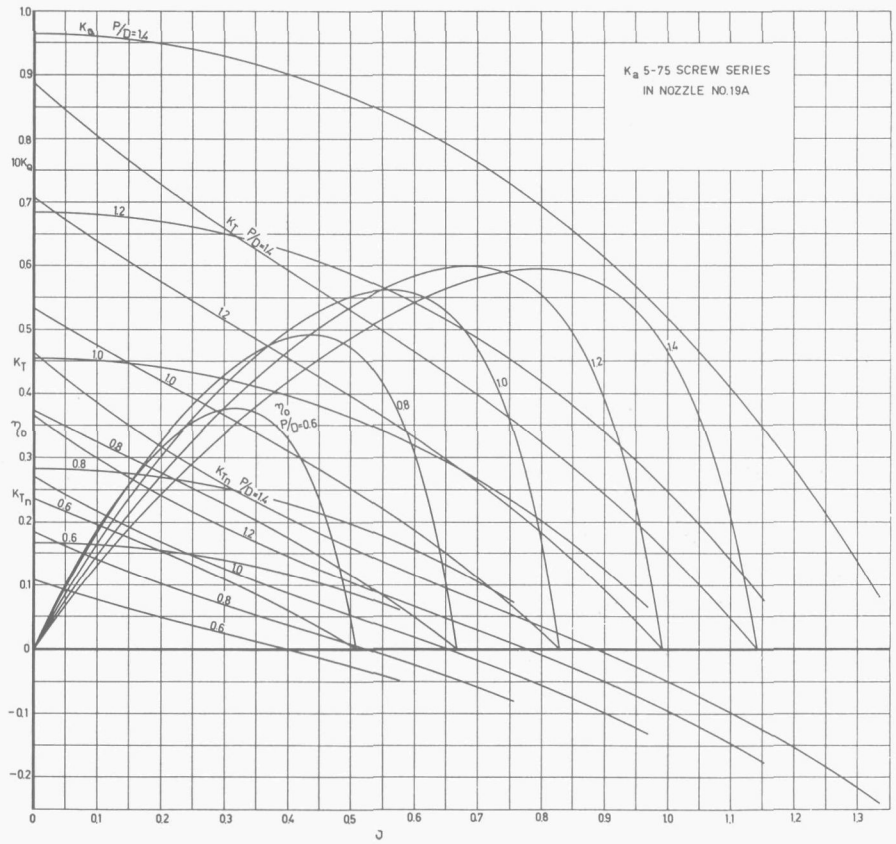

FIG. 24. Open-water test results of Ka 5–75 screw series with nozzle no. 19 A.

The $B_P - \delta$ diagrams of the different Ka screw series in nozzle no. 19A are given in Figs. 25 through 28.

In cases where V_A, T and N or V_A, T and D are given, the problem of determining the optimum diameter or the optimum number of revolutions can be solved by plotting η_o and J as functions of

$$K_T/J^4 \text{ and } K_T/J^2$$

For the different K_a screw series the curves for optimum diameter (on base of $K_Q^{1/2} \cdot J^{-5/2}$ and $K_T^{1/2} \cdot J^{-2}$) and optimum rpm (on base of $K_T \cdot J^{-2}$) are given in Figs. 29, 30 and 31 respectively.

In order to obtain data for analyzing the manoeuvres of ships, submersibles, drilling vessels (dynamic positioning) and so on fitted with ducted propellers, open-water tests with the Ka 4-70 screw series in combination with nozzle no. 19A were conducted

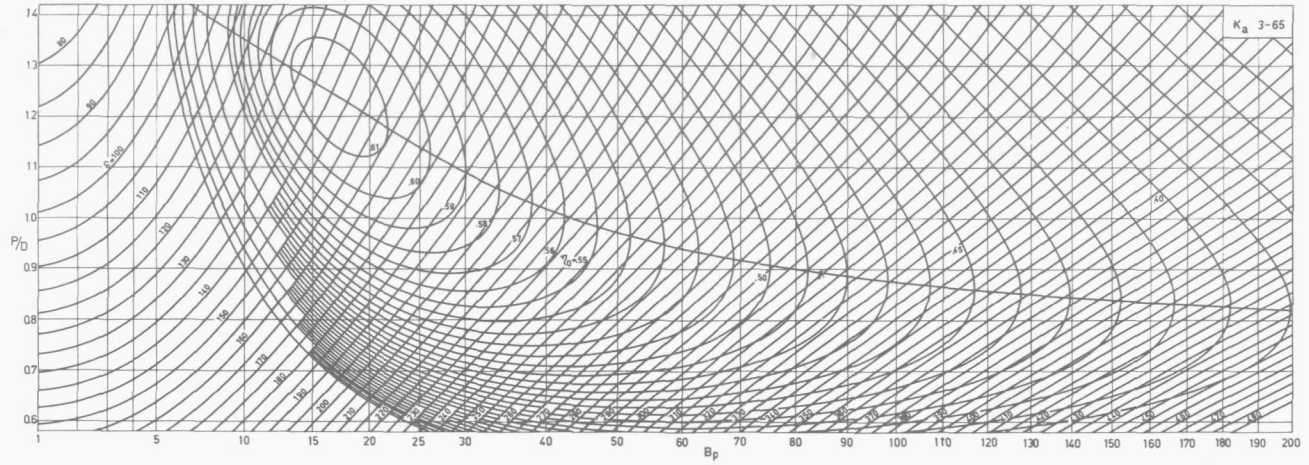

FIG. 25. B_P–δ diagram of Ka 3–65 screw series with nozzle no. 19 A.

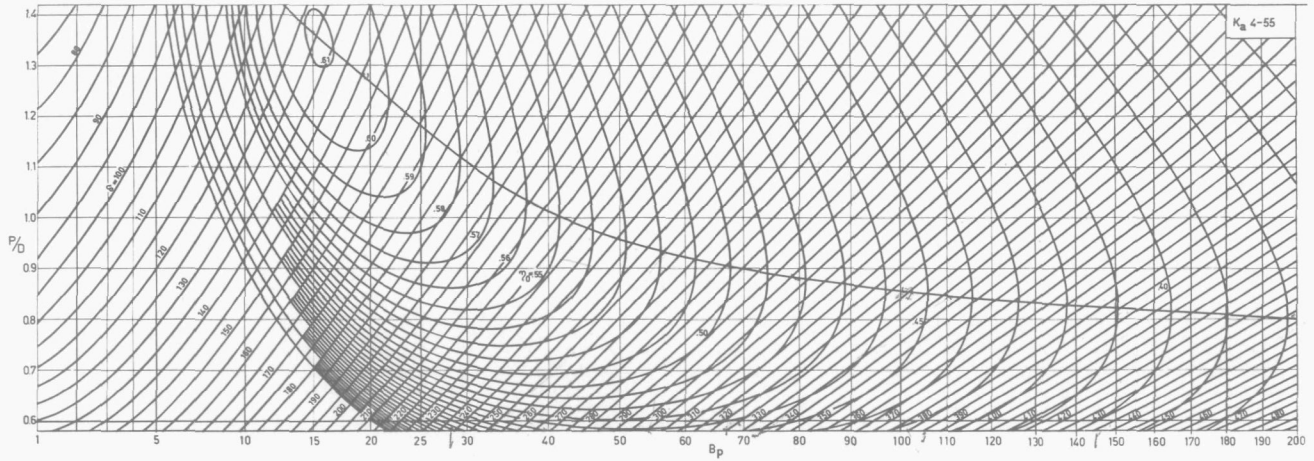

FIG. 26. B_P–δ diagram of Ka 4–55 screw series with nozzle no. 19 A.

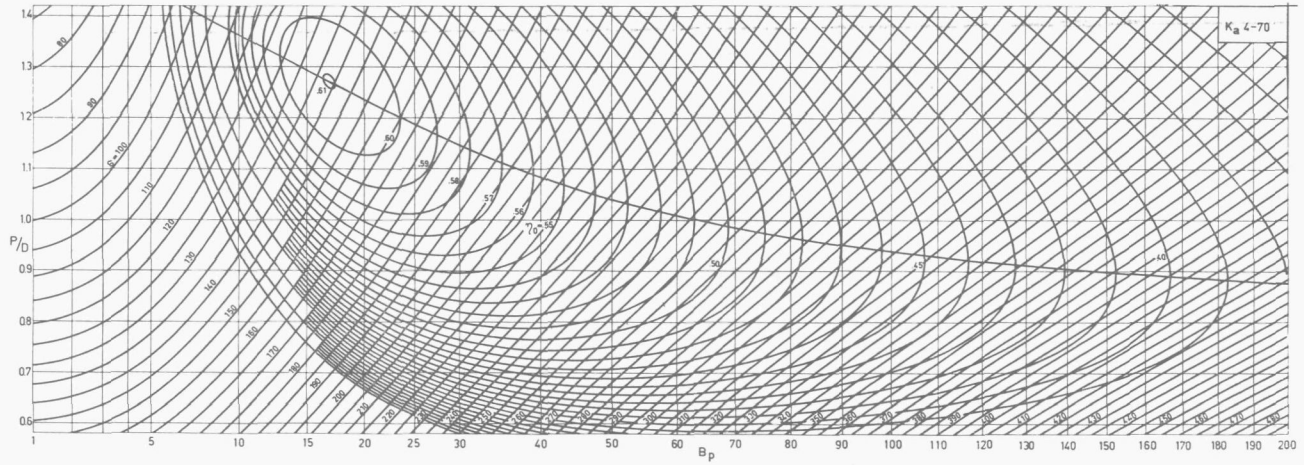

FIG. 27. B_P–δ diagram of Ka 4–70 screw sereis with nozzle no. 19A.

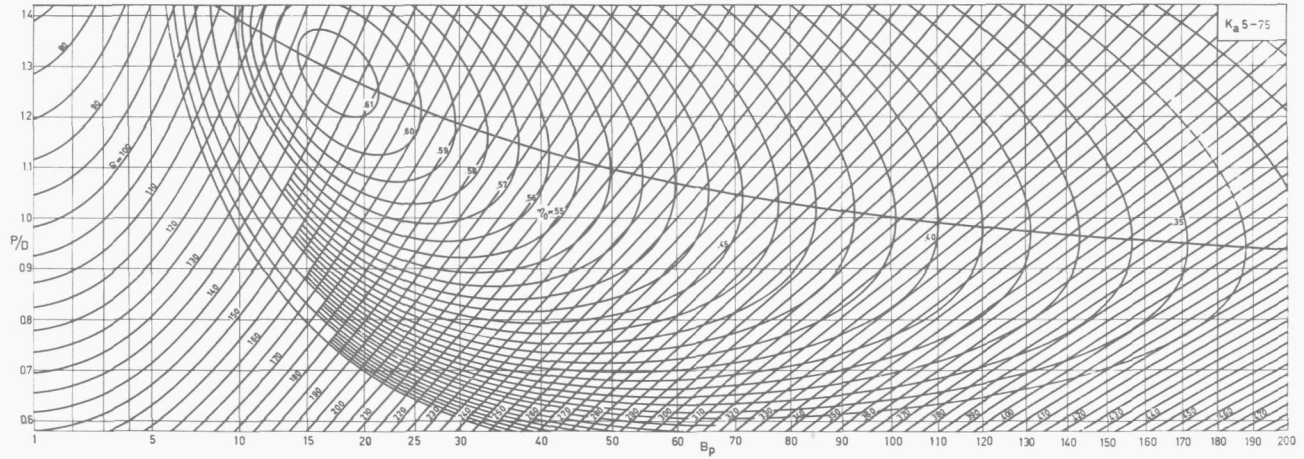

FIG. 28. B_P–δ diagram of Ka 5–75 screw series with nozzle no. 19A.

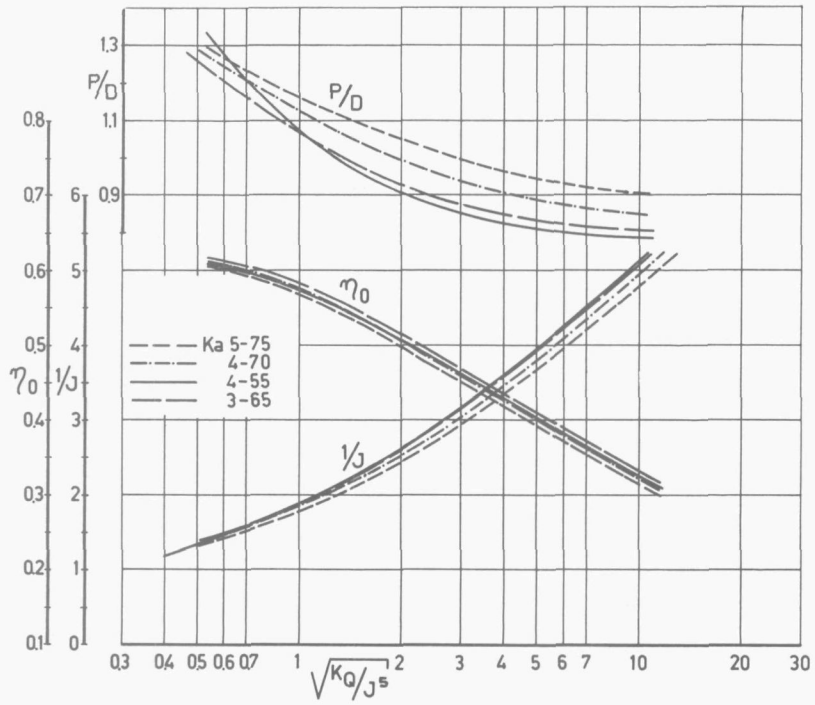

FIG. 29. Curves for optimum diameter of Ka screw series in nozzle no. 19 A.

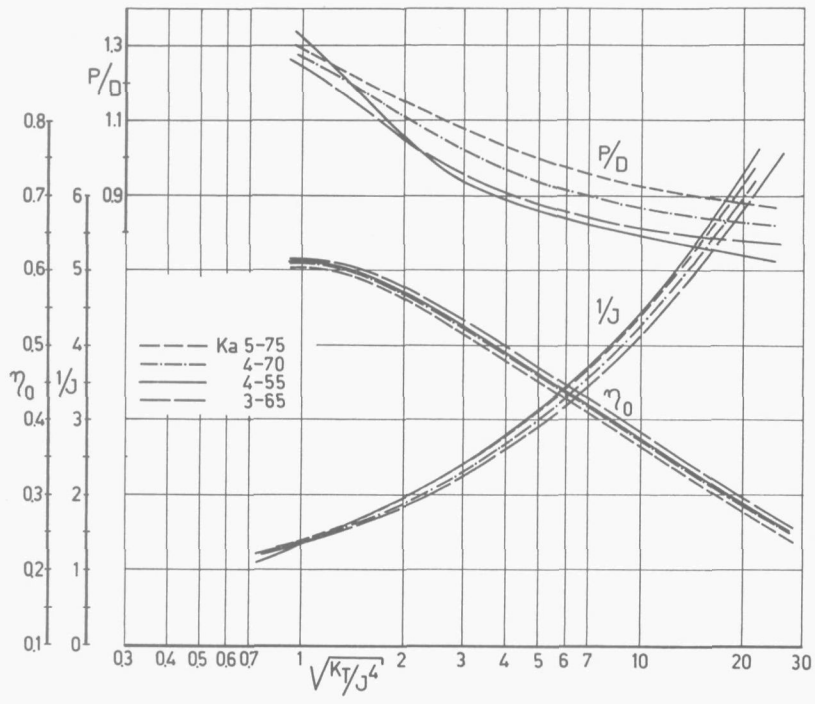

FIG. 30. Curves for optimum diameter of Ka screw series in nozzle no. 19 A.

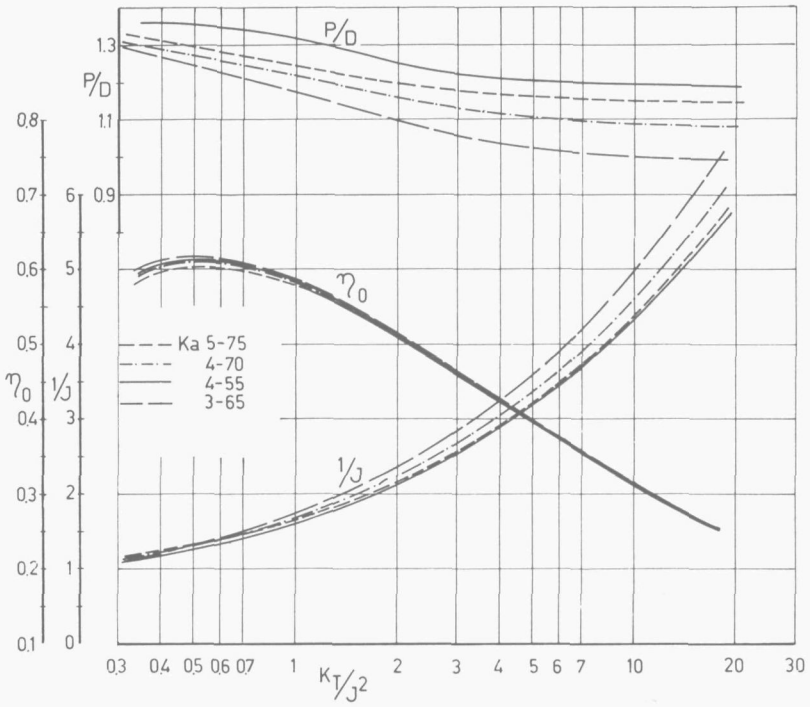

FIG. 31. Curves for optimum rpm of Ka screw series in nozzle no. 19A.

over a wider range of advance coefficients. In addition, it was of importance to have data available to determine the thrust which can be developed at bollard pull condition either with the propeller running ahead or astern for towing vessels (tugs, push-boats).

The ducted propellers were tested at the following combinations of speed and rpm:

1st quadrant: speed ahead, rpm ahead. In this quadrant the results of normal open-water tests are given. The measurements are, however, extended to operating conditions where the thrust of the ducted propeller system becomes negative. The advance angle β ($\tan \beta = V_A/0.7\,\pi nD$) varies between 0 and 90 degrees,
$0° \leqslant \beta \leqslant 90°$

2nd quadrant: speed ahead, rpm astern
$90° \leqslant \beta \leqslant 180°$

3rd quadrant: speed astern, rpm astern
$180° \leqslant \beta \leqslant 270°$

4th quadrant: speed astern, rpm ahead
$270° \leqslant \beta \leqslant 360°$

The measurements were performed with the usual apparatus for open-water tests with ducted propellers. The immersion of the propeller shaft was equal to the screw

diameter. Before the tests were carried out, the system friction and dummy hub thrust and torque were determined so that the measured propeller thrust and torque could be corrected accordingly.

The tests with the negative propeller advance velocities were conducted with a reversely mounted nozzle and with reversely mounted impellers without change in the carriage motion direction.

Within the normal test range of a ducted propeller it is generally possible to perform the tests at a constant rpm. Outside this range, the tests must be performed at different rpm and speeds of advance, to operate within the range of capabilities of the dynamometer and on account of the maximum speed of the towing carriage. Usually the rpm and speed were chosen as high as possible to maintain a high Reynolds number.

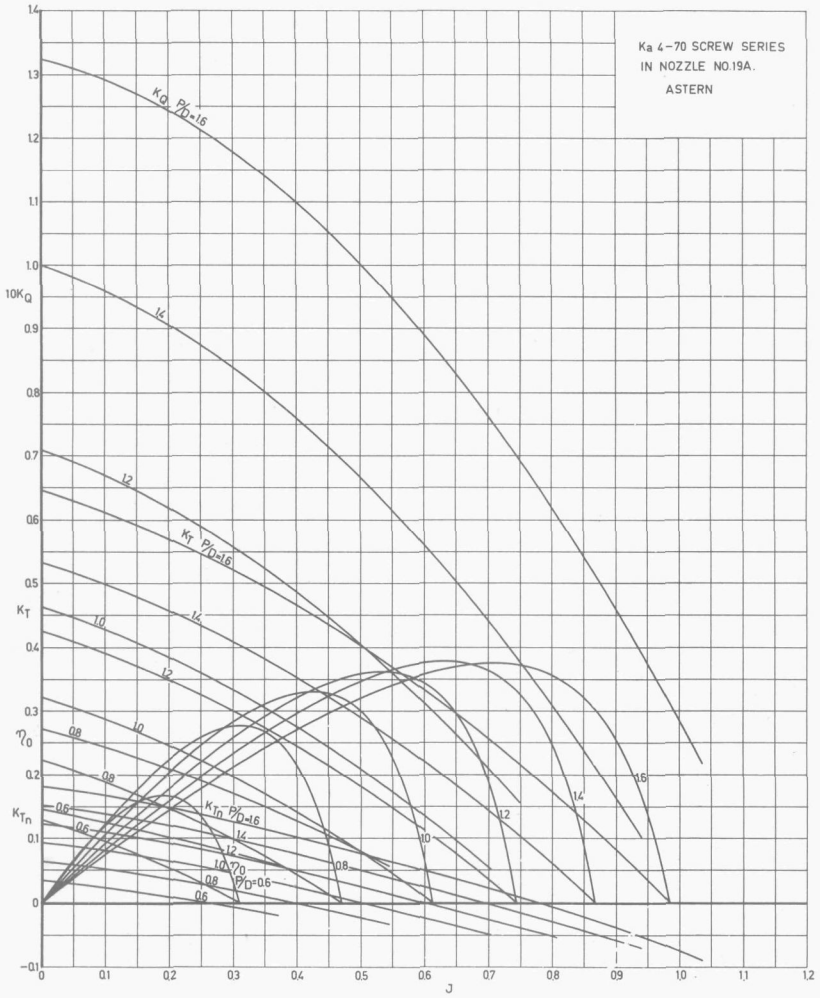

FIG. 32. Open-water test results of Ka 4–70 screw series with nozzle no. 19 A with reversely mounted nozzle and impeller.

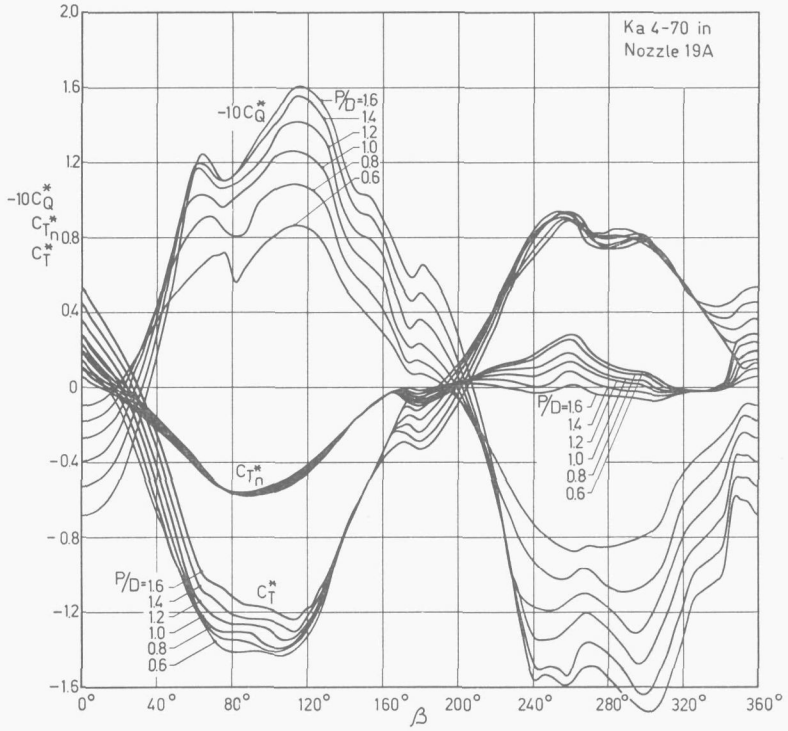

FIG. 33. Open-water test results of Ka 4–70 screw series with nozzle no. 19A in four quadrants.

In Fig. 32, the open-water results with the reversely mounted duct and impellers with speed and rpm astern (3rd quadrant) are given.

The test results over the whole range of operating conditions of the ducted propeller system are given in Fig. 33. The usually accepted way of presenting the results of open-water tests in the form of the thrust and torque coefficients K_T, K_{TN}, K_Q as functions of the advance coefficient J is unsuitable for representation of the ducted propeller characteristics in all of the cases encountered during the four-quadrant measurements. When n approaches zero, the advance coefficient J as well as the thrust and torque coefficients K_T and K_Q approach infinity and thus these coefficients cannot be used to describe the propeller characteristics. Therefore the modified thrust and torque coefficients

$$C_T^* = \frac{T}{\frac{1}{2}\rho\,[V_A^2 + (0.7\,\pi nD)^2]\,\pi/4\,D^2}$$

$$C_{TN}^* = \frac{T_N}{\frac{1}{2}\rho\,[V_A^2 + (0.7\,\pi nD)^2]\,\pi/4\,D^2}$$

$$C_Q^* = \frac{Q}{\frac{1}{2}\rho\,[V_A^2 + (0.7\,\pi nD)^2]\,\pi/4\,D^2 \cdot D}$$

FIG. 34. Profile of nozzle no. 37.

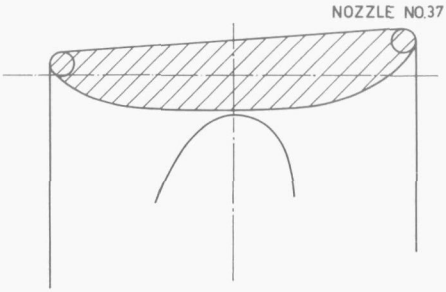

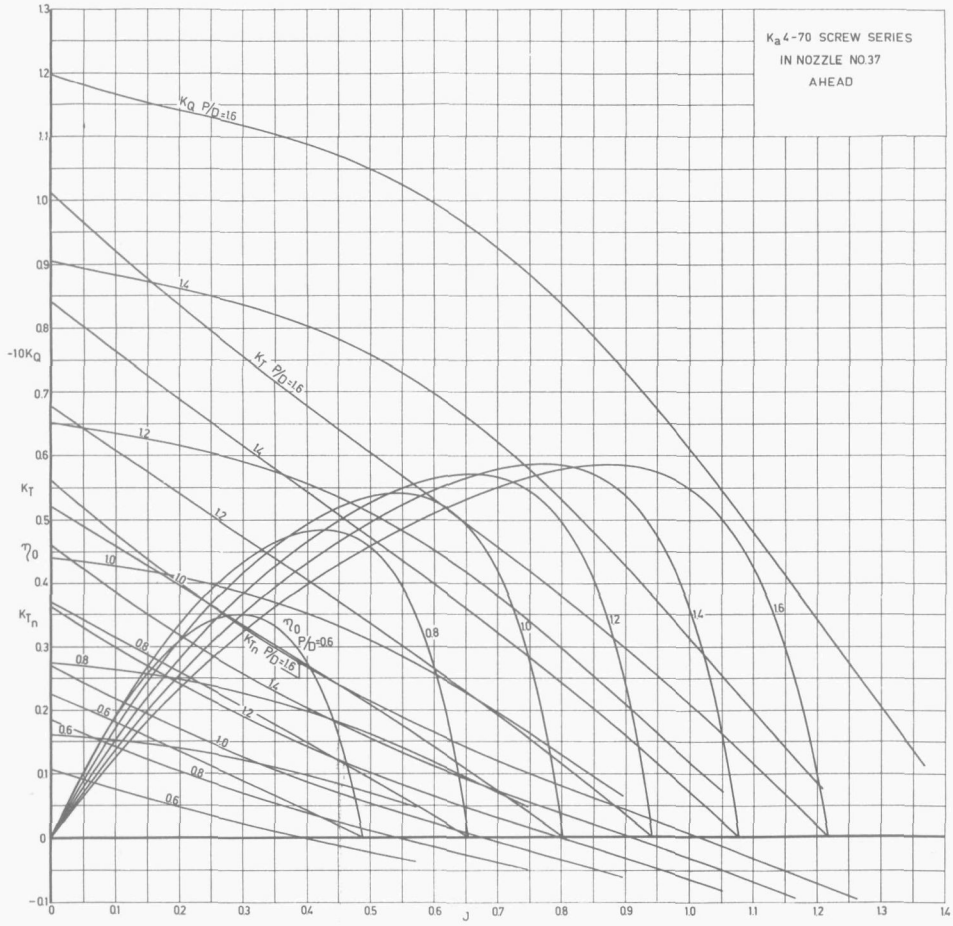

FIG. 35. Open-water test results of Ka 4–70 screw series with nozzle no. 37.

are given as functions of the advance angle β:

$$\beta = \arctan \frac{V_A}{0.7\,\pi n D}$$

in the diagram. This is about the same representation as used by MINIOVICH (19), BAKER and PATTERSON (20) and VAN LAMMEREN et al (18).

For towing vessels (especially pushboats), the thrust which can be developed at bollard pull condition either with the propeller running ahead or astern is of utmost importance. In such cases it is attractive to use a nozzle with a relatively thick trailing edge. Such a nozzle (nozzle no. 37) is shown in Fig. 34.

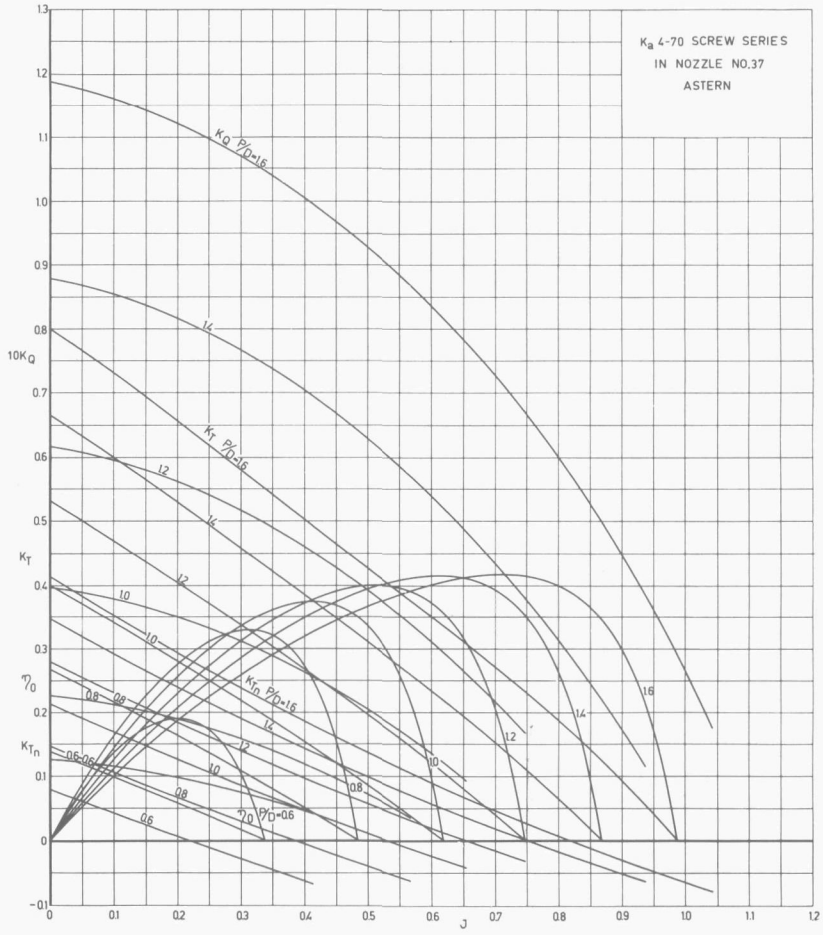

FIG. 36. Open-water test results of Ka 4–70 screw series with nozzle no. 37; with reversely mounted nozzle and impeller.

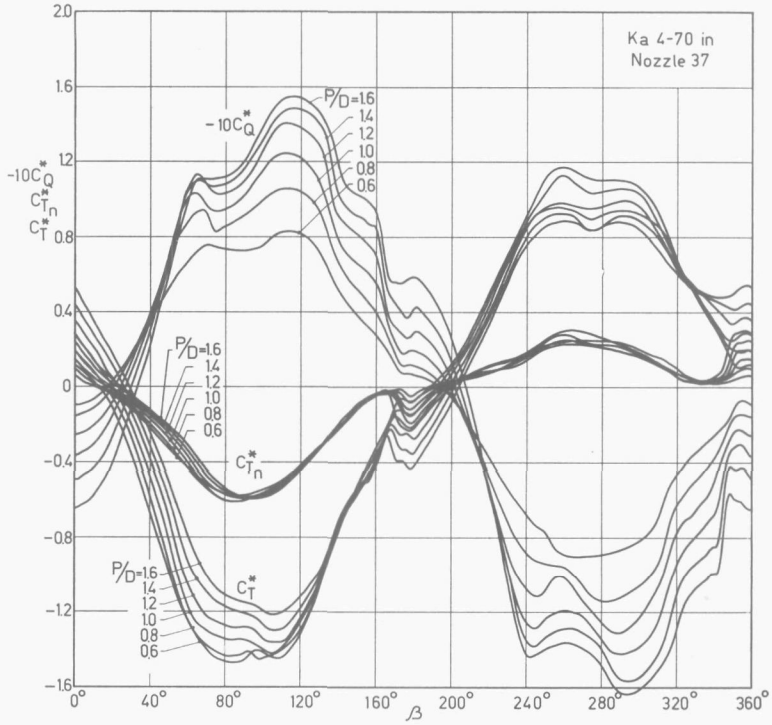

FIG. 37. Open-water test results of Ka 4–70 screw series with nozzle no. 37 in four quadrants.

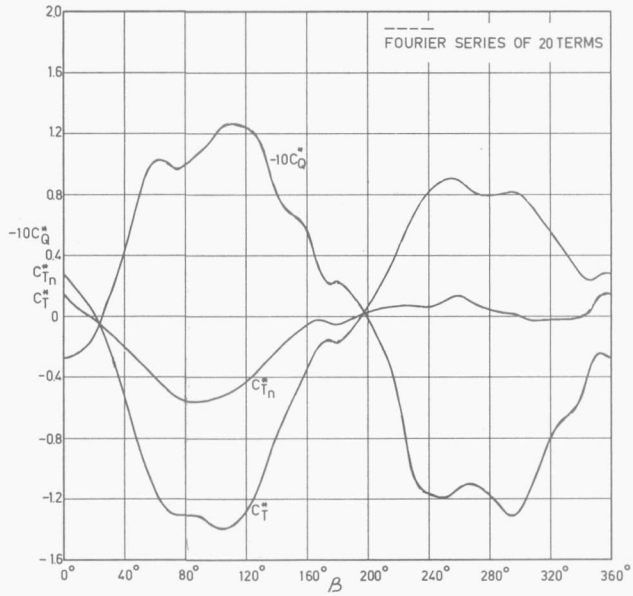

FIG. 38. Result of four-quadrant measurements of Ka 4–70 screw series with nozzle no. 19A approximated by Fourier series of 20 terms.

TABLE 5. Coefficients of Fourier series by which results are approximated of four-quadrant measurements with Ka 4-70 series screws in nozzle no. 19A

		$P/D = 0.6$		$P/D = 0.8$	
	K	A (K)	B (K)	A (K)	B (K)
C_T^*	0	$-.14825 \neq 0$	$+.00000 \neq +0$	$-.13080 \neq 0$	$+.00000 \neq +0$
	1	$+.84697 \neq -1$	$-.10838 \neq +1$	$+.10985 \neq 0$	$-.10708 \neq +1$
	2	$+.16700 \neq 0$	$+.18023 \neq -1$	$+.15810 \neq 0$	$+.24163 \neq -1$
	3	$+.96610 \neq -3$	$+.11825 \neq 0$	$+.18367 \neq -1$	$+.12784 \neq 0$
	4	$+.14754 \neq -1$	$-.70713 \neq -2$	$+.16168 \neq -1$	$-.14064 \neq -2$
	5	$-.11806 \neq -1$	$+.62894 \neq -1$	$-.37402 \neq -2$	$+.76213 \neq -1$
	6	$-.14888 \neq -1$	$+.11519 \neq -1$	$-.11736 \neq -1$	$+.13259 \neq -1$
	7	$+.73311 \neq -2$	$+.17070 \neq -2$	$+.25483 \neq -2$	$-.42300 \neq -2$
	8	$+.75022 \neq -2$	$+.22990 \neq -2$	$+.12350 \neq -2$	$-.26246 \neq -2$
	9	$-.15128 \neq -1$	$+.13458 \neq -1$	$-.20772 \neq -2$	$+.16328 \neq -1$
	10	$+.33002 \neq -2$	$+.54810 \neq -3$	$+.69749 \neq -2$	$-.33979 \neq -3$
	11	$+.31416 \neq -2$	$+.42076 \neq -2$	$+.59838 \neq -2$	$+.23506 \neq -2$
	12	$-.21144 \neq -2$	$-.57232 \neq -2$	$-.14599 \neq -2$	$-.69497 \neq -2$
	13	$+.29438 \neq -2$	$+.74689 \neq -2$	$+.83533 \neq -2$	$+.61925 \neq -2$
	14	$+.33857 \neq -3$	$-.84815 \neq -4$	$+.11093 \neq -2$	$+.35046 \neq -3$
	15	$+.41236 \neq -2$	$-.13374 \neq -2$	$+.41885 \neq -2$	$-.11571 \neq -2$
	16	$+.16259 \neq -2$	$-.91934 \neq -3$	$-.12438 \neq -3$	$-.32566 \neq -3$
	17	$+.12759 \neq -2$	$+.27412 \neq -2$	$+.38034 \neq -2$	$+.63420 \neq -3$
	18	$+.20647 \neq -2$	$-.10198 \neq -2$	$+.90073 \neq -3$	$-.22749 \neq -2$
	19	$+.34157 \neq -2$	$+.19845 \neq -2$	$+.31147 \neq -2$	$-.36805 \neq -3$
	20	$-.58703 \neq -3$	$-.13980 \neq -2$	$-.10633 \neq -3$	$-.12350 \neq -2$
$C_{T_N}^*$	0	$-.14276 \neq 0$	$+.00000 \neq +0$	$-.12764 \neq 0$	$+.00000 \neq +0$
	1	$-.55945 \neq -2$	$-.21875 \neq 0$	$+.68679 \neq -3$	$-.24100 \neq 0$
	2	$+.15519 \neq 0$	$+.10114 \neq -1$	$+.14639 \neq 0$	$+.18919 \neq -1$
	3	$+.15915 \neq -1$	$+.47120 \neq -1$	$+.23195 \neq -1$	$+.55513 \neq -1$
	4	$+.66633 \neq -2$	$-.58914 \neq -3$	$+.10292 \neq -1$	$-.12453 \neq -2$
	5	$+.89343 \neq -3$	$-.12958 \neq -2$	$+.86651 \neq -2$	$-.14748 \neq -2$
	6	$-.38876 \neq -2$	$-.20824 \neq -2$	$-.39124 \quad -2$	$-.21899 \neq -2$
	7	$+.10976 \neq -1$	$+.52475 \neq -2$	$+.15984 \neq -1$	$+.56694 \neq -2$
	8	$+.31959 \neq -2$	$-.15428 \neq -2$	$+.46295 \neq -2$	$-.49911 \neq -2$
	9	$+.14201 \neq -2$	$+.23580 \neq -2$	$+.68371 \neq -3$	$+.13631 \neq -2$
	10	$+.13507 \neq -2$	$+.23491 \neq -3$	$+.16740 \neq -2$	$+.12877 \neq -2$
	11	$+.50526 \neq -2$	$-.26868 \neq -2$	$+.83495 \neq -2$	$-.35176 \neq -2$
	12	$-.90855 \neq -3$	$-.45635 \neq -2$	$-.77063 \neq -3$	$-.55571 \neq -2$
	13	$+.42758 \neq -4$	$-.44554 \neq -4$	$+.14936 \neq -2$	$+.31438 \neq -3$
	14	$+.42084 \neq -3$	$-.18564 \neq -4$	$+.11017 \neq -2$	$-.11179 \neq -2$
	15	$+.20269 \neq -2$	$-.80547 \neq -3$	$+.16804 \neq -2$	$-.24577 \neq -2$
	16	$-.79748 \neq -3$	$-.10170 \neq -2$	$-.10338 \neq -2$	$-.55484 \neq -3$
	17	$+.97452 \neq -3$	$-.46721 \neq -4$	$+.22409 \neq -2$	$+.10968 \neq -3$
	18	$+.48897 \neq -3$	$-.17088 \neq -3$	$+.11000 \neq -2$	$-.73945 \neq -3$
	19	$+.84347 \neq -3$	$-.60673 \neq -3$	$+.48406 \neq -3$	$-.15400 \neq -2$
	20	$-.39298 \neq -3$	$-.36317 \neq -3$	$-.33008 \neq -3$	$+.22408 \neq -3$
C_Q^*	0	$+.17084 \neq -1$	$+.00000 \neq +0$	$+.19368 \neq -1$	$+.00000 \neq +0$
	1	$+.10550 \neq 0$	$-.78070 \neq 0$	$+.17050 \neq 0$	$-.99912 \neq 0$
	2	$-.27380 \neq -1$	$+.38134 \neq -1$	$-.11901 \neq -1$	$+.31924 \neq -1$
	3	$-.11827 \neq -1$	$+.74292 \neq -1$	$-.25601 \neq -2$	$+.81384 \neq -1$
	4	$+.28671 \neq -1$	$-.13568 \neq -1$	$+.17763 \neq -1$	$-.35096 \neq -3$
	5	$+.42504 \neq -2$	$+.66595 \neq -1$	$+.82085 \neq -2$	$+.10631 \neq 0$
	6	$-.78835 \neq -2$	$+.10330 \neq -1$	$-.34336 \neq -2$	$+.15116 \neq -1$
	7	$-.70981 \neq -2$	$-.17885 \neq -1$	$-.24534 \neq -1$	$-.27045 \neq -1$
	8	$+.76691 \neq -2$	$-.36187 \neq -2$	$-.10289 \neq -2$	$-.59389 \neq -2$
	9	$-.12506 \neq -1$	$+.10015 \neq -1$	$-.74938 \neq -2$	$+.11085 \neq -1$
	10	$-.70343 \neq -2$	$+.55926 \neq -2$	$+.15444 \neq -2$	$+.83787 \neq -2$
	11	$-.10254 \neq -1$	$+.69688 \neq -2$	$-.14173 \neq -1$	$+.15192 \neq -1$
	12	$+.25186 \neq -2$	$-.47676 \neq -2$	$-.28034 \neq -2$	$-.51507 \neq -2$
	13	$+.96613 \neq -2$	$+.88889 \neq -2$	$+.14246 \neq -1$	$+.14836 \neq -1$
	14	$+.14934 \neq -2$	$+.49081 \neq -2$	$+.34663 \neq -2$	$+.25041 \neq -2$
	15	$-.28323 \neq -2$	$-.58150 \neq -4$	$+.20764 \neq -2$	$-.78615 \neq -3$
	16	$-.30360 \neq -2$	$-.52044 \neq -2$	$-.29424 \neq -2$	$-.24526 \neq -2$
	17	$+.20889 \neq -2$	$+.12522 \neq -2$	$+.30149 \neq -2$	$-.32187 \neq -3$
	18	$+.31929 \neq -2$	$+.33190 \neq -2$	$+.27714 \neq -2$	$-.48551 \neq -3$
	19	$-.91635 \neq -3$	$+.52446 \neq -2$	$+.18423 \neq -3$	$+.35455 \neq -2$
	20	$-.23922 \neq -2$	$-.20591 \neq -2$	$-.81634 \neq -4$	$-.34936 \neq -3$

$P/D = 1.0$		$P/D = 1.2$		$P/D = 1.4$	
A (K)	B (K)	A (K)	B (K)	A (K)	B (K)
−.10985 ≠ 0	+.00000 ≠ +0	−.90888 ≠ −1	+.00000 ≠ +0	−.73487 ≠ −1	+.00000 ≠ +0
+.14064 ≠ 0	−.10583 ≠ +1	+.17959 ≠ 0	−.10260 ≠ +1	+.22861 ≠ 0	− ≠98101 ≠ 0
+.15785 ≠ 0	+.47284 ≠ −1	+.14956 ≠ 0	+.61459 ≠ −1	+.14853 ≠ 0	+.71510 ≠ −1
+.45544 ≠ −1	+.13126 ≠ 0	+.65675 ≠ −1	+.13715 ≠ 0	+.75328 ≠ −1	+.14217 ≠ 0
+.51639 ≠ −2	−.77539 ≠ −2	+.52107 ≠ −2	−.17280 ≠ −1	+.34084 ≠ −2	−.22675 ≠ −1
−.25560 ≠ −2	+.93507 ≠ −1	−.68232 ≠ −2	+.96579 ≠ −1	−.11643 ≠ −2	+.91082 ≠ −1
−.60502 ≠ −2	+.92520 ≠ −2	−.62896 ≠ −2	+.58809 ≠ −2	+.18576 ≠ −3	−.40283 ≠ −2
+.67368 ≠ −2	−.14828 ≠ −1	+.18178 ≠ −1	−.22587 ≠ −1	+.26970 ≠ −1	−.22759 ≠ −1
+.68571 ≠ −2	−.96554 ≠ −2	+.60694 ≠ −2	−.14819 ≠ −1	+.20616 ≠ −2	−.16727 ≠ −1
+.47245 ≠ −2	+.96216 ≠ −2	+.61942 ≠ −2	+.10398 ≠ +1	+.78666 ≠ −2	+.86970 ≠ −2
+.23591 ≠ −2	−.75453 ≠ −3	+.26482 ≠ −2	−.29324 ≠ −2	+.46912 ≠ −2	−.47515 ≠ −2
+.87912 ≠ −2	+.24453 ≠ −2	+.12137 ≠ −1	+.40913 ≠ −2	+.14771 ≠ −1	+.22828 ≠ −2
+.11968 ≠ −2	−.87981 ≠ −2	−.35705 ≠ −2	−.44436 ≠ −2	−.75056 ≠ −2	−.49383 ≠ −2
+.83808 ≠ −2	+.18184 ≠ −2	+.32985 ≠ −2	−.12190 ≠ −2	+.14983 ≠ −2	−.25924 ≠ −2
−.82098 ≠ −3	−.20077 ≠ −2	−.88652 ≠ −3	−.22551 ≠ −2	+.24058 ≠ −2	−.25143 ≠ −2
+.27371 ≠ −2	−.33070 ≠ −2	+.69807 ≠ −2	−.32272 ≠ −2	+.55647 ≠ −2	−.33659 ≠ −2
−.26121 ≠ −3	−.79201 ≠ −3	−.17560 ≠ −3	+.17533 ≠ −2	−.38178 ≠ −2	+.28153 ≠ −2
+.19133 ≠ −2	−.36311 ≠ −3	+.21643 ≠ −2	+.14875 ≠ −2	+.26704 ≠ −2	−.22162 ≠ −3
+.32290 ≠ −3	−.19377 ≠ +2	+.35362 ≠ −3	+.45353 ≠ −4	+.15745 ≠ −2	−.53749 ≠ −3
+.15223 ≠ −2	−.12135 ≠ −2	+.25772 ≠ −2	−.88702 ≠ −3	+.24500 ≠ −3	−.35190 ≠ −2
−.10151 ≠ −2	−.31678 ≠ −3	−.18279 ≠ −2	−.94609 ≠ −3	−.42370 ≠ −4	−.42846 ≠ −3
−.11257 ≠ 0	+.00000 ≠ +0	−.10166 ≠ 0	+.00000 ≠ +0	−.86955 ≠ −1	+.00000 ≠ +0
+.93340 ≠ −2	−.26265 ≠ 0	+.18593 ≠ −1	−.27769 ≠ 0	+.30046 ≠ −1	−.29799 ≠ ≠0
+.13788 ≠ 0	+.27587 ≠ −1	+.13408 ≠ 0	+.35459 ≠ −1	+.12651 ≠ 0	+.43403 ≠ −1
+.33223 ≠ −1	+.65262 ≠ −1	+.43767 ≠ −1	+.72317 ≠ −1	+.55034 ≠ −1	+.83309 ≠ −1
+.12672 ≠ −1	−.40234 ≠ −2	+.13604 ≠ −1	−.83408 ≠ −2	+.19376 ≠ −1	−.14571 ≠ −1
+.14250 ≠ −1	+.10255 ≠ −2	+.18658 ≠ −1	+.44854 ≠ −2	+.22082 ≠ −1	+.43398 ≠ −2
−.30407 ≠ −3	−.32045 ≠ −2	+.26598 ≠ −2	−.37642 ≠ −2	+.76282 ≠ −2	−.39256 ≠ −2
+.19888 ≠ −1	+.21752 ≠ −2	+.24907 ≠ −1	+.75727 ≠ −3	+.31821 ≠ −1	−.23504 ≠ −2
+.48334 ≠ −2	−.59535 ≠ −2	+.47924 ≠ −2	−.88802 ≠ −2	+.51835 ≠ −2	−.13633 ≠ −1
+.28427 ≠ −2	+.90664 ≠ −3	+.36556 ≠ −2	+.40541 ≠ −3	+.38898 ≠ −2	−.14000 ≠ −2
+.32326 ≠ −2	−.10222 ≠ −2	+.39850 ≠ −2	−.12811 ≠ −2	+.49300 ≠ −2	−28212 ≠ −2
+.97693 ≠ −2	−.48133 ≠ −2	+.10643 ≠ −1	−.55230 ≠ −2	+.10731 ≠ −1	−.77360 ≠ −2
−.28378 ≠ −3	−.56355 ≠ −2	+.25495 ≠ −3	−.63566 ≠ −2	+.11388 ≠ −2	−.68665 ≠ −2
+.29395 ≠ −2	−.18248 ≠ −2	+.29347 ≠ −2	−.25338 ≠ −2	+.31378 ≠ −2	−.42392 ≠ −2
+.53177 ≠ −3	−.20263 ≠ −2	+.36599 ≠ −3	−.20504 −2	−.82607 ≠ −3	−.33252 ≠ −2
+.16229 ≠ −2	−.30382 ≠ −2	+.13115 ≠ −2	−.38485 ≠ −2	−.17537 ≠ −4	−.45496 ≠ −2
−.27265 ≠ −3	−.11128 ≠ −2	−.13511 ≠ −2	−.63908 ≠ −3	−.36227 ≠ −2	−.12282 ≠ −2
+.20276 ≠ −2	−.15327 ≠ −2	+.17101 ≠ −2	−.10819 ≠ −2	−.22400 ≠ −3	−.15759 ≠ −2
+.35477 ≠ −3	−.12433 ≠ −2	+.33765 ≠ −3	−.96321 ≠ −3	−.58416 ≠ −3	−.77655 ≠ −6
+.39082 ≠ −3	−.20069 ≠ −2	−.39681 ≠ −3	−.20969 ≠ −2	−.12806 ≠ −2	−.17787 ≠ −2
−.92513 ≠ −3	−.48842 ≠ −3	−.11814 ≠ −2	−.19298 ≠ −3	−.19870 ≠ −2	+.49570 ≠ −3
+.31589 ≠ −1	+.00000 ≠ +0	+.43800 ≠ −1	+.00000 ≠ +0	+.73202 ≠ −1	+.00000 ≠ +0
+.24406 ≠ 0	−.11717 ≠ +1	+.35299 ≠ 0	−.12949 ≠ +1	+.47301 ≠ 0	−.14062 ≠ +1
−.73880 ≠ −2	+.51155 ≠ −1	−.10917 ≠ −1	+.59030 ≠ −1	−.33300 ≠ −1	+.71683 ≠ −1
+.28260 ≠ −1	+.89069 −1	+.47062 ≠ −1	+.93540 ≠ −1	+.62786 ≠ −1	+.11449 ≠ 0
−.55959 ≠ −2	−.65670 ≠ −2	−.10779 ≠ −1	−.61148 ≠ −2	−.19511 ≠ −1	−.13400 ≠ −1
+.26558 ≠ −3	+.14204 ≠ 0	−.10193 ≠ −1	+.16121 ≠ 0	−.27569 ≠ −1	+.17547 ≠ 0
+.11368 ≠ −1	+.77052 ≠ −2	−.88824 ≠ −3	+.14624 ≠ −1	−.38296 ≠ −2	+.25715 ≠ −1
−.47401 ≠ −1	−.36091 ≠ −1	−.37893 ≠ −1	−.53549 ≠ −1	−.23310 ≠ −1	−.54967 ≠ −1
−.65686 ≠ −2	+.42036 ≠ −2	−.70346 ≠ −2	−.31589 ≠ −2	−.84525 ≠ −2	−.12576 ≠ −1
−.74990 ≠ −2	+.21139 ≠ −2	−.80130 ≠ −2	+.14382 ≠ −1	−.48956 ≠ −2	+.13084 ≠ −1
+.12873 ≠ +2	+.13095 ≠ −1	+.72622 ≠ −2	+.99836 ≠ −2	+.48544 ≠ −2	+.10733 ≠ −1
+.46502 ≠ −2	+.30961 ≠ −1	−.54390 ≠ −2	+.38781 ≠ −1	−.71945 ≠ −2	+.44142 ≠ −1
−.46676 ≠ −2	−.99459 ≠ −2	−.20038 ≠ −2	−.46749 ≠ −2	−.53186 ≠ −2	−.10945 ≠ −2
+.33438 −2	+.17921 ≠ −1	+.39281 ≠ −2	+.14944 ≠ −1	+.13281 ≠ −2	+.12209 ≠ −1
+.22046 ≠ −2	−.81917 ≠ −2	−.65256 ≠ −3	−.63253 ≠ −2	+.68695 ≠ −2	−.14074 ≠ −2
+.70034 ≠ −2	−.78428 ≠ −3	+.15414 ≠ −1	+.22275 ≠ −2	+.18071 ≠ −1	+.17837 ≠ −2
+.39147 ≠ −1	+.72661 ≠ −2	+.30356 ≠ −2	+.71826 ≠ −2	−.15725 ≠ −2	+.37948 ≠ −2
+.73719 ≠ −2	−.47316 ≠ −2	+.59073 ≠ −2	+.10229 ≠ −2	+.11527 ≠ −1	+.49971 ≠ −2
−.94083 ≠ −3	−.25731 ≠ −2	+.41433 ≠ −2	−.59201 ≠ −2	+.10168 ≠ −1	−.42398 ≠ −2
+.60560 ≠ −2	+.11136 ≠ −2	+.46102 ≠ −2	−.14814 ≠ −2	+.81504 ≠ −3	−.77298 ≠ −2
−.42390 ≠ −3	−.15470 ≠ −2	−.57423 ≠ −3	−.43092 ≠ −2	+.14051 ≠ −2	−.34485 ≠ −2

TABLE 6. Coefficients of Fourier series by which results are approximated of four-quadrant measurements with Ka 4-70 series screws in nozzle no. 37

		$P/D = 0.6$		$P/D = 0.8$	
	K	A (K)	B (K)	A (K)	B (K)
C_T^*	0	$-.78522 \neq -1$	$+.00000 \neq +0$	$-.81169 \neq -1$	$+.00000 \neq +0$
	1	$+.91962 \neq -1$	$-.12241 \neq +1$	$+.12849 \neq 0$	$-.11842 \neq +1$
	2	$+.96733 \neq -1$	$-.10805 \neq -1$	$+.11331 \neq 0$	$+.58341 \neq -3$
	3	$-.14657 \neq -2$	$+.16207 \neq 0$	$+.15131 \neq -1$	$+.16441 \neq 0$
	4	$+.10810 \neq -1$	$+.10642 \neq -2$	$+.41567 \neq -2$	$+.62103 \neq -2$
	5	$-.20708 \neq -1$	$+.78648 \neq -1$	$-.16220 \neq -1$	$+.76506 \neq -1$
	6	$-.80316 \neq -2$	$+.14098 \neq -1$	$-.11305 \neq -1$	$+.96359 \neq -2$
	7	$+.11052 \neq -1$	$-.11329 \neq -1$	$+.93452 \neq -2$	$-.18036 \neq -1$
	8	$+.21070 \neq -2$	$-.52596 \neq -2$	$+.17779 \neq -2$	$-.12146 \neq -1$
	9	$-.16466 \neq -1$	$+.11815 \neq -1$	$-.62214 \neq -2$	$+.92879 \neq -2$
	10	$+.85238 \neq -3$	$-.23771 \neq -2$	$+.46290 \neq -2$	$+.40488 \neq -2$
	11	$+.39384 \neq -2$	$+.64113 \neq -2$	$+.69293 \neq -2$	$+.73891 \neq -2$
	12	$-.32905 \neq -2$	$+.50027 \neq -2$	$-.20445 \neq -2$	$-.40761 \neq -2$
	13	$+.25672 \neq -2$	$+.60467 \neq -2$	$+.59366 \neq -2$	$+.59307 \neq -2$
	14	$+.24770 \neq -2$	$-.28242 \neq -2$	$-.44055 \neq -3$	$-.22663 \neq -2$
	15	$+.62208 \neq -2$	$+.20489 \neq -2$	$+.72301 \neq -2$	$-.15148 \neq -2$
	16	$+.34143 \neq -3$	$+.31069 \neq -3$	$-.53198 \neq -3$	$-.13262 \neq -3$
	17	$+.19780 \neq +2$	$+.63925 \neq -3$	$+.26809 \neq -2$	$+.40086 \neq -2$
	18	$+.60762 \neq -3$	$-.22082 \neq -2$	$-.85582 \neq -3$	$-.11431 \neq -2$
	19	$+.34488 \neq -2$	$+.30421 \neq -2$	$+.32728 \neq -2$	$-.25883 \neq -2$
	20	$-.17166 \neq -2$	$-.52892 \neq -3$	$-.11347 \neq -2$	$-.93290 \neq -4$
$C_{T_N}^*$	0	$-.75854 \neq -1$	$+.00000 \neq +0$	$-.85104 \neq -1$	$+.00000 \neq +0$
	1	$+.91152 \neq -2$	$-.34397 \neq -0$	$+.15122 \neq -1$	$-.33237 \neq -0$
	2	$+.85316 \neq -1$	$-.60863 \neq -2$	$+.10325 \neq 0$	$+.24803 \neq -2$
	3	$+.47203 \neq -2$	$+.82506 \neq -1$	$+.15649 \neq -1$	$+.89761 \neq -1$
	4	$+.31838 \neq -2$	$+.51816 \neq -2$	$+.75680 \neq -3$	$+.45883 \neq -2$
	5	$+.45464 \neq +2$	$+.99282 \neq -2$	$+.92408 \neq -2$	$+.26548 \neq -2$
	6	$+.31828 \neq -2$	$+.59292 \neq -3$	$-.25160 \neq -8$	$-.42819 \neq -2$
	7	$+.95481 \neq -2$	$-.19148 \neq -2$	$+.18041 \neq -1$	$-.24385 \neq -2$
	8	$-.19432 \neq -2$	$-.17686 \neq -2$	$-.14737 \neq -2$	$-.45051 \neq -2$
	9	$+.58607 \neq -2$	$-.78198 \neq -3$	$+.48237 \neq -2$	$-.15233 \neq -2$
	10	$-.15047 \neq -2$	$-.30445 \neq -2$	$-.99338 \neq -3$	$-.15358 \neq -2$
	11	$+.38003 \neq -2$	$-.27783 \neq -2$	$+.48625 \neq -2$	$-.32041 \neq -2$
	12	$-.63250 \neq -3$	$+.17514 \neq -3$	$-.11657 \neq -2$	$+.17286 \neq -4$
	13	$+.10102 \neq -2$	$-.60004 \neq -3$	$+.43615 \neq -2$	$-.80871 \neq -3$
	14	$-.28923 \neq -3$	$-.32771 \neq -3$	$-.38004 \neq -3$	$-.21661 \neq -2$
	15	$+.26588 \neq -2$	$+.16418 \neq -3$	$+.32422 \neq -2$	$-.21791 \neq -3$
	16	$-.11302 \neq -3$	$-.14323 \neq -2$	$-.37155 \neq -3$	$-.72641 \neq -3$
	17	$+.19966 \neq -2$	$-.11456 \neq -2$	$+.22704 \neq -2$	$-.13466 \neq -2$
	18	$-.56644 \neq -3$	$-.74530 \neq -3$	$-.11253 \neq -2$	$-.23762 \neq -3$
	19	$+.95964 \neq -3$	$-.83559 \neq -3$	$+.19759 \neq -2$	$-.10735 \neq -2$
	20	$-.58527 \neq -3$	$-.54179 \neq -4$	$-.96980 \neq -3$	$-.57005 \neq -5$
C_Q^*	0	$+.14884 \neq -1$	$+.00000 \neq +0$	$+.20089 \neq -1$	$+.00000 \neq +0$
	1	$+.10044 \neq 0$	$-.79096 \neq 0$	$+.16636 \neq 0$	$-.99219 \neq 0$
	2	$-.25182 \neq -1$	$+.12206 \neq -1$	$-.18388 \neq -1$	$+.12892 \neq -1$
	3	$-.10918 \neq -1$	$+.90718 \neq -1$	$-.19051 \neq -1$	$+.95272 \neq -1$
	4	$+.27502 \neq -1$	$+.72669 \neq -2$	$+.16808 \neq -1$	$+.16045 \neq +1$
	5	$-.26072 \neq -2$	$+.57653 \neq -1$	$+.52434 \neq -2$	$+.94354 \neq -1$
	6	$-.11409 \neq -1$	$+.11032 \neq -3$	$-.11019 \neq -1$	$-.36169 \neq -2$
	7	$+.93808 \neq +3$	$-.99388 \neq -2$	$-.26942 \neq -1$	$-.22539 \neq -1$
	8	$+.82783 \neq -2$	$-.22892 \neq -2$	$+.94780 \neq -2$	$-.30457 \neq -4$
	9	$-.17756 \neq -1$	$+.53796 \neq -2$	$-.19689 \neq -2$	$+.21436 \neq -2$
	10	$-.42598 \neq -2$	$+.36876 \neq -2$	$+.16447 \neq -2$	$+.37463 \neq -2$
	11	$-.46664 \neq -2$	$+.96603 \neq -2$	$-.14766 \neq -1$	$+.21398 \neq -1$
	12	$+.10278 \neq -2$	$+.41719 \neq -3$	$-.22670 \neq -2$	$+.19168 \neq -2$
	13	$+.20667 \neq -2$	$+.72900 \neq -2$	$+.93023 \neq -2$	$+.76358 \neq -2$
	14	$+.18501 \neq -2$	$+.96970 \neq -3$	$+.41823 \neq -2$	$-.33249 \neq -2$
	15	$+.26112 \neq -2$	$+.87227 \neq -3$	$+.77675 \neq -2$	$+.24934 \neq -2$
	16	$-.32505 \neq -2$	$+.21002 \neq -3$	$-.13283 \neq -2$	$+.39206 \neq -3$
	17	$-.77389 \neq -3$	$+.28832 \neq -2$	$-.92032 \neq -3$	$-.83670 \neq -3$
	18	$+.13220 \neq -2$	$+.70445 \neq -3$	$+.25952 \neq -3$	$-.31653 \neq -2$
	19	$+.16856 \neq -2$	$+.39547 \neq -2$	$+.23462 \neq -2$	$+.41032 \neq -2$
	20	$-.48127 \neq -3$	$+.17791 \neq -2$	$+.69823 \neq -3$	$+.20375 \neq -2$

$P/D = 1.0$		$P/D = 1.2$		$P/D = 1.4$	
A (K)	B (K)	A (K)	B(K)	A (K)	B (K)
$-.78681 \neq -1$	$+.00000 \neq +0$	$-.60256 \neq -1$	$+.00000 \neq +0$	$-.47437 \neq -1$	$+.00000 \neq +0$
$+.17005 \neq 0$	$-.11152 \neq +1$	$+.22360 \neq 0$	$-.10687 \neq +1$	$+.26393 \neq 0$	$-.10004 \neq +1$
$+.12604 \neq 0$	$+.20371 \neq -1$	$+.12353 \neq 0$	$+.29643 \neq -1$	$+.11478 \neq 0$	$+.46145 \neq -1$
$+.24444 \neq -1$	$+.15275 \neq 0$	$+.24086 \neq -1$	$+.14275 \neq 0$	$+.47309 \neq -1$	$+.14074 \neq 0$
$-.69987 \neq -2$	$+.28881 \neq -2$	$-.14518 \neq -1$	$-.14016 \neq -1$	$-.11061 \neq -1$	$-.21940 \neq -1$
$-.52998 \neq -2$	$+.78299 \neq -1$	$-.62461 \neq -2$	$+.73413 \neq -1$	$+.11308 \neq -1$	$+.67294 \neq -1$
$-.77500 \neq -2$	$+.18865 \neq -2$	$-.43441 \neq -2$	$+.70950 \neq -3$	$-.83647 \neq -3$	$-.44987 \neq -2$
$+.67088 \neq -2$	$-.24665 \neq -1$	$+.17726 \neq -1$	$-.26735 \neq -1$	$+.24933 \neq -1$	$-.25518 \neq -1$
$+.78818 \neq -2$	$-.82956 \neq -2$	$+.10820 \neq -1$	$-.10309 \neq -1$	$+.19552 \neq -2$	$-.12518 \neq -1$
$+.83058 \neq -2$	$+.15085 \neq -1$	$+.89902 \neq -2$	$+.15399 \neq -1$	$+.60531 \neq -2$	$+.14151 \neq -1$
$+.20833 \neq -2$	$+.15879 \neq -2$	$-.24474 \neq -2$	$-.72466 \neq -2$	$-.28748 \neq -2$	$-.12588 \neq -2$
$+.72262 \neq -2$	$+.95129 \neq -2$	$+.51620 \neq -2$	$+.93292 \neq -2$	$+.64118 \neq -2$	$+.55618 \neq -2$
$-.58329 \neq -3$	$-.73249 \neq -2$	$-.48962 \neq -2$	$-.39241 \neq -2$	$-.48164 \neq -2$	$-.53289 \neq -2$
$+.88467 \neq -2$	$+.34931 \neq -2$	$+.80184 \neq -2$	$+.55616 \neq -2$	$+.64267 \neq -2$	$+.44079 \neq -2$
$-.29559 \neq -2$	$-.63570 \neq -2$	$-.25019 \neq -2$	$-.31513 \neq -3$	$-.40358 \neq -2$	$+.48467 \neq -3$
$+.11530 \neq -1$	$-.22474 \neq -2$	$+.14983 \neq -1$	$-.17566 \neq -2$	$+.16051 \neq -1$	$-.18905 \neq -2$
$-.83057 \neq -3$	$+.25069 \neq -2$	$-.28220 \neq -3$	$+.18409 \neq -2$	$-.32816 \neq -2$	$+.29965 \neq -2$
$+.31339 \neq -2$	$-.12990 \neq -2$	$+.23533 \neq -2$	$-.29180 \neq -2$	$+.30250 \neq -2$	$-.37761 \neq -2$
$-.13290 \neq -2$	$-.41905 \neq -3$	$-.64457 \neq -3$	$+.63270 \neq -3$	$-.13567 \neq -2$	$+.32763 \neq -2$
$+.30666 \neq -2$	$-.28288 \neq -2$	$+.12248 \neq -2$	$-.31003 \neq -2$	$+.31794 \neq -2$	$-.44109 \neq -2$
$-.13749 \neq -2$	$-.45929 \neq -3$	$-.17391 \neq -2$	$-.31826 \neq -3$	$+.44946 \neq -3$	$+.10459 \neq -2$
$-.80432 \neq -1$	$+.00000 \neq +0$	$-.72310 \neq -1$	$+.00000 \neq +0$	$-.63893 \neq -1$	$+.00000 \neq +0$
$+.29904 \neq -1$	$-.32774 \neq 0$	$+.47220 \neq -1$	$-.32899 \neq 0$	$+.60260 \neq -1$	$-.33060 \neq 0$
$+.10546 \neq 0$	$+.81952 \neq -2$	$+.10455 \neq 0$	$+.17983 \neq -1$	$+.10016 \neq 0$	$+.28880 \neq -1$
$+.21277 \neq -1$	$+.93073 \neq -1$	$+.23912 \neq -1$	$+.93061 \neq -1$	$+.33369 \neq -1$	$+.99036 \neq -1$
$-.14818 \neq -2$	$+.38289 \neq -2$	$-.32961 \neq -2$	$-.63572 \neq -2$	$-.17785 \neq -2$	$-.10075 \neq -1$
$+.15667 \neq -1$	$+.21950 \neq -3$	$+.24863 \neq -1$	$+.74431 \neq -3$	$+.38604 \neq -1$	$+.71186 \neq -3$
$+.17592 \neq -2$	$-.63045 \neq -2$	$+.17700 \neq -3$	$-.30252 \neq -2$	$+.43713 \neq -2$	$-.48584 \neq -2$
$+.25671 \neq -1$	$-.23125 \neq -2$	$+.30933 \neq -1$	$-.26122 \neq -2$	$+.35035 \neq -1$	$-.18671 \neq -2$
$-.90447 \neq -3$	$-.36290 \neq -2$	$+.15955 \neq -2$	$-.64419 \neq -2$	$+.50841 \neq -3$	$-.10093 \quad -1$
$+.88204 \neq -2$	$-.90853 \neq -3$	$+.12406 \neq -1$	$+.33704 \neq -3$	$+.12764 \neq -1$	$+.24435 \neq -4$
$-.18008 \neq -2$	$-.18997 \neq -2$	$-.13918 \neq -2$	$-.29805 \neq -2$	$-.24911 \neq -3$	$-.22708 \neq -2$
$+.81643 \neq -2$	$-.40480 \neq -2$	$+.10216 \neq -1$	$-.50133 \neq -2$	$+.13320 \neq -1$	$-.77347 \neq -2$
$-.97356 \neq -3$	$-.34197 \neq -3$	$+.16203 \neq -4$	$-.28858 \neq -2$	$-.18539 \neq -2$	$-.40802 \neq -2$
$+.69039 \neq -2$	$-.13522 \neq -2$	$+.72150 \neq -2$	$-.28057 \neq -2$	$+.77057 \neq -2$	$-.20523 \neq -2$
$-.56244 \neq -3$	$-.22322 \neq -2$	$-.39249 \neq -3$	$-.11737 \neq -2$	$+.22148 \neq -3$	$-.21040 \neq -2$
$+.45475 \neq -2$	$-.14808 \neq -2$	$+.48746 \neq -2$	$-.34043 \neq -2$	$+.51024 \neq -2$	$-.47028 \neq -2$
$-.38196 \neq -3$	$-.11481 \neq -2$	$-.21174 \neq -2$	$-.20546 \neq -2$	$-.26606 \neq -2$	$-.19265 \neq -2$
$+.31160 \neq -2$	$-.28678 \neq -2$	$+.31669 \neq -2$	$-.31834 \neq -2$	$+.24555 \neq -2$	$-.39615 \neq -2$
$-.11878 \neq -2$	$-.25410 \neq -3$	$-.13671 \neq -2$	$-.11222 \neq -2$	$-.26363 \neq -2$	$-.60252 \neq -3$
$+.19158 \neq -2$	$-.25631 \neq -2$	$+.16721 \neq -2$	$-.26716 \neq -2$	$+.10883 \neq -2$	$-.27663 \neq -2$
$-.13129 \neq -2$	$+.22029 \neq -4$	$-.19020 \neq -2$	$-.49627 \neq -3$	$-.28978 \neq -2$	$+.10214 \neq -3$
$+.30767 \neq -1$	$+.00000 \neq +0$	$+.44351 \neq -1$	$+.00000 \neq +0$	$+.64033 \neq -1$	$+.00000 \neq +0$
$+.24472 \neq 0$	$-.11315 \neq +1$	$+.34230 \neq 0$	$-.12562 \neq +1$	$+.45620 \neq 0$	$-.13383 \neq +1$
$-.11316 \neq -1$	$+.33712 \neq -1$	$-.18087 \neq -1$	$+.55298 \neq -1$	$-.26747 \neq -1$	$+.57075 \neq -1$
$-.81658 \neq -2$	$+.90343 \neq -1$	$+.35568 \neq -2$	$+.92837 \neq -1$	$+.16152 \neq -1$	$+.89051 \neq -1$
$+.16208 \neq -2$	$+.12113 \neq -1$	$-.63786 \neq -2$	$-.49373 \neq -2$	$-.15846 \neq -1$	$-.97724 \neq -2$
$+.86632 \neq -2$	$+.12138 \neq 0$	$-.13513 \neq -1$	$+.14129 \neq 0$	$-.19336 \neq -1$	$+.15575 \neq 0$
$-.34936 \neq -2$	$-.54322 \neq -2$	$+.94572 \neq -3$	$-.31662 \neq -2$	$+.55030 \neq -2$	$+.25599 \neq -2$
$-.46075 \neq -1$	$-.35712 \neq -1$	$-.35793 \neq -1$	$-.45159 \neq -1$	$-.28670 \neq -1$	$-.42572 \neq -1$
$+.66651 \neq -2$	$+.63862 \neq -2$	$+.10295 \neq -1$	$+.56348 \neq -2$	$+.28700 \neq -3$	$+.29638 \neq -2$
$+.61510 \neq -2$	$+.14021 \neq -1$	$+.22438 \neq -2$	$+.28053 \neq -1$	$-.49652 \neq -2$	$+.24850 \neq -1$
$+.51947 \neq -2$	$+.28095 \neq -2$	$-.26275 \neq -2$	$+.23267 \neq -2$	$+.23913 \neq -2$	$+.30607 \neq -2$
$-.13702 \neq -1$	$+.32828 \neq -1$	$-.17427 \neq -1$	$+.38309 \neq -1$	$-.20976 \neq -1$	$+.41837 \neq -1$
$+.12766 \neq -3$	$-.19195 \neq -2$	$-.21233 \neq -2$	$-.69986 \neq -2$	$+.14416 \neq -2$	$-.32116 \neq -2$
$+.61680 \neq -2$	$+.88817 \neq -2$	$+.98031 \neq -2$	$+.14268 \neq -1$	$+.39953 \neq -2$	$+.17848 \neq -1$
$+.12713 \neq -2$	$-.71309 \neq -2$	$+.38115 \neq -2$	$-.77495 \neq -3$	$-.13605 \neq -2$	$+.30114 \neq -2$
$+.14570 \neq -1$	$+.30977 \neq -2$	$+.22608 \neq -1$	$+.32200 \neq -2$	$+.28437 \neq -1$	$+.75977 \neq -2$
$+.44360 \neq -2$	$+.64517 \neq -3$	$-.37227 \neq -3$	$+.69956 \neq -2$	$+.19337 \neq -2$	$+.27087 \neq -2$
$+.18140 \neq -2$	$-.22876 \neq -2$	$+.14353 \neq -3$	$-.21184 \neq -3$	$+.75472 \neq -2$	$-.13255 \neq -2$
$-.43127 \neq -2$	$-.98748 \neq -4$	$+.16375 \neq -2$	$-.84958 \neq -3$	$+.29007 \neq -2$	$+.30258 \neq -3$
$+.38794 \neq -2$	$+.10718 \neq -2$	$+.51490 \neq -2$	$-.14700 \neq -2$	$+.32369 \neq -2$	$-.37368 \neq -2$
$+.14728 \neq -3$	$-.23283 \neq -2$	$+.26719 \neq -2$	$-.27758 \neq -2$	$+.32247 \neq -2$	$-.23794 \neq -2$

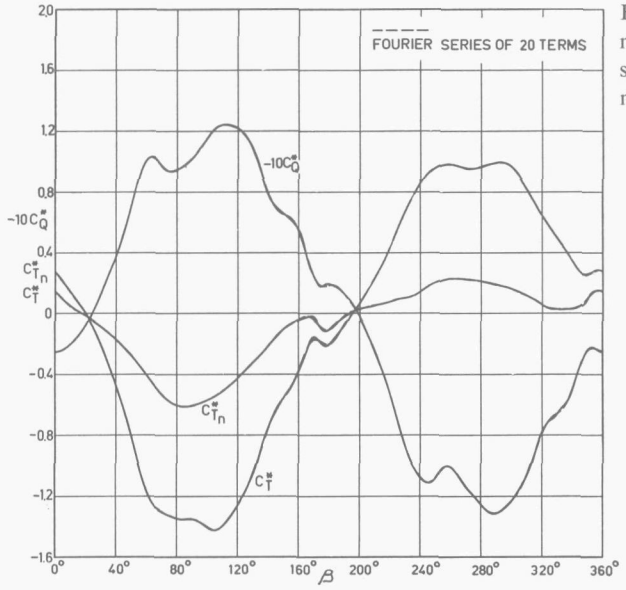

FIG. 39. Result of four-quadrant measurements of Ka 4–70 screw series with nozzle no. 37 approximated by Fourier series of 20 terms.

The results of the four-quadrant measurements with nozzle no. 37 in combination with the Ka 4-70 screw series are shown in the Figs. 35 through 37. The open-water test results over the normal test range (speed and rpm ahead) and the results with the reversely mounted nozzle and impeller with speed and rpm astern (3rd quadrant) are given in the form of $K_T - K_{TN} - K_Q - J$ diagrams in Figs. 35 and 36 respectively. The test results over the whole range of operating conditions are given in the form of a $C_T^* - C_{TN}^* - C_Q^* - \beta$ diagram in Fig. 37.

In ship control studies, it is necessary to have a mathematical representation of the data suitable for use on a computer. Therefore calculations were carried out to represent the results of the four-quadrant measurements by a Fourier series. The thrust and torque coefficients C_T^*, C_{TN}^* and C_Q^* were approximated by the following series:

$$C_T^* = \sum_{k=0} [A(k) \cos \beta k + B(k) \sin \beta k]$$

$$C_{TN}^* = \quad \text{ditto}$$

$$C_Q^* = \quad \text{ditto}$$

In Figs. 38 and 39, the test results and their approximations by a Fourier series of 20 terms are given for the Ka 4-70 screw series in nozzle no. 19A and nozzle no. 37 successively. From the results given in these diagrams it can be seen that the characteristics of ducted propellers in the four-quadrants can be adequately represented by a Fourier series of 20 terms. The values of the Fourier coefficients of the ducted propellers with nozzles no. 19A and no. 37 are given in the Tables 5 and 6.

6. THE FLOW DECELERATING NOZZLE

In section 3 a simple method for the calculation of the characteristics of ducted propellers was discussed. This method has been followed for the determination of the characteristics of systematic series of ducted propellers with decelerating nozzles.

The data used for the computations and the results are given in Tables I, II and III of the Appendix. Some results are presented in Figs. 40 through 45. Figs. 40 and 41 show the effect of the thrust ratio τ_0 on the shape of the nozzle and the characteristics of the ducted propeller systems. The effects of the nozzle length-diameter ratio L/D and the thickness ratio of the nozzle profile S/L are shown in Figs. 42 through 45. The pressure distribution along the interior and the exterior surface of the various nozzles are given in Figs. 46 and 47.

Based on the theory a number of nozzle shapes with the following variations of the design coefficients were manufactured and tested:

- variations in the thrust ratio τ_0 at the design thrust coefficient C_{T0} (nozzles nos. 30, 31 and 32).
- variations in the length-diameter ratio L/D (nozzles nos. 33, 35 and 36)
- variations in the thickness ratio of the nozzle profiles S/L (nozzles nos. 33 and 34).

The design coefficients for these nozzles are summarized in Table 7. The nozzle shapes are presented in Figs. 48, 49 and 50 and are tabulated in Table 8.

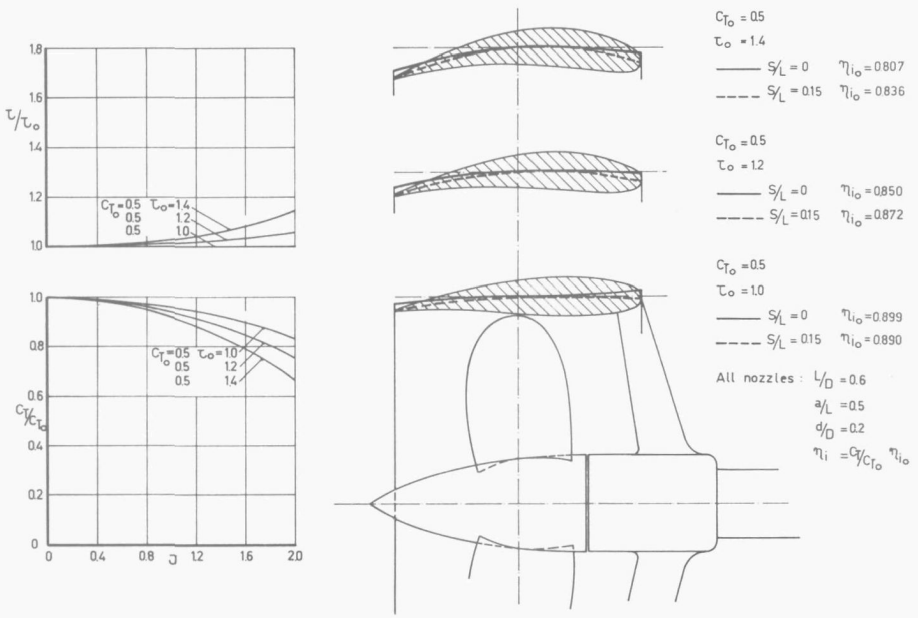

FIG. 40. Meanlines and characteristics of systematic series of nozzles with $C_{T_o} = 0.5$ and $\tau_o = 1.0$; 1.2 and 1.4.

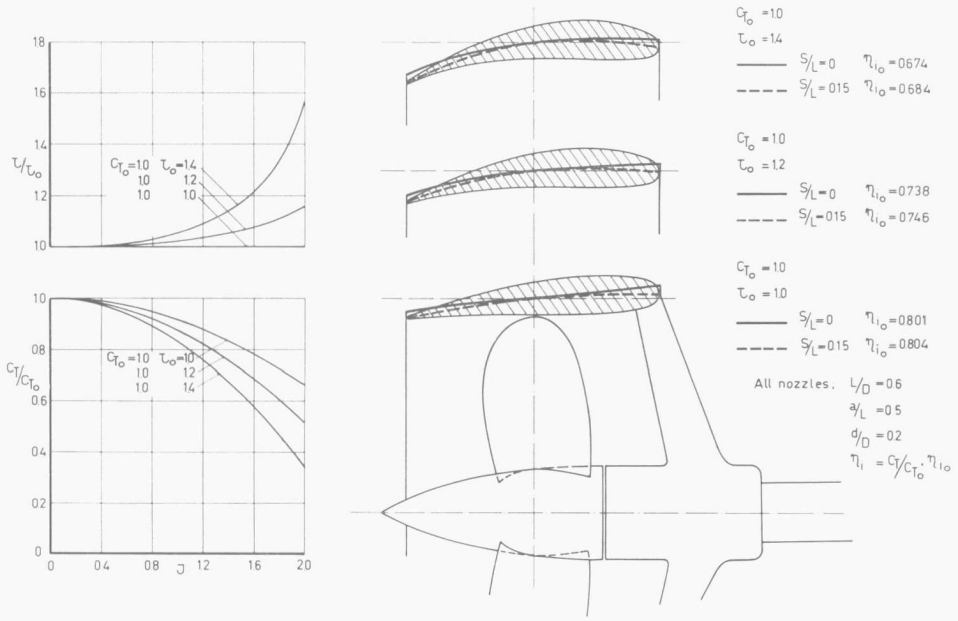

FIG. 41. Mean lines and characteristics of systematic series of nozzles with $C_{To} = 1.0$ and $\tau_o = 1.0$; 1.2 and 1.4.

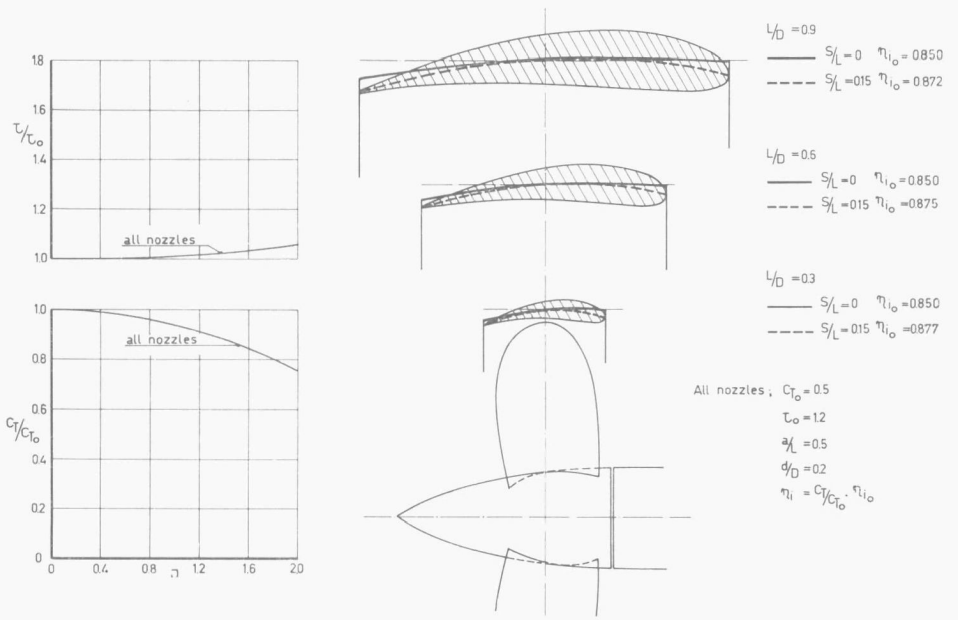

FIG. 42. Mean lines and characteristics of systematic series of nozzles with $C_{To} = 0.5$; $\tau_o = 1.2$ and different length diameter ratios.

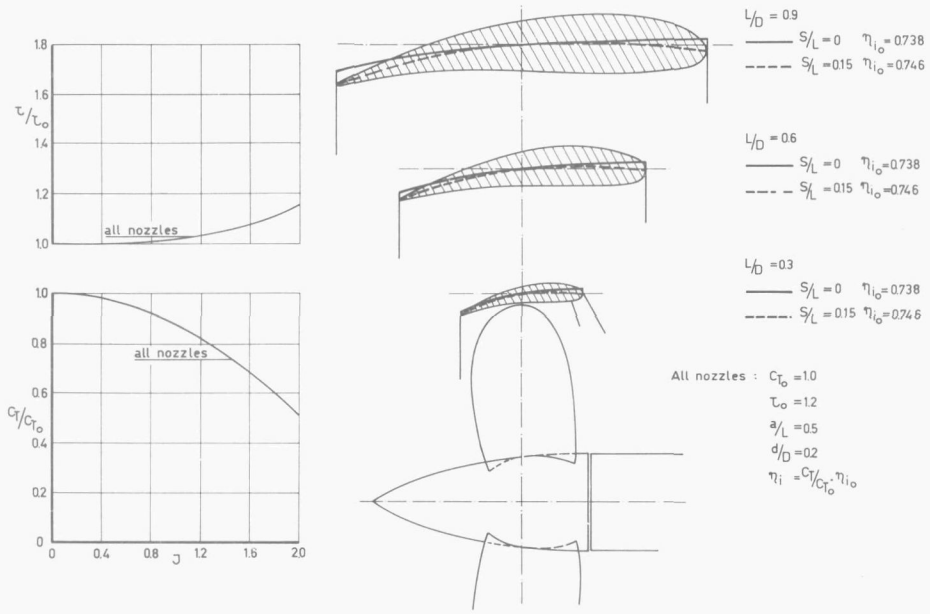

FIG. 43. Mean lines and characteristics of systematic series of nozzles with $C_{To} = 1.0$; $\tau_o = 1.2$ and different length diameter ratios.

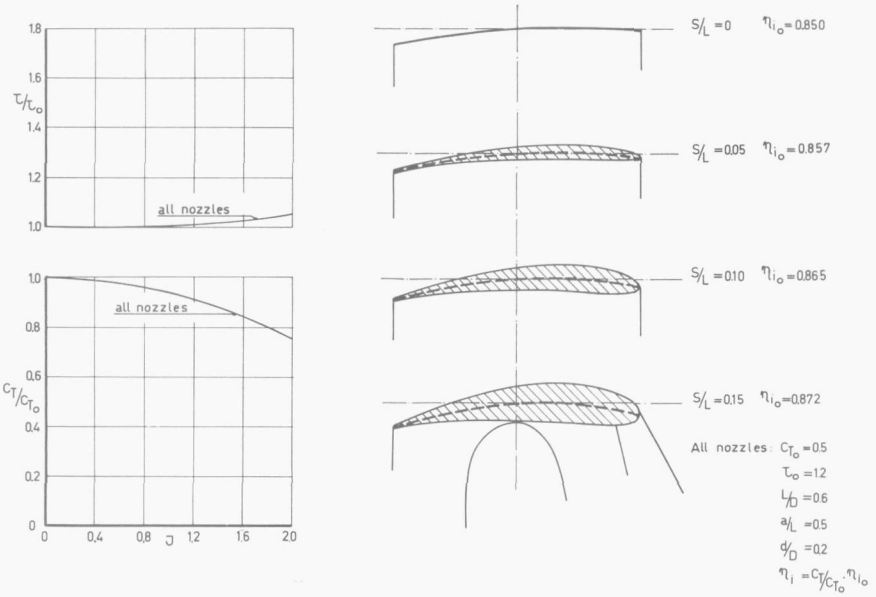

FIG. 44. Meanlines and characteristics of systematic series of nozzles with $C_{To} = 0.5$; $\tau_o = 1.2$ and with different thickness ratios of the nozzle profile.

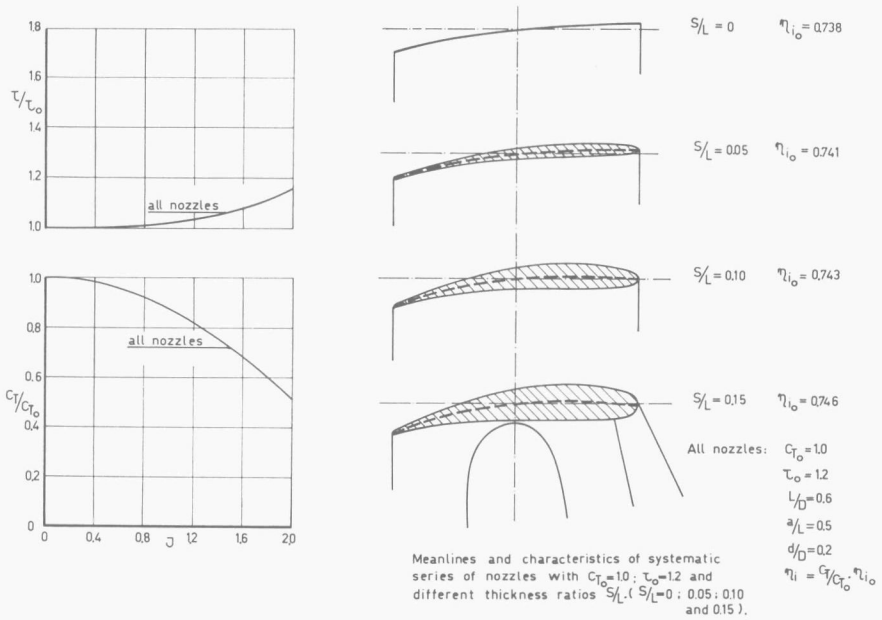

FIG. 45. Mean lines and characteristics of systematic series of nozzles with $C_{To} = 1.0$; $\tau_o = 1.2$ and with different thickness ratios of the nozzle profiles.

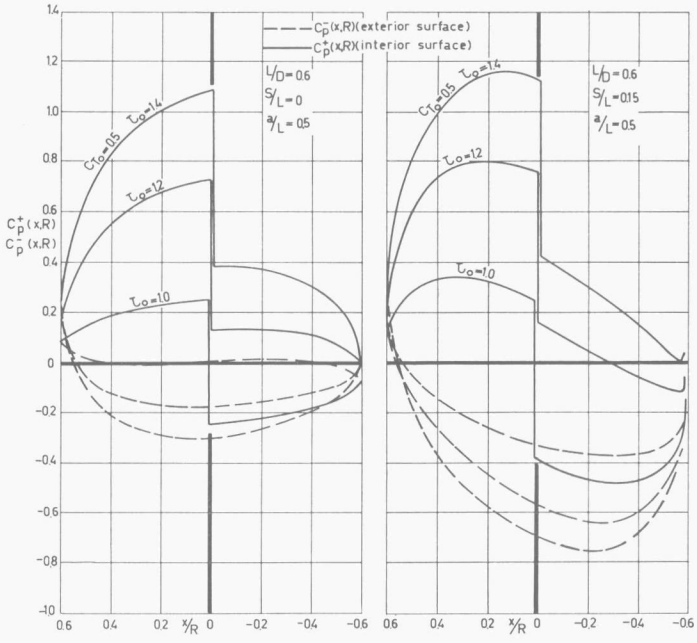

FIG. 46. Pressure distribution along interior and exterior surface of nozzles with $C_{To} = 0.5$ and $\tau_o = 1.0$; 1.2 and 1.4.

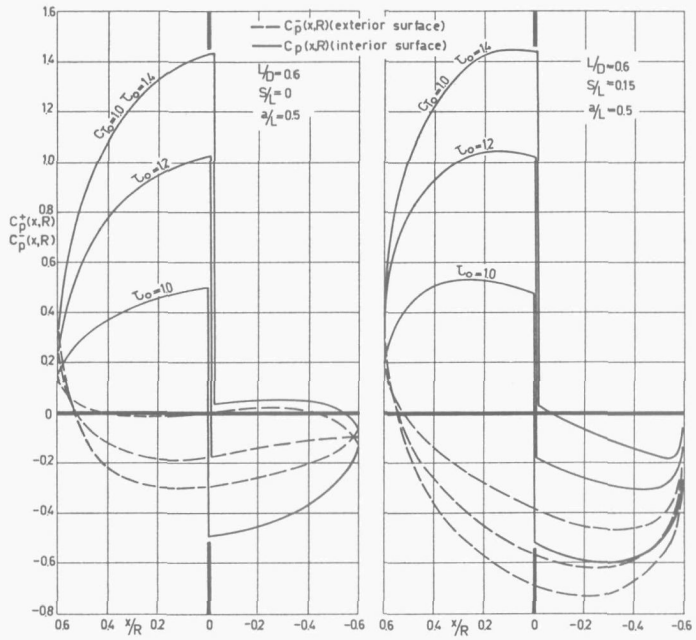

FIG. 47. Pressure distribution along interior and exterior surface of nozzles with $C_{To} = 1.0$ and $\tau_o = 1.0$; 1.2 and 1.4.

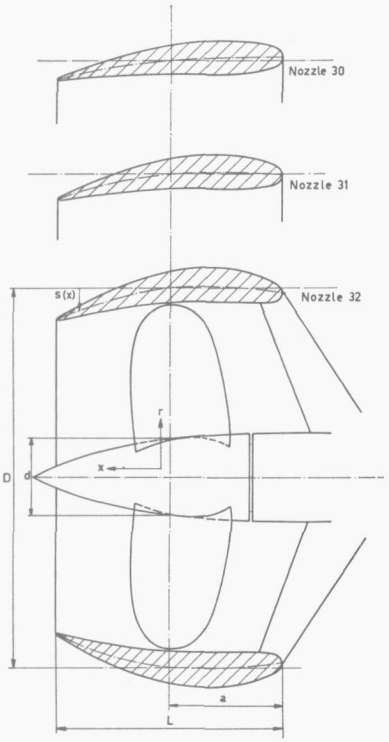

FIG. 48. Particulars of nozzles nos. 30, 31 and 32.

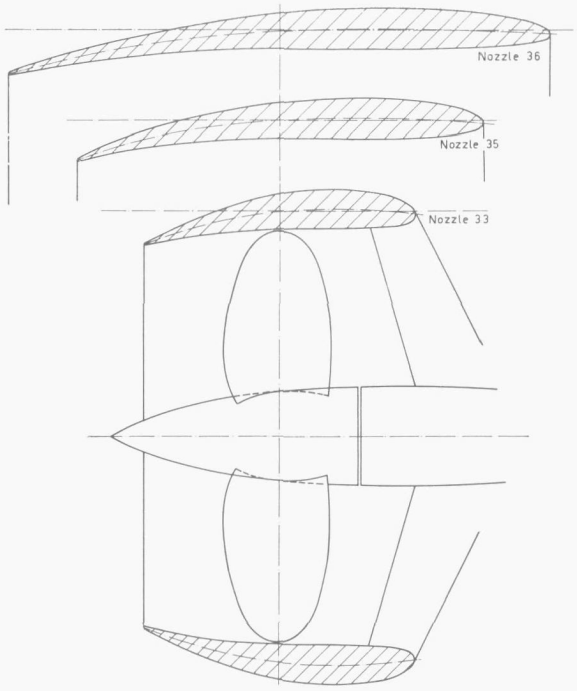

FIG. 49. Particulars of nozzles nos. 33, 35 and 36.

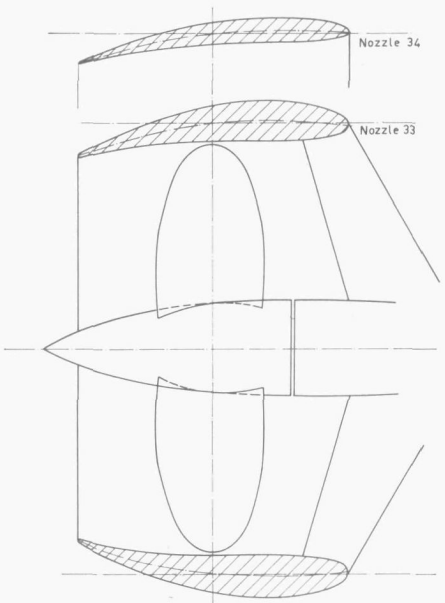

FIG. 50. Particulars of nozzles nos. 33 and 34.

TABLE 7. Design parameters of tested nozzle shapes.

Nozzle number	C_{T0}	τ_0	L/D	a/L	S/L	d/D
30	0.95	*1.00*	0.6	0.5	0.15	0.20
31	0.95	*1.15*	0.6	0.5	0.15	0.20
32	0.95	*1.30*	0.6	0.5	0.15	0.20
33	1.0	1.2	*0.6*	0.5	*0.15*	0.20
34	1.0	1.2	0.6	0.5	*0.09*	0.20
35	1.0	1.2	*0.9*	0.5	0.10	0.20
36	1.0	1.2	*1.2*	0.5	0.075	0.20

TABLE 8. Particulars of nozzles nos. 30 through 36.

x/L	$s(x)/L$						
	nozzle number 30	31	32	33	34	35	36
− 0.500	+ 0.0112	− 0.0073	− 0.0232	− 0.0083	+ 0.0005	− 0.0067	− 0.0071
− 0.416	+ 0.0130	+ 0.0008	− 0.0096	+ 0	+ 0.0007	− 0.0008	− 0.0034
− 0.333	+ 0.0139	+ 0.0067	+ 0.0006	+ 0.0058	+ 0.0008	+ 0.0033	− 0.0008
− 0.250	+ 0.0128	+ 0.0093	+ 0.0067	+ 0.0083	+ 0.0011	+ 0.0056	+ 0.0004
− 0.167	+ 0.0102	+ 0.0091	+ 0.0085	+ 0.0083	+ 0.0012	+ 0.0055	+ 0.0012
− 0.084	+ 0.0059	+ 0.0060	+ 0.0063	+ 0.0058	+ 0.0011	+ 0.0037	+ 0.0008
+ 0	0	+ 0	+ 0	+ 0	+ 0	0	0
+ 0.084	− 0.0081	− 0.0096	− 0.0112	− 0.0010	− 0.0009	− 0.0064	− 0.0054
+ 0.167	− 0.0186	− 0.0229	− 0.0276	− 0.0023	− 0.0021	− 0.0152	− 0.0158
+ 0.250	− 0.0316	− 0.0404	− 0.0496	− 0.0042	− 0.0038	− 0.0389	− 0.0279
+ 0.333	− 0.0476	− 0.0622	− 0.0773	− 0.0066	− 0.0058	− 0.0460	− 0.0417
+ 0.416	− 0.0661	− 0.0881	− 0.1106	− 0.0092	− 0.0083	− 0.0675	− 0.0592
+ 0.500	− 0.0874	− 0.1182	− 0.1498	− 0.0124	− 0.0112	− 0.0951	− 0.0816

The experiments were all carried out with a series of five bladed Kaplan type screws (Kd 5-100 series). The pitch distributions of the screws depend on the velocities induced by the nozzle at the impeller plane and on the radial load distribution of the screw. The design method is discussed at length in (11) and (13). Particulars of the screw models are given in Table 9 and in Fig. 51. The screws were located in the nozzles

TABLE 9. Particulars of screw models of the Kd 5-100 series

Diameter	D	240 mm
Number of blades	Z	5
Pitch ratio (at 0.7 D)	P/D	1.0−1.2−1.4−1.6−1.8
Blade area ratio	A_E/A_0	1.00
Blade outline		Kaplan type
Blade section		NASA 16-parabolic camberline
Propellers indicated by nos.		3930−3931−3932−3933−3934

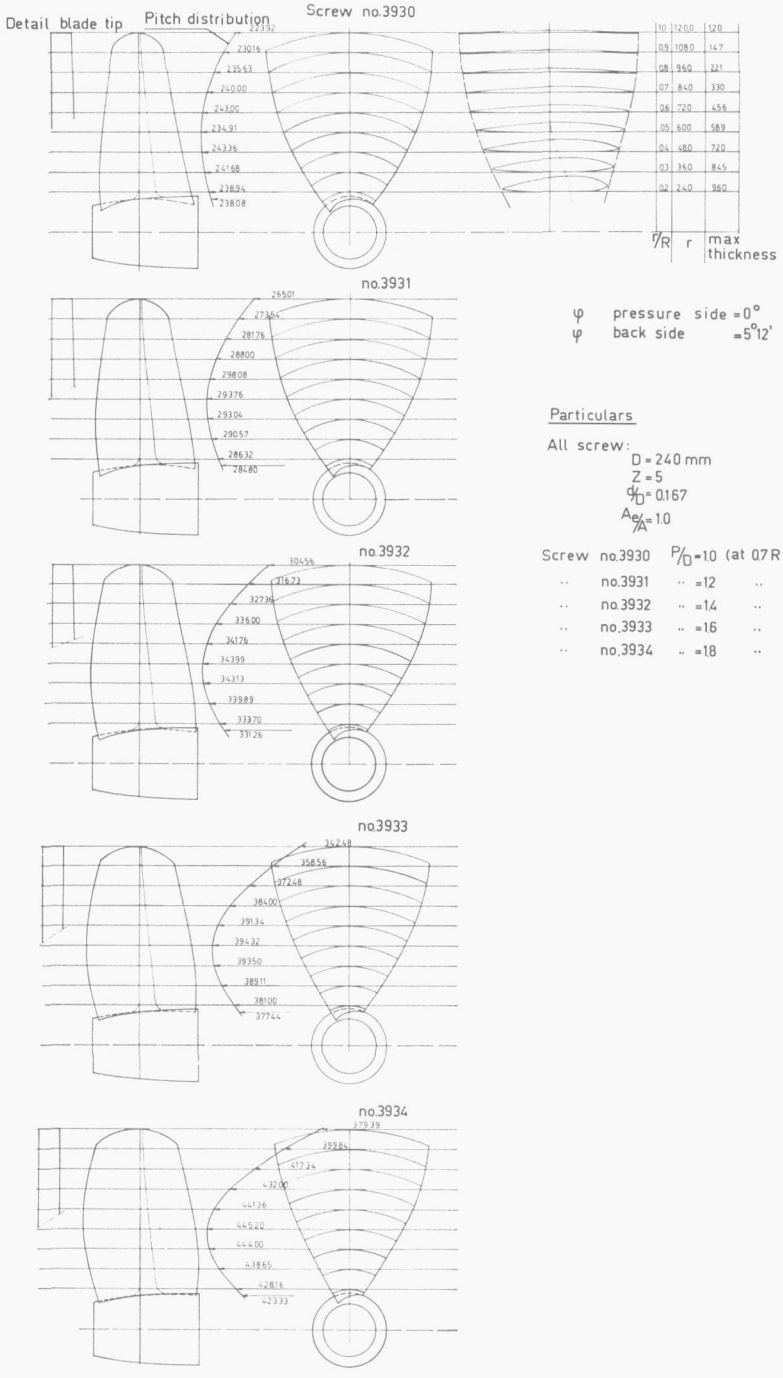

φ pressure side = 0°
φ back side = 5°12'

Particulars

All screw:
D = 240 mm
Z = 5
d/D = 0.167
A_e/A = 1.0

Screw no.3930 P/D = 1.0 (at 0.7 R)
.. no.3931 .. = 1.2 ..
.. no.3932 .. = 1.4 ..
.. no.3933 .. = 1.6 ..
.. no.3934 .. = 1.8 ..

FIG. 51. Particulars of screw models of the Kd 5–100 screw series.

with a uniform tip clearance of 1 mm. (about 0.4 percent of the screw diameter D). It must be noted that in the presentation of the test results the diameter now denotes the tip diameter of the screw.

The tests were carried out with the usual tank apparatus for open-water tests of ducted propellers as described in the preceding section.

All the open-water test results were faired by computer and plotted in the conventional way with the coefficients K_T, K_{TN}, K_Q and η_o as functions of the advance coefficient J. The diagrams are given as Figs. 52 through 58. The experimentally obtained relations between the thrust coefficient C_T and the thrust ratio τ of the various nozzles are given in the Figs. 59 and 60. In addition, the design thrust coefficient C_T and the design thrust ratio τ are given in these diagrams.

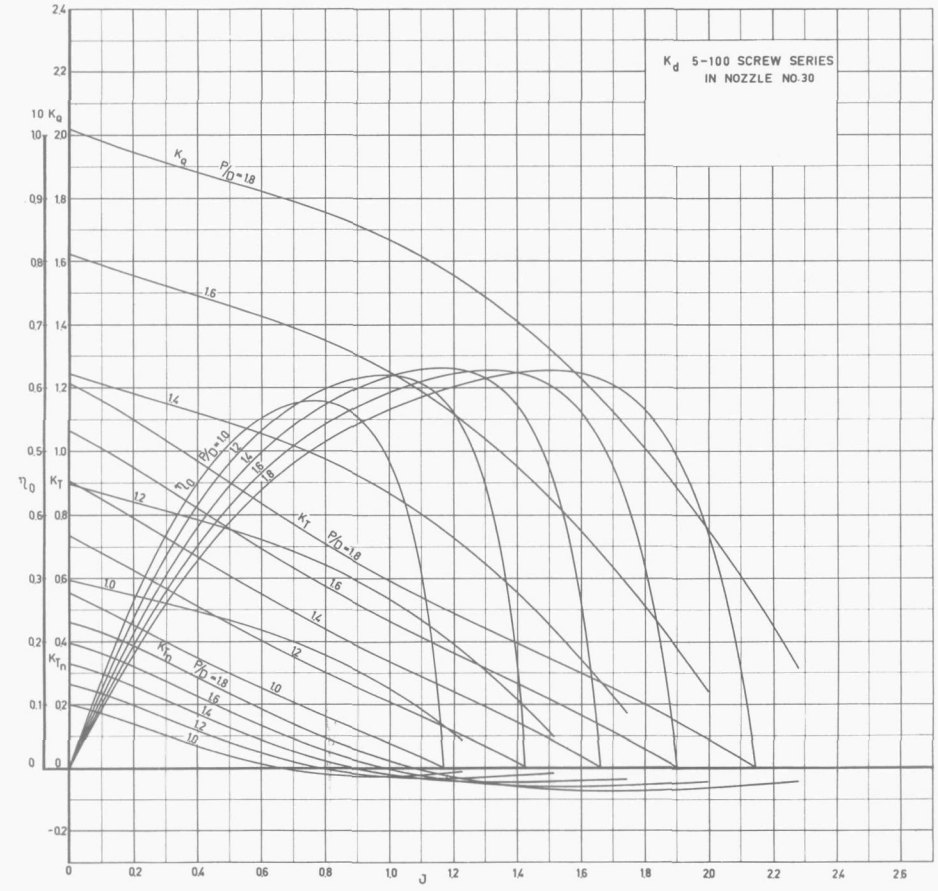

FIG. 52. Open-water test results of Kd 5–100 screw series with nozzle no. 30.

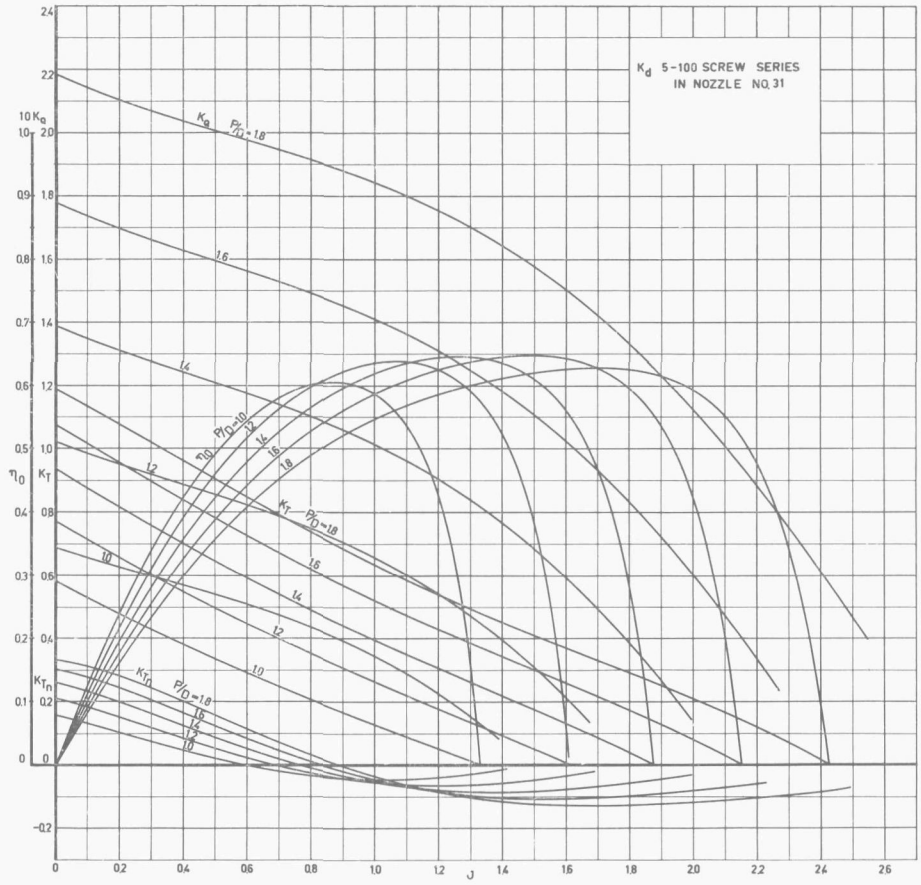

FIG. 53. Open-water test results of Kd 5–100 screw series with nozzle no. 31.

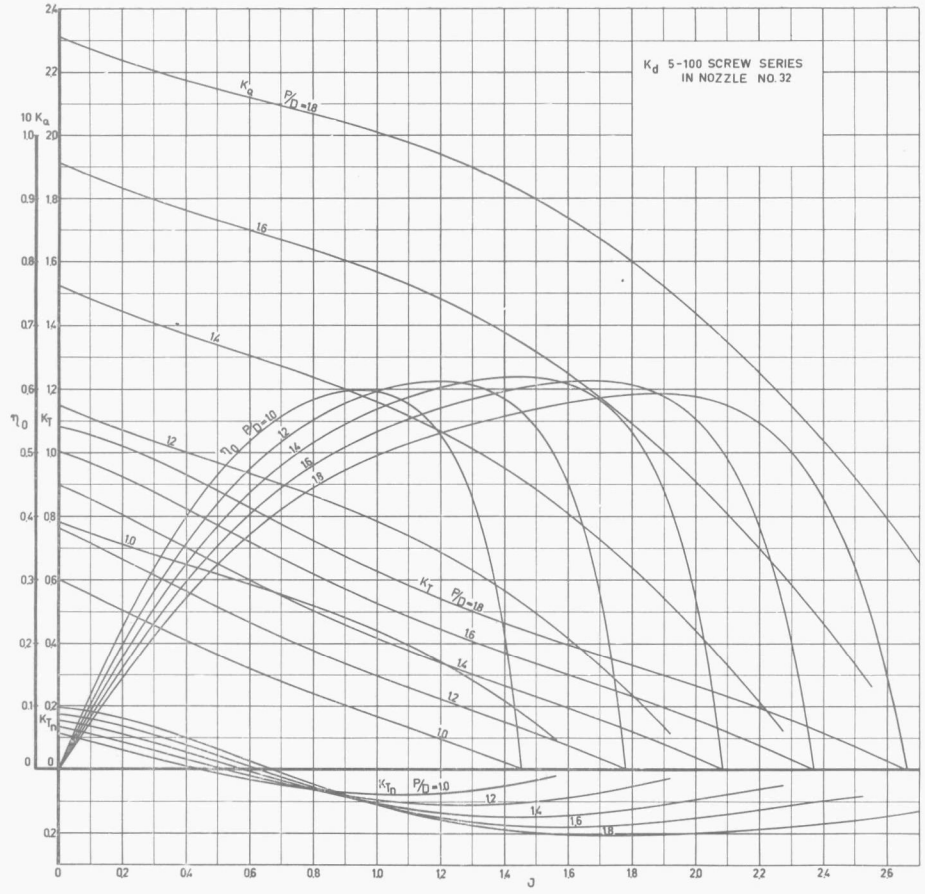

FIG. 54. Open-water test results of Kd 5–100 screw series with nozzle no. 32.

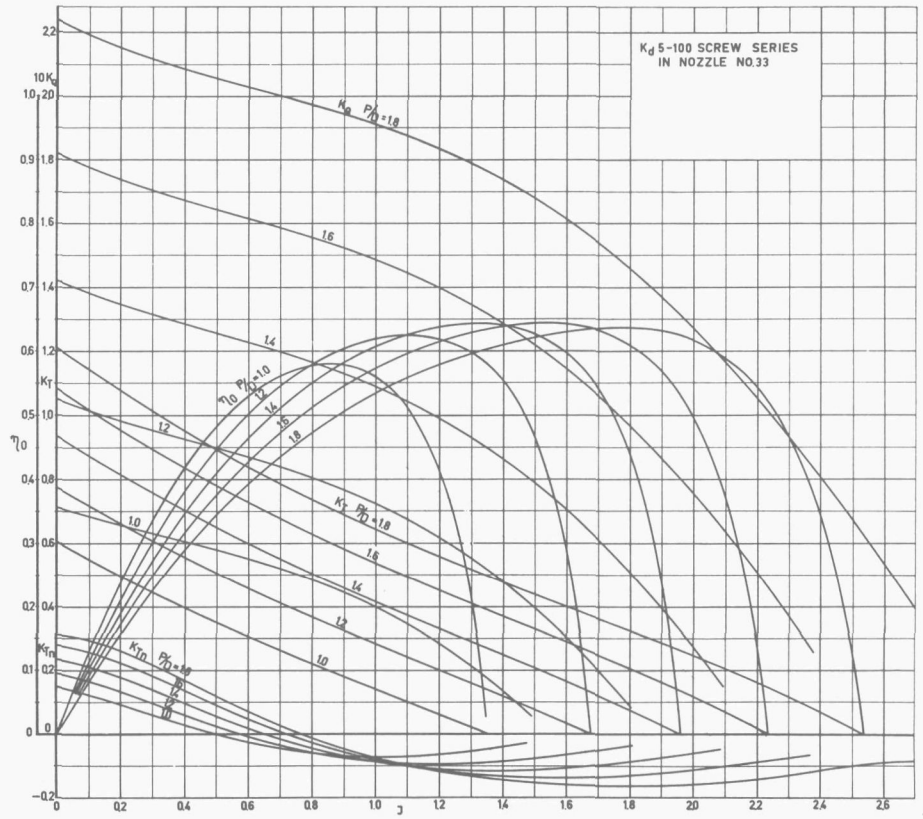

FIG. 55. Open-water test results of Kd 5–100 screw series with nozzle no. 33.

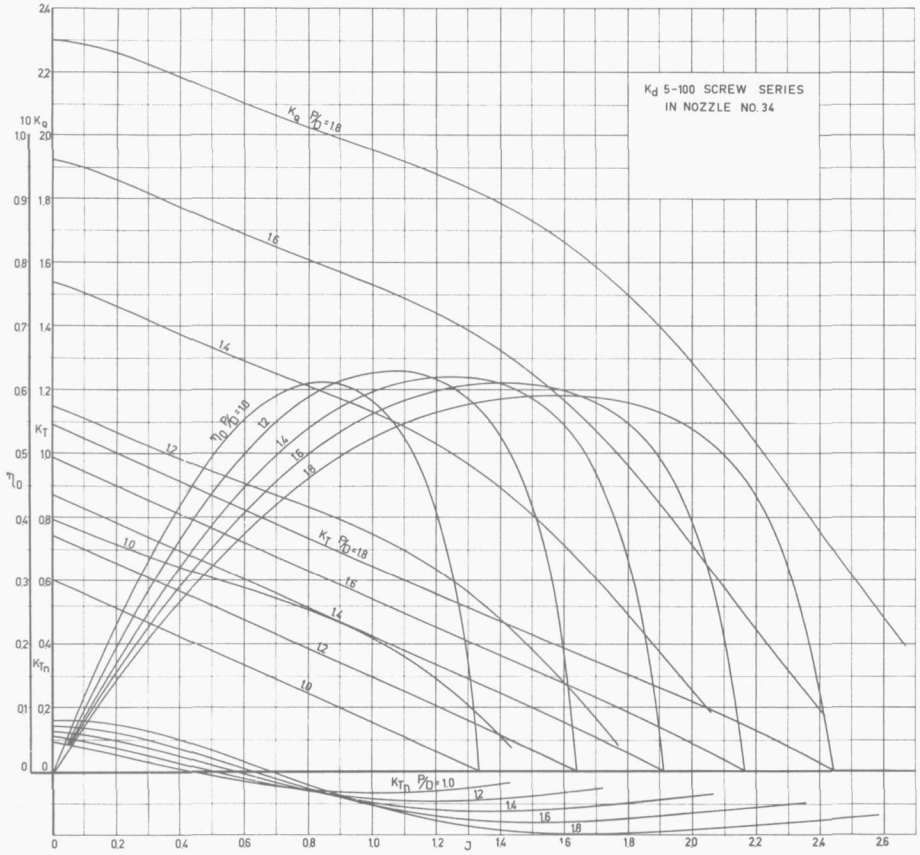

FIG. 56. Open-water test results of Kd 5–100 screw series with nozzle no. 34.

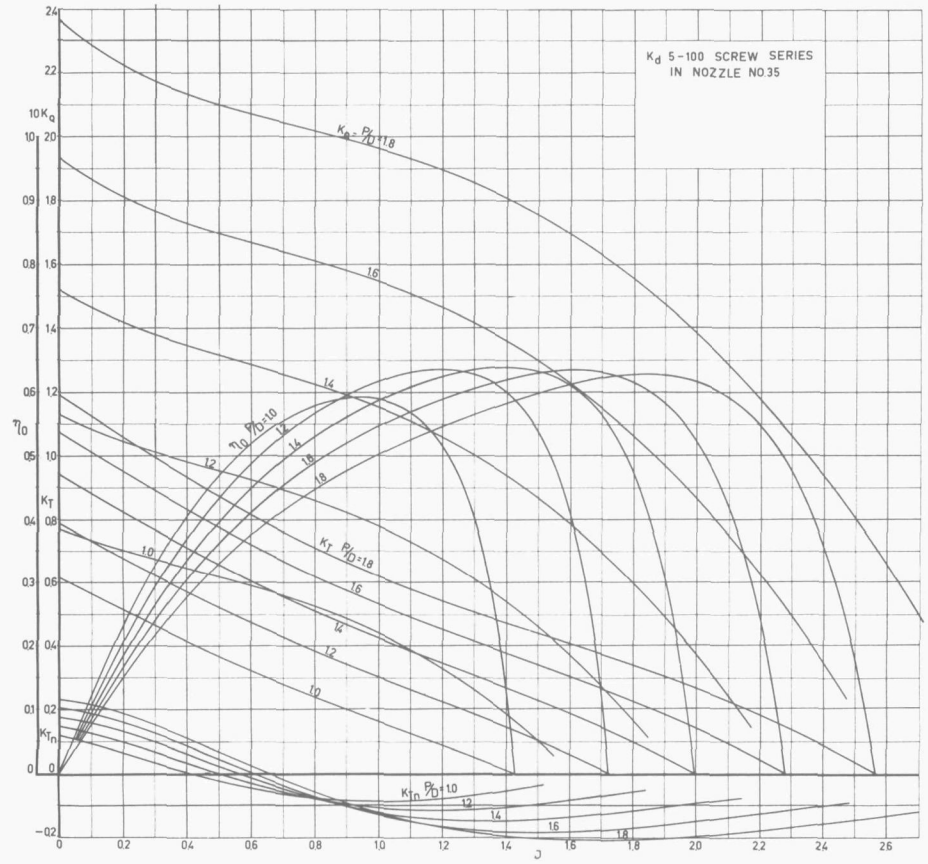

FIG. 57. Open-water test results of Kd 5–100 screw series with nozzle no. 35.

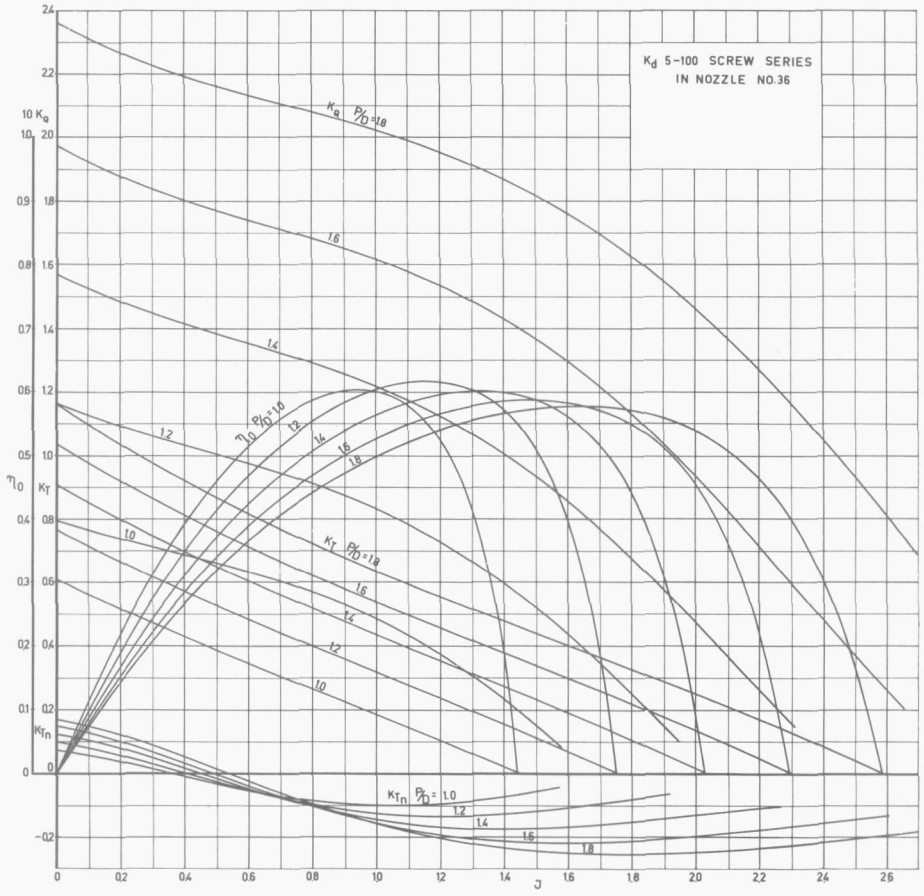

FIG. 58. Open-water test results of Kd 5–100 screw series with nozzle no. 36.

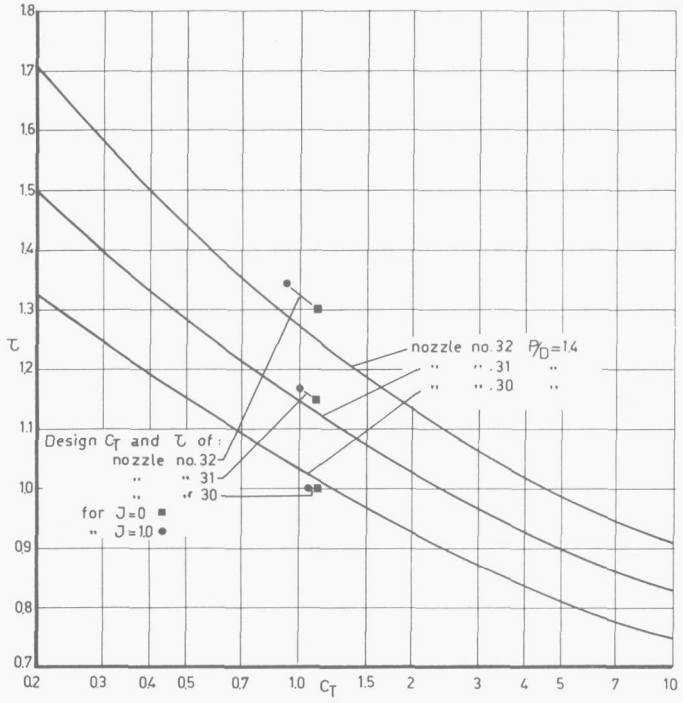

FIG. 59. Relationship between C_T and τ of nozzles nos. 30, 31 and 32.

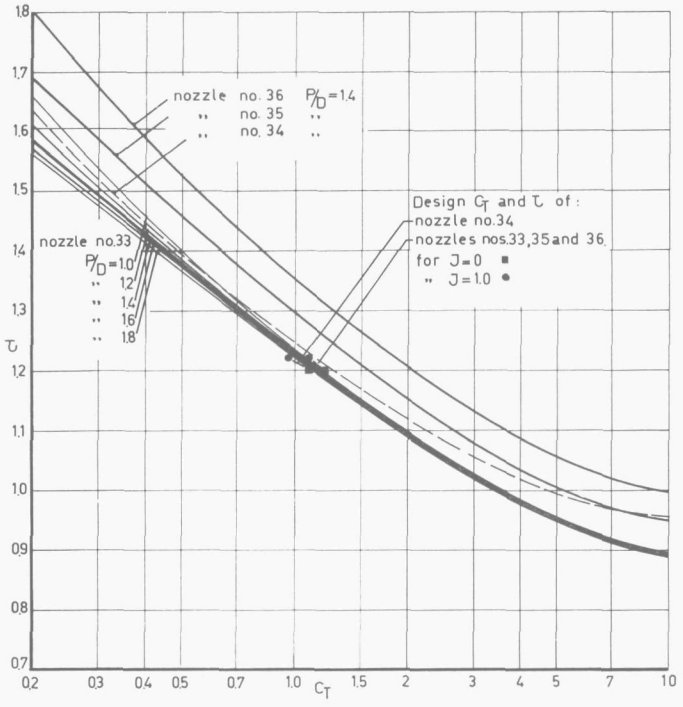

FIG. 60. Relationship between C_T and τ of nozzles nos. 33, 34, 35 and 36.

The relationship between the thrust coefficient C_T and the thrust ratio τ of nozzle no. 33 in combination with the various screws of the Kd 5-100 screw series is shown in Fig. 60. It can be seen from this diagram that, as might be expected, this relationship is approximately independent of the pitch ratio of the screws. The small differences which occur may be explained by the differences in rotational losses and radial load distributions of the screws and by frictional effects.

The relationships between C_T and τ of nozzles nos. 30, 31 and 32 (Fig. 59) and nozzles nos. 34, 35 and 36 (Fig. 60) were, therefore, only given for the screw with a pitch ratio of 1.4. Although a number of simplifying assumptions were made in the development of the theory for the numerical calculations of the nozzles shapes (it was a linearized theory, the impeller was represented by a uniformly loaded actuator disk, tip clearance effects were not taken into account, the effect of friction was neglected) a reasonable agreement between the calculated relationship of C_T and τ of the various nozzles and those obtained by the open-water tests was found.

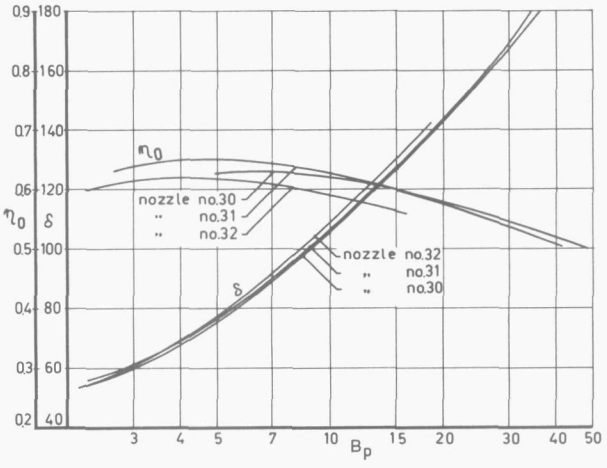

FIG. 61. Optimum relationship between η_o, δ and B_P of nozzles nos. 30, 31 and 32.

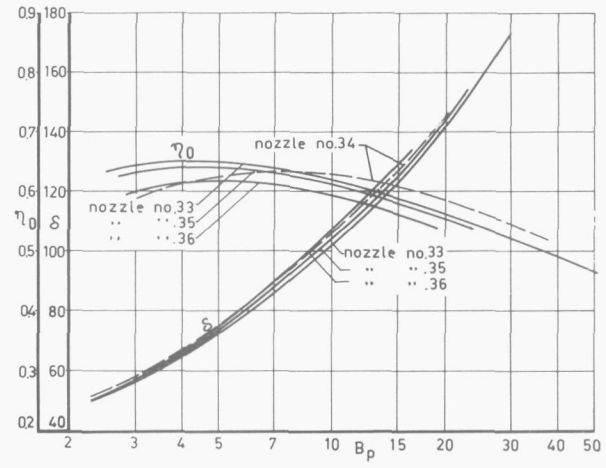

FIG. 62. Optimum relationship between η_o, δ and B_P of nozzles nos. 33, 34, 35 and 36.

The open-water efficiency η_o and the diameter coefficient δ of the various nozzles were given for optimum condition from the viewpoint of efficiency in the Figs. 61 and 62 on a base of B_P. In combination with Figs. 59 and 60, these diagrams show clearly that by comparing the properties of the different nozzles, the open-water efficiency decreases with increasing thrust ratio τ. The diameter coefficients of the various nozzles are nearly the same.

The prevention of strong vortices along the hub of the decelerating ducted propeller is of importance because these vortices may result in hub vortex cavitation. This can be achieved by the application of vanes or a stator located downstream of the impeller. It may also increase the efficiency if the vanes eliminate the rotational losses without incurring excessive frictional resistance.

Based on the theory as discussed in (11) and (13), a six-bladed stator was designed for application downstream of the Kd 5-100 screw with $P/D = 1.4$ in nozzle no. 33. Particulars of the stator are given in Fig. 63. Open-water tests with the Kd 5-100 screw series in combination with nozzle no. 33 and the six-bladed stator were performed. The result is given in Fig. 64. The stator was fitted to the nozzle, consequently, K_{TN} denotes the thrust coefficient of nozzle and stator.

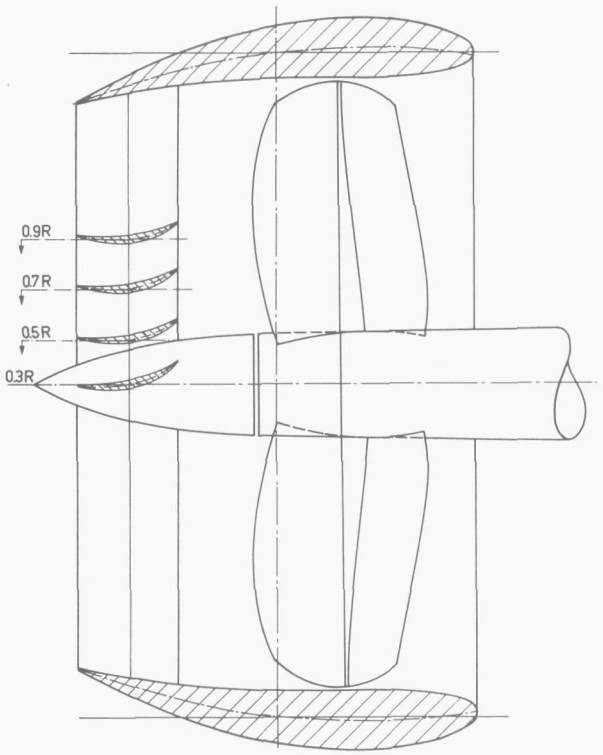

FIG. 63. Particulars of six-bladed stator.

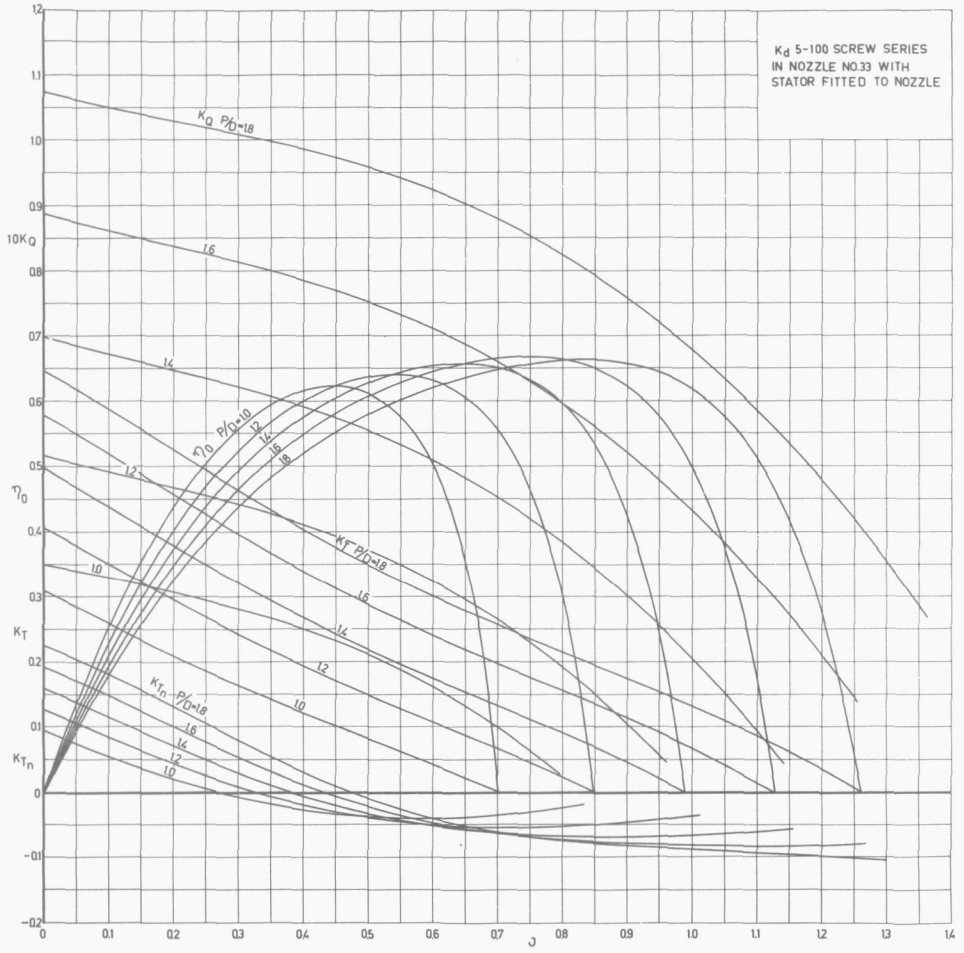

FIG. 64. Open-water test results of Kd 5–100 screw series and nozzle no. 33 fitted with stator.

In the case of application of a screw or a ducted propeller behind a ship, a part of the rotational losses of the screw or impeller is already eliminated due to the presence of the rudder in the propeller slipstream. Consequently, the gain in efficiency due to the stator will be lower as may be expected from comparing the results given in Figs. 55 and 64.

For comparison purposes, model tests have been carried out to determine the effect of the presence of a rudder on the characteristics of a ducted propeller system. A more or less common rudder configuration was therefore fitted to nozzle no. 33 and open-water tests were performed with this system in combination with the Kd 5-100 screw series. Particulars of the nozzle-rudder system are given in Fig. 65. The results of the open-water tests are presented in Fig. 66.

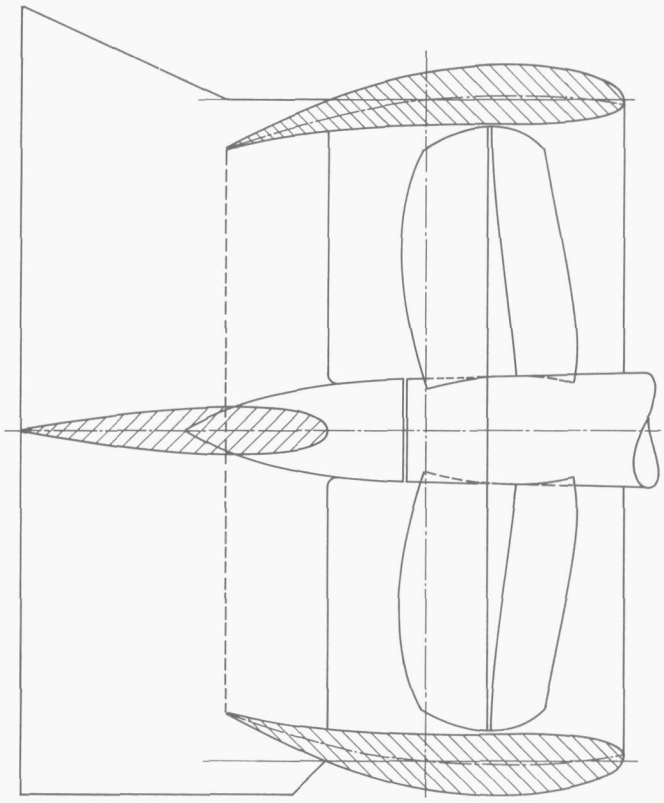

FIG. 65. Particulars of rudder fitted to nozzle no. 33.

The optimum curves for efficiency of the Kd 5-100 screw series in combination with successively nozzle no. 33, nozzle 33 with six-bladed stator and nozzle no. 33 with rudder, are given in Fig. 67. From this diagram it can be seen that both the stator and the rudder give an increase of the efficiency. The ducted propeller equipped with stator has the smallest optimum diameter.

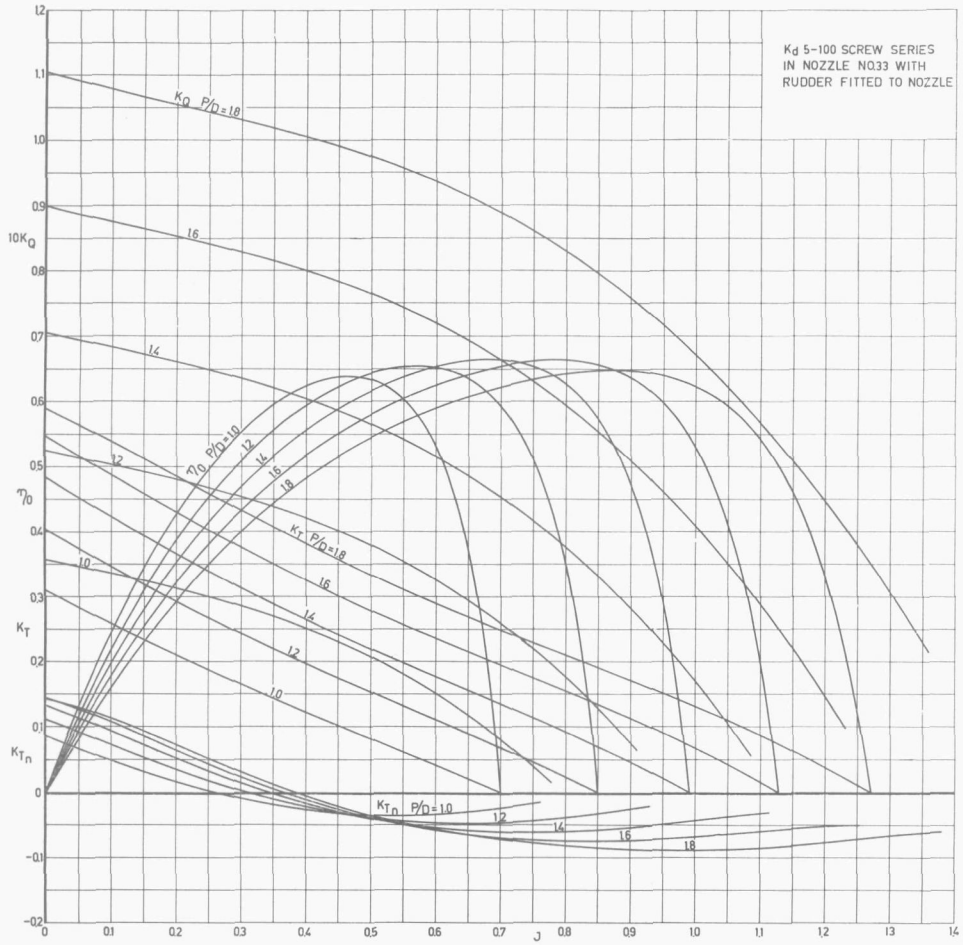

FIG. 66. Open-water test results of Kd 5–100 screw series and nozzle no. 33 fitted with rudder.

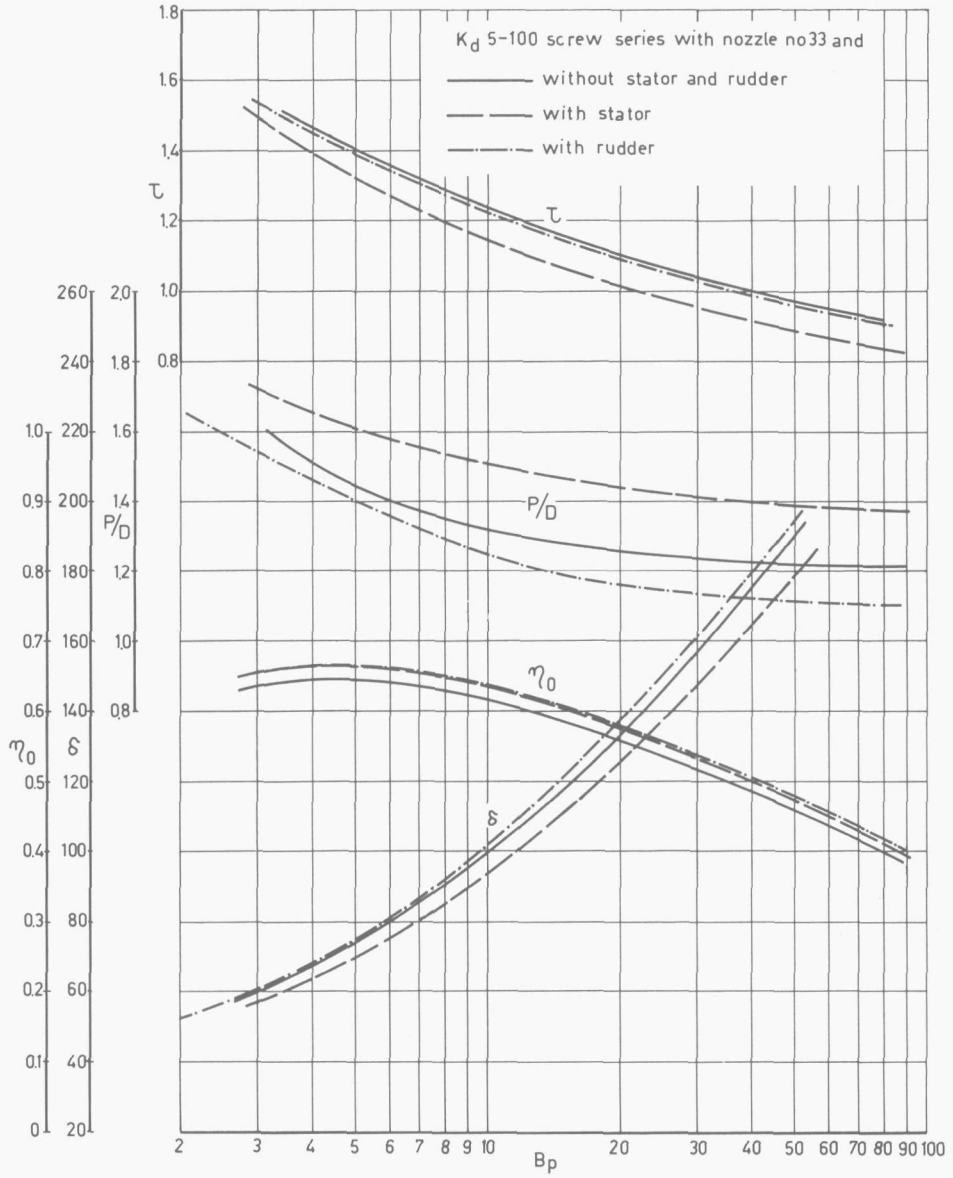

FIG. 67. Optimum relationship between η_o, δ and B_P of Kd 5–100 screw series and successively nozzle no. 33 and nozzle no. 33 fitted with stator and with rudder.

7. GENERAL DISCUSSION OF TEST RESULTS

In section 6, it was found that the relation between the thrust coefficient C_T and the thrust ratio τ of a ducted propeller system was approximately independent of the pitch ratio of the impeller. This result was for the Kd 5-100 screw series in combination with nozzle no. 33 shown in Fig. 60.

The experimentally obtained relation between C_T and τ of the Ka 4-70 screw series with nozzle no. 19A is shown in Fig. 68. The results presented in this diagram confirm the above mentioned conclusion.

In section 2, the following relation between the impeller disk area-nozzle exit area ratio A_o/A_{EX}, the thrust coefficient C_T and the thrust ratio τ was derived:

$$\frac{A_o}{A_{EX}} = \frac{2\,[1 + \tau C_T - \sqrt{1+\tau\,C_T}]}{C_T}$$

In the derivation of this expression it was assumed that the tangentially induced velocities and consequently the losses due to the rotation of the fluid were zero.

For the range of impeller pitch ratios of ducted propellers normally considered, it can be expected that the rotation of the fluid slightly influences the forces developed on the nozzle or the nozzle thrust. A rough indication of the decrease in propeller thrust due to the rotation of the fluid can be obtained from axial flow pump theory. With the aid of this theory, the ratio between the propeller thrust influenced by rotation C^*_{TP} and the propeller thrust for zero rotational losses C_{TP} can be written as:

$$\frac{C^*_{TP}}{C_{TP}} = 1 - \left(\frac{P}{D}\right)^2 \frac{\ln R_1/R_0}{2\pi^2\,[1 - (R_0/R_1)^2]}$$

Some results of the calculations performed with these relations are also presented in Fig. 68.

It must be noted that in the derivation of these relations a large number of simplifying assumptions were made. Therefore this theory is only useful to make a qualitative analysis of the characteristics of ducted propellers. It can be seen from Fig. 68, that the tendencies found from the theoretical calculations and the experimental results are in good agreement with each other.

From all model tests performed with accelerating and decelerating nozzles as described in the sections 5 and 6, it can be deduced that for the considered nozzles (with length-diameter ratios L/D between 0.4 and 1.0), there exists a fixed relation between C_T, τ and the ratio between the disk area of the nozzle. This result is shown in Fig. 69. The numbers of the considered nozzles are indicated in the diagram. This diagram gives a simple relation between the nozzle geometry and the characteristics

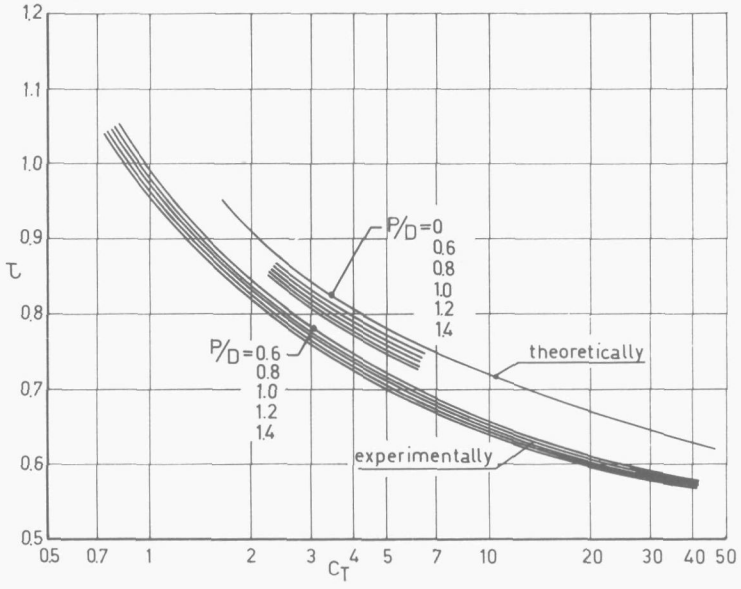

FIG. 68. Relationship between C_T and τ of nozzle no. 19 A.

of the ducted propeller system. The result will be used in the following sections for the design of various special nozzle shapes.

Another general result which can be obtained from the model tests is presented in Fig. 70. In this diagram the open-water efficiency of ducted propeller systems is given

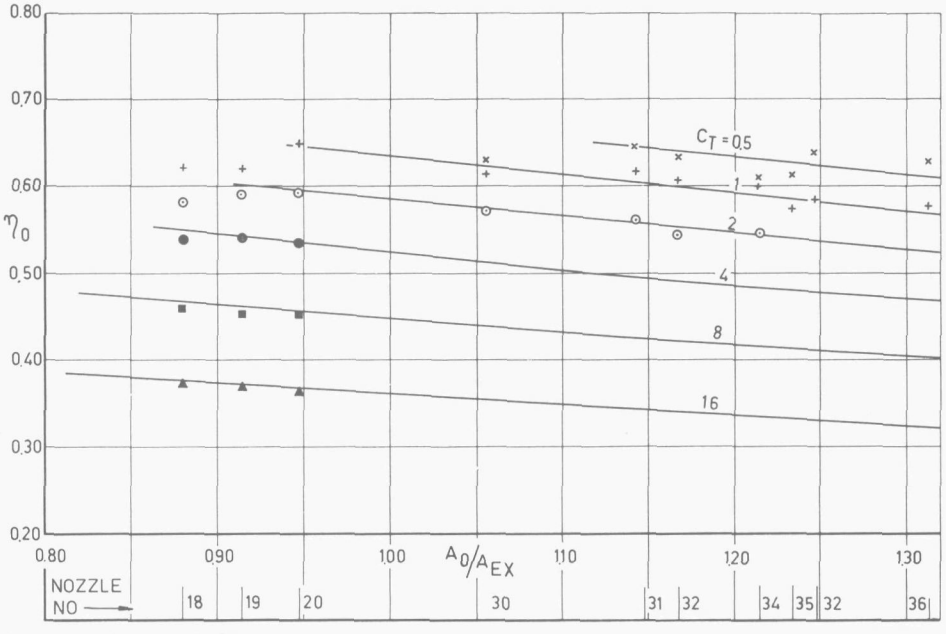

FIG. 69. Relationship between C_T, τ and nozzle geometry.

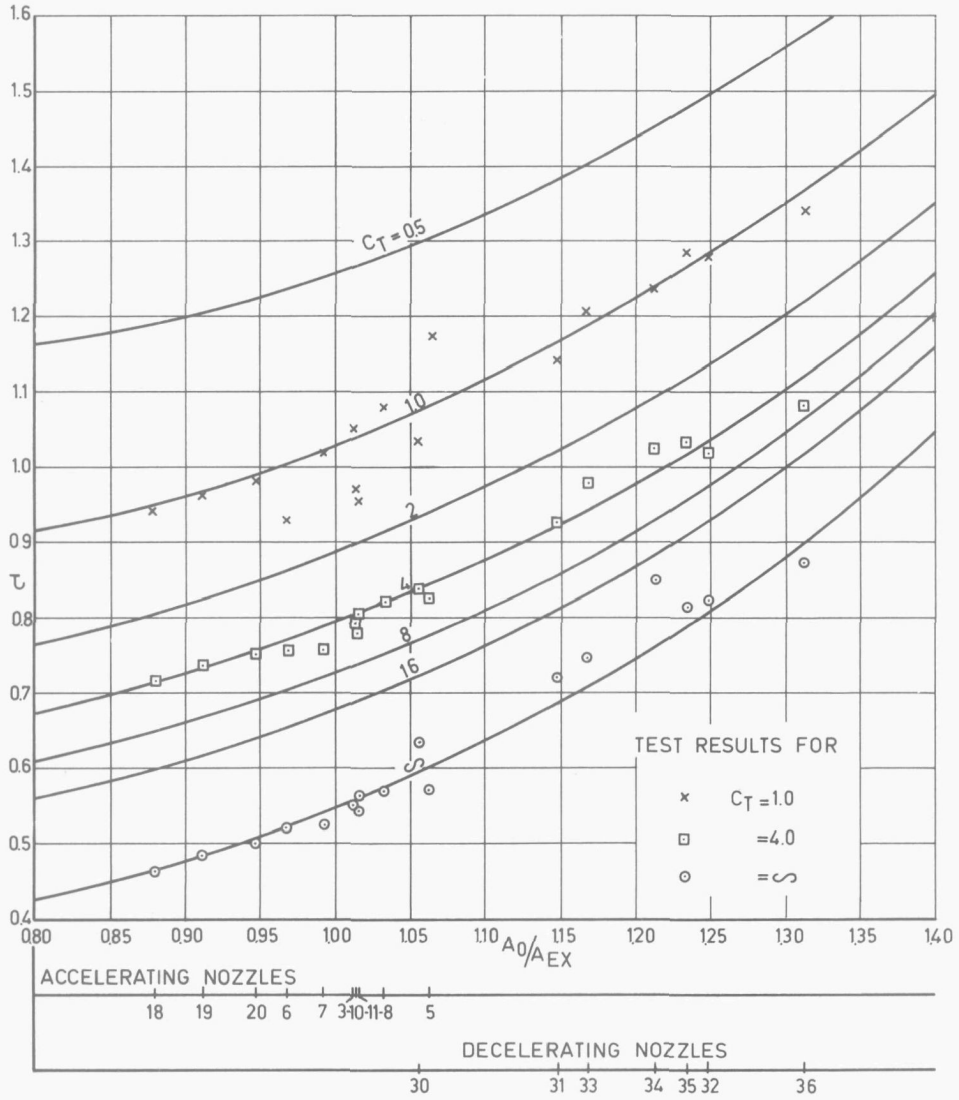

FIG. 70. Relationship between η_o, C_T and nozzle geometry.

on a base of the nozzle area ratio A_o/A_{EX} and for different values of the thrust coefficient C_T. By combining the results presented in Figs. 69 and 70 it can be seen that with decreasing value of the area ratio A_o/A_{EX}, the thrust ratio τ decreases and the efficiency η_o of the ducted propeller system increases. Thus with increasing positive loading of the nozzle, the efficiency of the ducted propeller system increases. The loading of the nozzle is limited by the risk of flow separation on the interior surface of the nozzle. A criterion for the nozzle loading was given in section 4.

As a comparison, the optimum curves for open-water efficiency η_o, diameter coefficient δ and thrust ratio τ of the Ka 4-70 screw series in nozzle no. 19A, the B 4-70 screw series and the Kd 5-100 screw series in nozzle no. 33 are given in Fig. 71 on a base of B_P. Screws of the B 4-70 screw series are usually applied behind single screw cargo ships (see for instance (17)). Typical B_P and C_T values for different ship types are indicated in Table 10. The lightly loaded screws of fast ships are on the left side of Fig. 71 while the heavily loaded propellers of towing vessels are on the right.

It can be seen from Fig. 71 that at low B_P-values the open-water efficiency of both the accelerating and the decelerating nozzle decrease with respect to the efficiency of the B 4-70 screw series. This fact can be explained by the relative increase of the frictional and the induced drag of the nozzle (see also Fig. 11). The curves of the diameter coefficient δ of the accelerating and the decelerating nozzle almost coincide; the B 4-70 screw series has a larger optimum screw diameter. It is interesting to note that the curves of the diameter coefficient based on the maximum diameter of the system δ^* of both accelerating and the decelerating nozzle and the B 4-70 screw series almost coincide.

The accelerating nozzle (nozzle no. 19A), if compared with a conventional screw propeller (B 4-70 screw series), gives rise to an improvement in open-water efficiency η_o in the case of heavy screw loads (see Fig. 71). The decelerating nozzle (nozzle no. 33) has a relatively low open-water efficiency.

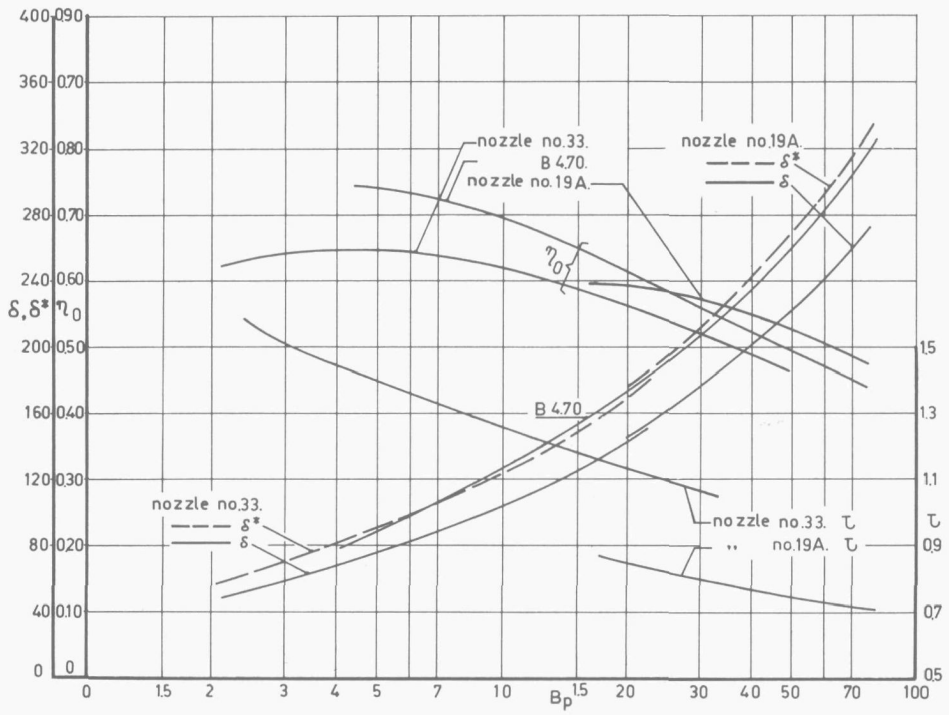

FIG. 71. Optimum relationship between η_o, δ and B_P of the Ka 4–70 screw series in nozzle no. 19A, the B 4–70 screw series and the Kd 5–100 screw series in nozzle no. 33.

TABLE 10. Typical B_P and C_T values for different ship types

	B_P	C_T
Torpedo's	<10	<0.5
Twin-screw ships	10– 15	0.5–1.0
Fast warships (frigates, destroyers)	10– 25	0.5–1.5
Single screw cargo ships	15– 35	1.0–2.5
Coasters	35– 60	2.5–4.0
Tankers	35 –70	2.5–5.0
Trawlers	60–100	4.0–8.0
Towing vessels (tugs, pushboats)	>80	>6.0

In the case of heavy screw loads (all types of towing vessels) the attractiveness with regard to propulsive efficiency of application of the accelerating nozzle has been demonstrated in practice in the course of the past thirty years.

For middle and lower screw loads (tankers and single-screw cargo ships) the increase in propulsive efficiency through application of an accelerating nozzle strongly depends on the stern-nozzle configuration. In the case of lightly loaded screws the application of a decelerating nozzle may become attractive when other requirements than the efficiency influence the choice. For naval ships it is of utmost importance that the inception speed, or the speed at which cavitation phenomena occur at the screw will be as high as possible. For tactical reasons a minimum sound radiation of propeller noise due to cavitation is necessary for these ships.

Finally it must be noted that the flow velocity at the impeller disk of a ducted propeller is far less sensitive to variations in ship speed than the flow velocity at an ordinary propeller. Consequently the power absorption of a ducted propeller is relatively less sensitive to variations in the ship speed. This feature has also been an important factor in the case of application of ducted propellers behind tugs, pushboats and trawlers. All these ships must operate satisfactorily at different loadings (towing and free-running) of the screw. For towing vessels the thrust which can be developed at bollard pull condition, either with the propeller running ahead or astern, is of importance. In such cases, as stated in section 5, the use of a nozzle with a relatively thick trailing edge is attractive. Such a nozzle (nozzle no. 37) was shown in Fig. 34.

The optimum curves for open-water efficiency η_o and diameter coefficient δ of the Ka 4-70 screw series in combination with successively nozzle no. 19A and nozzle no. 37 are given in Fig. 72 on a base of B_P. From this diagram it can be seen that, as may be expected due to the increase of the nozzle drag by the relatively thick trailing edge of the nozzle profile, the ducted propeller system with nozzle no. 37 has a lower open-water efficiency than the system with nozzle no. 19A.

In Figs. 73 through 76, the thrust force at bollard pull condition and with the impeller running ahead and astern is given on a base of the power with the diameter and

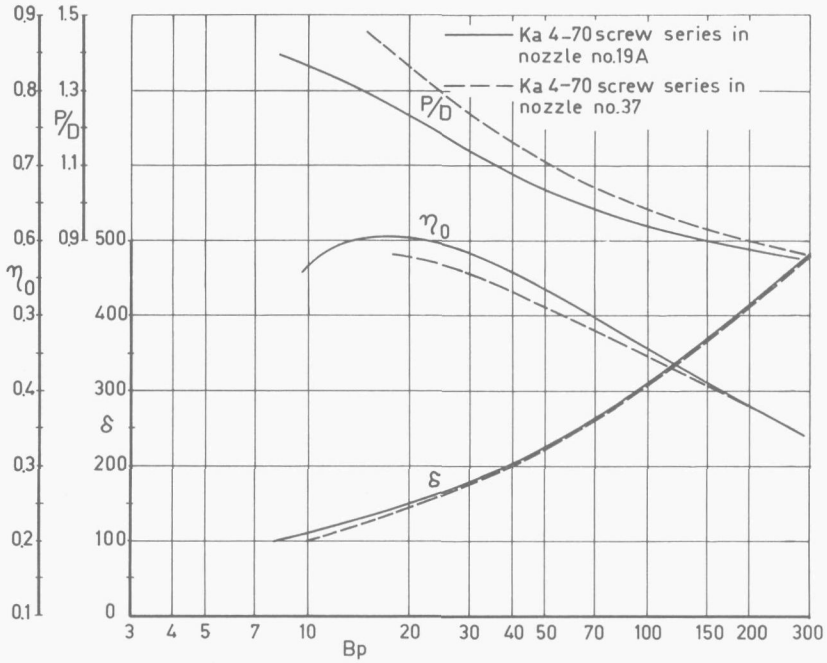

FIG. 72. Optimum relationship between η_{io}, δ and B_P of the Ka 4–70 screw series in respectively nozzle no. 19 A and nozzle no. 37.

the rpm as parameters. The result with nozzle no. 19A is given in Figs. 73 and 74 whereas this result for nozzle no. 37 is given in the Figs. 75 and 76.

The thrust-power ratios for the different nozzle configurations and flow conditions are for instance for a power absorption of 5000 HP and an impeller diameter of 4 m:

nozzle no. 19A,	ahead:	T/P = 13.6 kg/HP
	astern:	= 8.3 kg/HP
nozzle no. 37	ahead:	= 14.8 kg/HP
	astern:	= 12.2 kg/HP

From these results it can be seen that nozzle no. 37 at bollard pull condition has the best characteristics, even with the impeller running ahead.

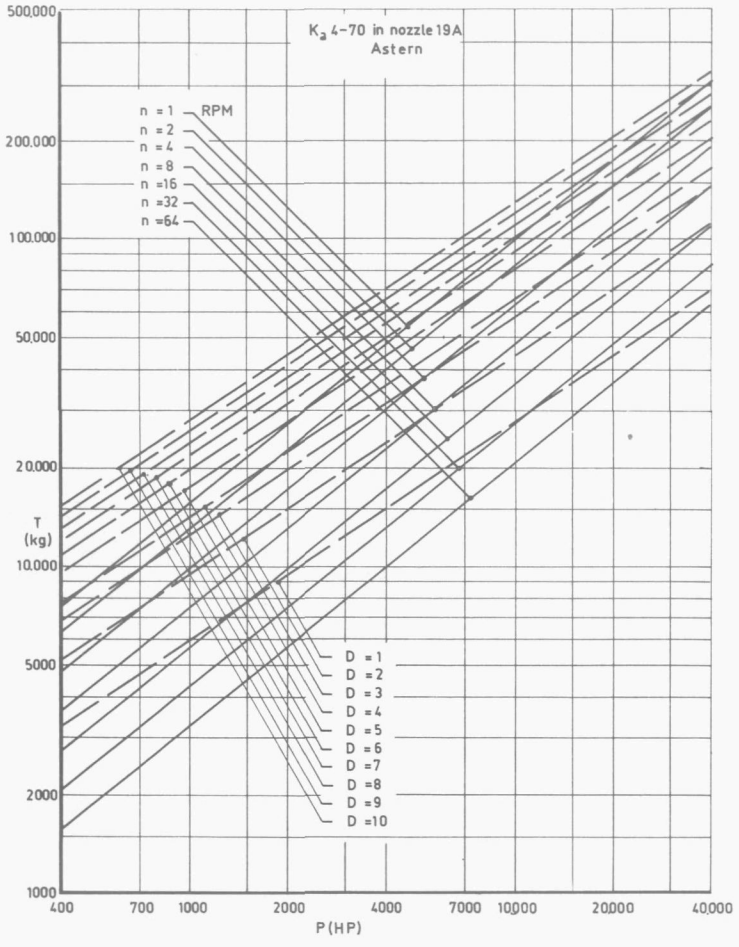

FIG. 74. Bollard pull thrust of nozzle no. 19A with Ka 4–70 series screw with $P/D = 1.0$; Impeller running *astern*.

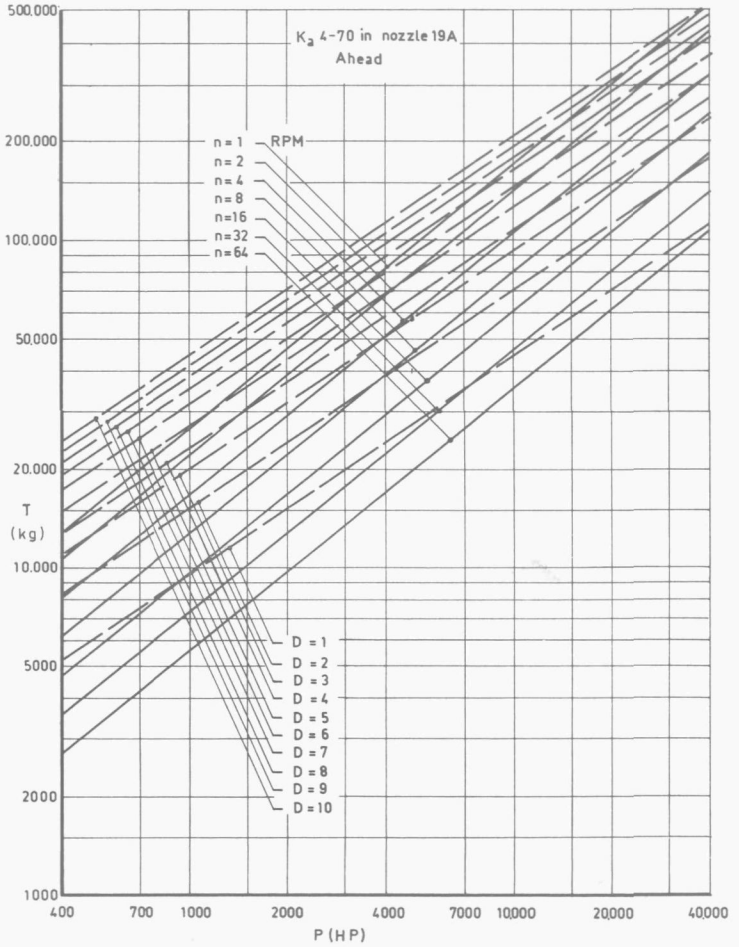

FIG. 73. Bollard pull thrust of nozzle no. 19A with Ka 4–70 series screw with $P/D = 1.0$. Impeller running *ahead*.

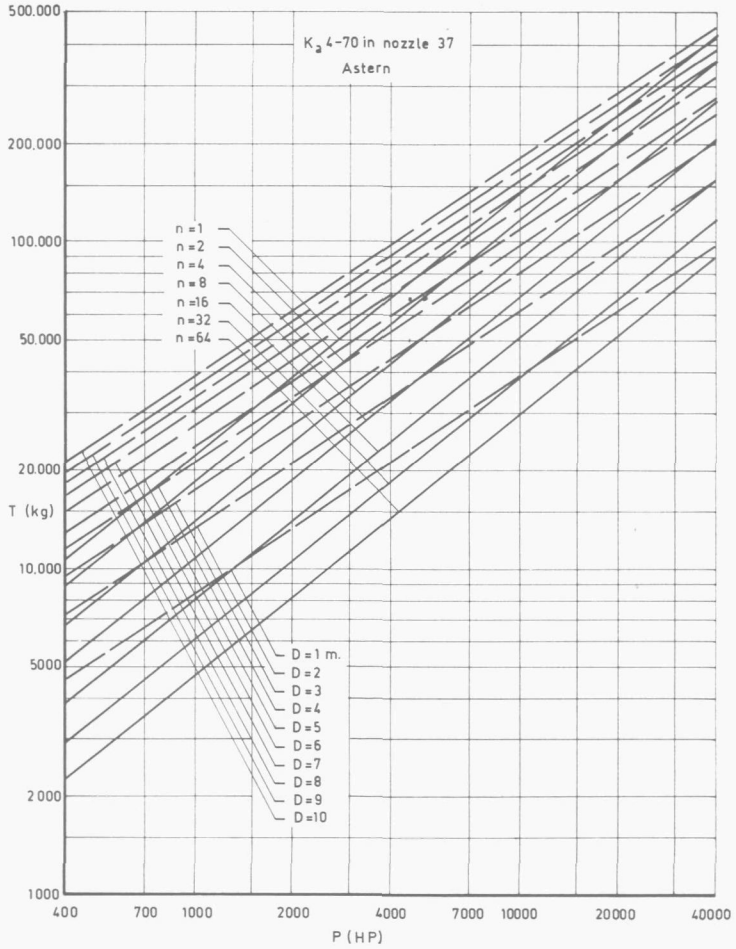

FIG. 76. Bollard pull thrust of nozzle no. 37 with Ka 4–70 series screw with $P/D = 1.0$. Impeller running *astern*.

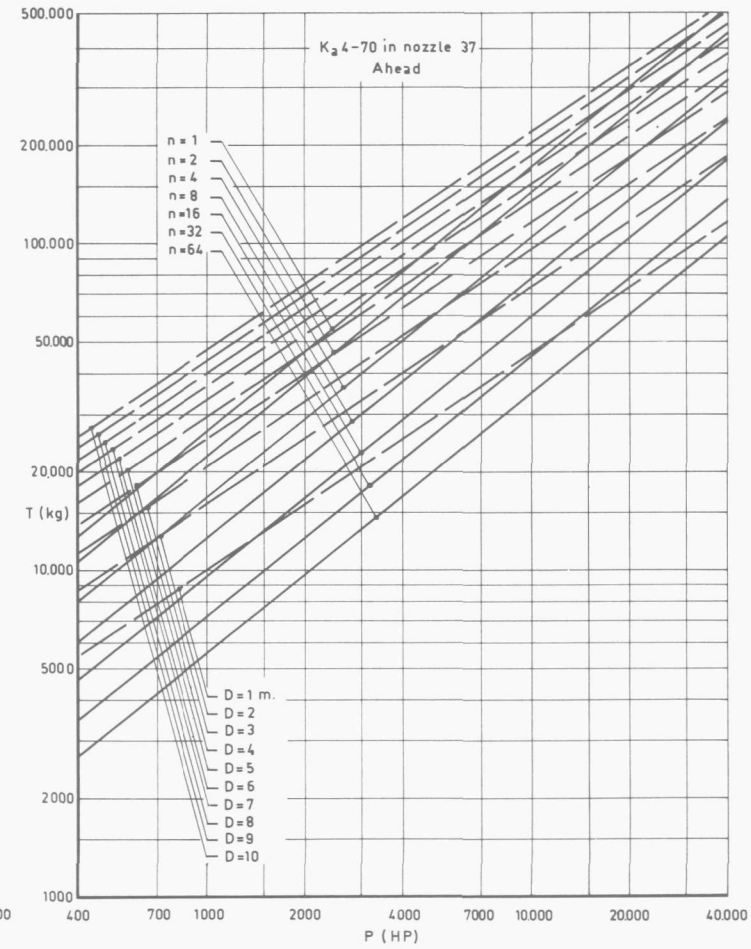

FIG. 75. Bollard pull thrust of nozzle no. 37 with Ka 4–70 series screw with $P/D = 1.0$. Impeller running *ahead*.

8. APPLICATION OF WAKE ADAPTED NOZZLES

8.1. Introduction

Before going into details of the design of wake adapted nozzles the wake behind a ship will be discussed. Usually the variations of the flow field at the screw can be split up into two components (see also (21)):

1. The radial variation, especially of the axial velocities. This variation does not lead to unsteady phenomena at the screw. A propeller working in such a velocity field has a steady flow- and force-pattern.
   Moreover, the propeller can be adjusted to this radially non-uniform flow by an appropriate distribution of pitch and camber, and optimum efficiency and cavitation properties may be expected in such cases.

2. The circumferential (at a given radius) variation of both the axial and tangential velocities. This non-uniformity is the origin of the periodically fluctuating pressure distributions along the blade chords and leads to the unsteady force-pattern at the screw and at the stern of the ship. These periodically fluctuating pressure distributions lead to unsteady cavitation phenomena which may be serious from a viewpoint of erosion and noise radiation. In addition, these unsteady pressure distributions lead to propeller induced vibrations.

The inflow velocity of the screw can be made more constant over the screw disk by surrounding the propeller by a *non-axisymmetrical* nozzle which is adapted to the wake distribution and flow direction behind the ship.

In the case of a single-screw ship the intake velocity will be lower in the upper part of the screw disk than in the lower part. Consequently, the propeller is more heavily loaded in the upper part of the screw disk. The inflow velocity of the propeller can be made more constant over the screw disk by a non-axisymmetrical nozzle which accelerates the flow in the upper part of the screw disk and decelerates the flow in the lower part of the disk.

In the case of twin-screw ships the propellers operate in a varying inflow, due to the shaft inclination. The inclination is a consequence of the fact that the propeller shaft has a sizeable inclination to both the horizon and the buttock lines in way of the propeller. The non-axisymmetrical nozzle must be designed here, from the viewpoint of retardation of screw cavitation, in such a way that the actual effective incidence changes of the blade sections of the impeller will be as low as possible during a revolution.

Investigations with respect to special nozzle configurations will be described in the following sections.

8.2. Application of wake adapted nozzles behind tankers

From Fig. 71 it could be seen that propellers in nozzles are to be recommended for heavy screw loadings such as occur on towing vessels, trawlers and very large tankers. The possibilities of using nozzles on towing vessels (tugs, push-boats) have been adequately demonstrated in practice.

The trend in the design of tankers has been towards large dimensions at nearly constant speed and therefore high-powered ships. Although the rpm has been decreased and consequently the diameter of the screw was chosen larger, the loading coefficient of the screw of these ships has still become larger. Therefore, according to Fig. 71, a larger reduction in shaft horsepower due to application of a ducted propeller in comparison with a conventional screw may be expected for these ships when their size is increased.

Based on results, as presented in Fig. 71, propulsion tests have been performed at the Netherlands Ship Model Basin with a large number of tanker models equipped with ducted propellers. Some results of these tests were given in (22, 23, 24, 25). The investigations performed by Lindgren et al (26) may be mentioned also in this respect. The results of these tests generally confirm the conclusion that an increase in propulsive efficiency can be obtained by application of a ducted propeller for this ship type if compared with a conventional screw. Some of the more extensive tests will be discussed here.

The total propulsive efficiency of a self-propelled ship depends on the open-water efficiency of the screw and on the mutual interference of screw and hull. A screw fitted behind a ship normally increases her drag, because of the decreasing pressure (suction field), which accompanies the acceleration of the flow in front of the screw. This additional drag is called thrust deduction. The open-water efficiency of a screw with an accelerating nozzle is, for the range of screw loadings of tankers, better than that of an open-screw, but the higher thrust deduction of the first system may reduce this gain.

Therefore, tests have been carried out with a model of a 95.000 TDW tanker with conventional stern and fitted with a conventional screw or one of a series of ducted propeller systems. The nozzles were designed for different acceleration ratios of the flow. The design of these nozzles was based on the results presented in Fig. 69. The profiles of the tested nozzle shapes are given in Fig. 77. The nozzle area ratio A_o/A_{EX} of the different nozzles are also indicated in the diagram, since this ratio is one of the important characteristics of a ducted propeller.

Analysis of the reduction in DHP due to the use of the different nozzles in comparison with the conventional screw propeller has been made for a ship speed of 16.5 knots and for the loaded and ballast condition of the vessel. The result is given in Fig. 77. This diagram clearly shows that for the loaded as well as for the ballast condition the most accelerating nozzle (nozzle II) still gives the largest reduction in DHP. Further, it can be seen that an increase in DHP of about 1 percent is found by making the trailing edge of the nozzle profile round instead of sharp.

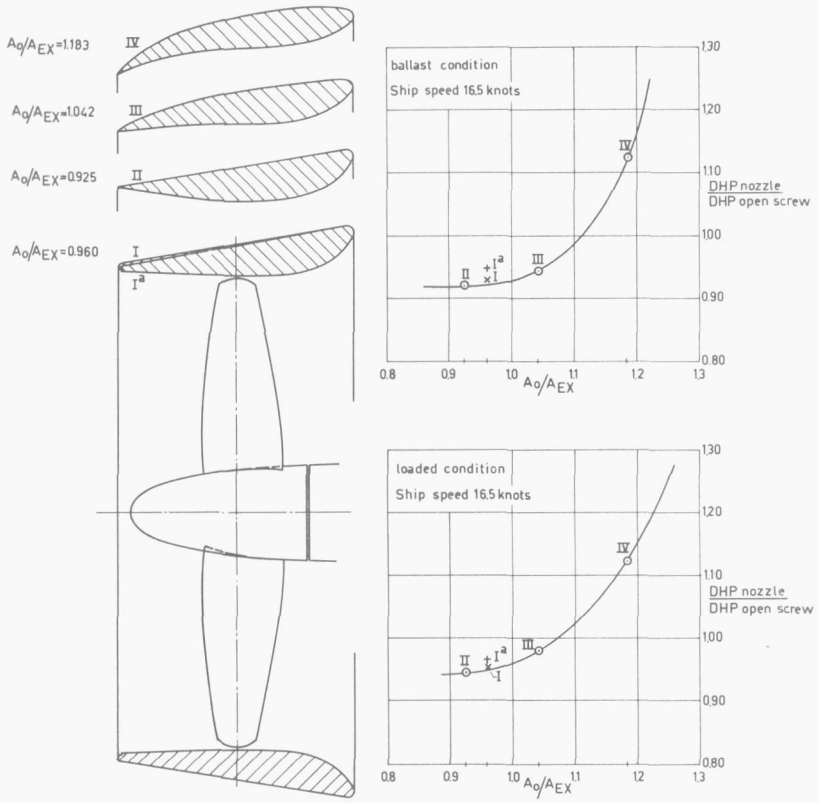

FIG. 77. Reduction in DHP due to the application of different axisymmetrical ducted propeller systems behind tankers.

It is a well known fact that the propulsive efficiency of a tanker can be further increased by application of a ducted propeller, in combination with a cigar-shaped stern. The cigar-shaped stern tends to make the flow more uniform and to bend the flow in a horizontal direction. In this respect a non-axisymmetrical nozzle behind a conventional stern may also be attractive.

Measurements performed by WERELDSMA (27) show that for large tankers a propeller thrust eccentricity of 0.1 D is common practice due to the fact that the propeller operates in the non-uniform wake. The inflow velocity of the propeller can be made more constant over the screw disk by a non-axisymmetrical nozzle which is adapted to the wake distribution behind the ship. This nozzle accelerates the flow in the upper part of the screw disk (by increasing the exit area of the nozzle) and decelerates the flow in the lower part (by decreasing the exit area of the nozzle). A view of a tanker with a conventional stern and equipped with a non-axisymmetrical ducted propeller is given in Fig. 78. The non-axisymmetrical nozzle is still cylindrical at the inside from the leading edge of the nozzle to the impeller; only the aft part is non-axisymmetrical but still cylindrical.

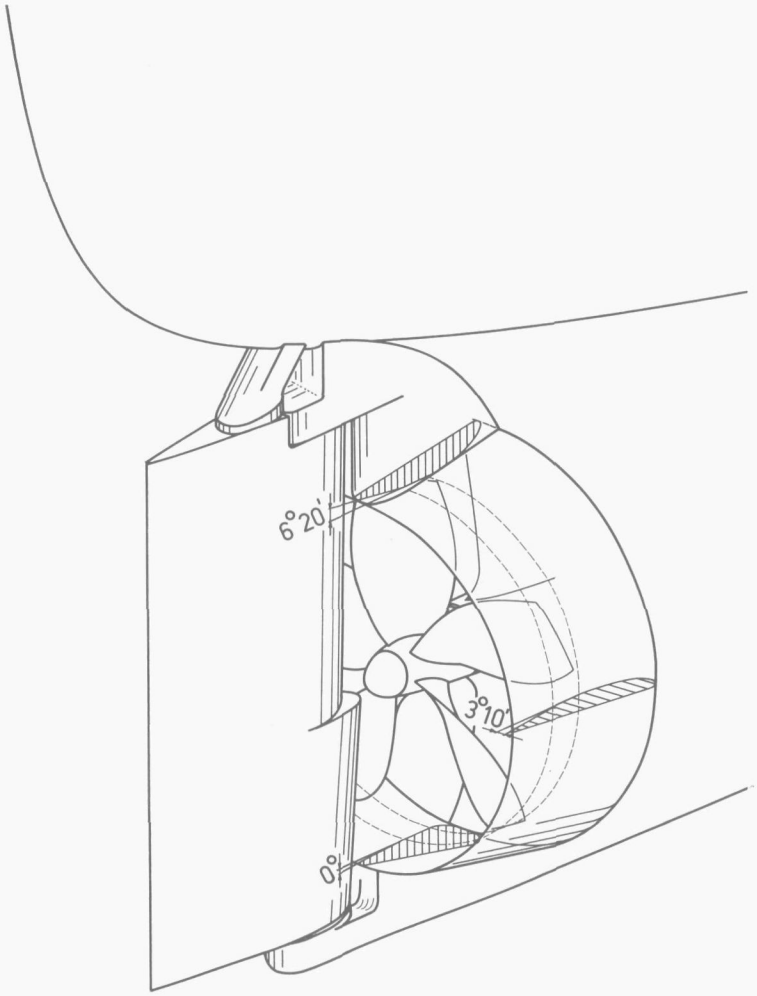

FIG. 78. View of stern of tanker fitted with non-axisymmetrical ducted propeller.

Tests have been carried out with the model of a 95.000 TDW tanker fitted with successively different non-axisymmetrical nozzles. The profiles of the tested nozzle shapes are given in Fig. 79. It can be seen from this diagram that the maximum diffusor angles (in the upper part of the screw disk) of the nozzles V, Va and VII are equal to the diffusor angle of nozzle II. Nozzle VI has a larger diffusor angle. Nozzles V, Va and VI are made non-axisymmetrical in the same degree. Nozzle VII is less non-axisymmetrical.

An analysis of the reduction in DHP due to the use of the different nozzles in comparison with the conventional screw propeller has again been made for a ship speed of 16.5 knots and for the loaded and the ballast condition of the vessel. The result is given in Fig. 79. The curves obtained with the axisymmetrical ducts are also indicated in the diagram. From this diagram it can be seen that nozzles V and Va give the largest reduction in DHP. Nozzle VI which is the most accelerating nozzle type of the series

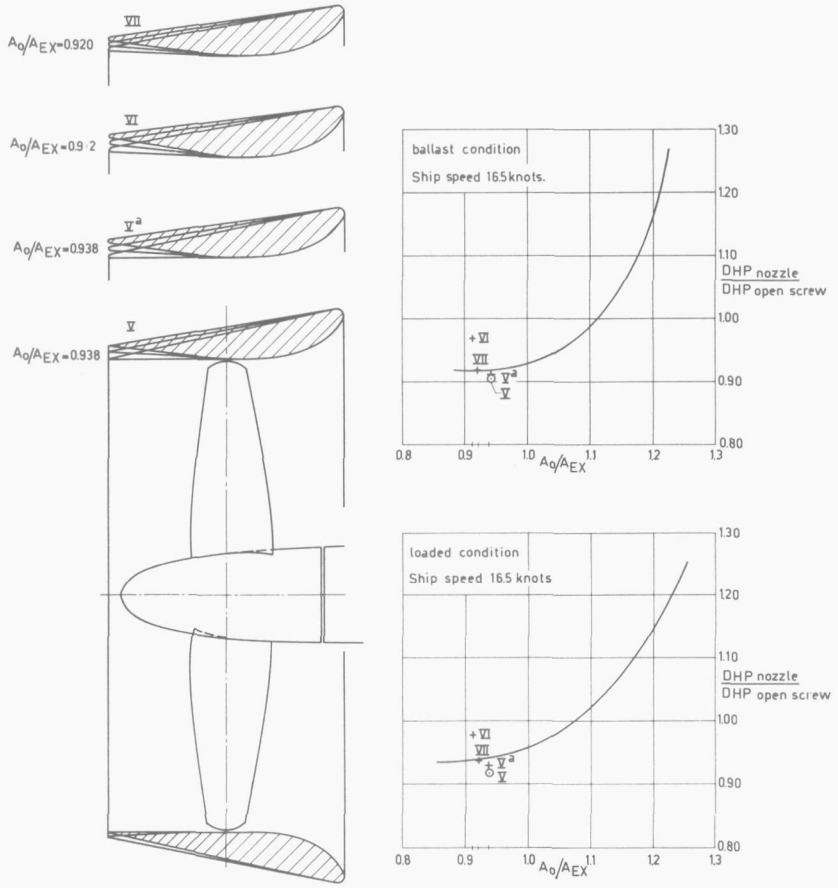

FIG. 79. Reduction in DHP due to the application of different non-axisymmetrical ducted propeller systems behind tankers.

probably suffers from flow separation in the upper part of the screw disk at the inside of the nozzle, as the diffusor angle of the nozzle is too large. Nozzle Va is slightly better than nozzle VII. It can be seen once more that a small increase in DHP is found by making the trailing edge of the nozzle profile round instead of sharp. By comparing the results presented in Figs. 77 and 79 it can be seen that the best non-axisymmetrical nozzle (nozzle Va or V) in comparison with the best axi-symmetrical nozzle gives a reduction in DHP of about 2 percent.

In Table 11 the results are compared of a large number of model self-propulsion tests, performed with tankers with conventional and cigar-shaped stern arrangements and fitted with conventional screws, ducted propellers (nozzles I and Ia) and non-axisymmetrical ducted propellers (nozzle Va).

From this table it can be seen that the conventional stern with non-axisymmetrical ducted propeller gives a reduction in DHP which is still larger than can be obtained by

TABLE 11. Reduction in DHP if compared with tanker with conventional stern and screw

Configuration	Loaded condition	Ballast condition
Ship with conventional stern and axisymmetrical ducted propeller	2–6%	
Ship with conventional stern and non-axisymmetrical ducted propeller	6–9%	reductions about 2–3% larger
Ship with cigar-shaped stern and axisymmetrical ducted propeller	5–8%	

application of a cigar-shaped stern with an axisymmetrical nozzle. In addition, it can be expected from the homogenizing effect of the non-axisymmetrical nozzle on the inflow velocity of the impeller that the non-axisymmetrical ducted propeller offers a means of minimizing propeller induced vibration and cavitation problems.

The suitable non-axisymmetrical nozzle shapes for large tankers discussed so far were determined experimentally. For the development of a more refined design method the wake-field behind the ship must be known. Normally wake surveys are made without running propeller. In the case of tankers which have a full form a region of flow separation occurs above the propeller. This causes quite different wake fields with and without the propeller running. This fact is illustrated in Fig. 80. In this diagram the results of wake surveys conducted on the model of a 240.000 TDW tanker are given. The pitot-tube wake surveys were made in a plane about 0.15 D upstream of the screw propeller. The tests were performed for the full load condition and at the service speed of the ship.

It can be seen from the wake survey without running propeller that the mean flow

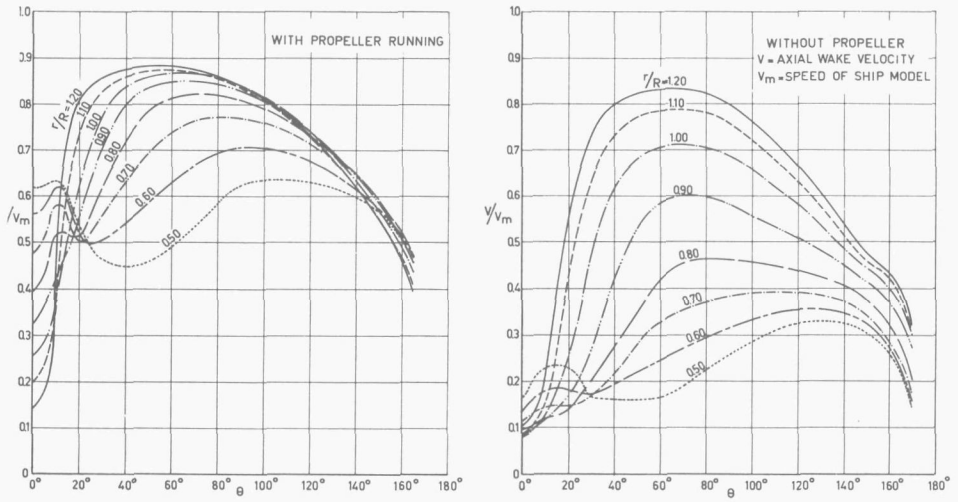

FIG. 80. Wake of large tanker with and without running propeller.

velocity in the upper part of the screw disk is larger than in the lower part. Based on this result it should be expected that the screw is relatively more heavily loaded in the lower part of the screw disk. This is in contradiction with the results of measurements of the thrust excentricity and the results of observations in a cavitation tunnel.

However, from analyzing the wake survey with running propeller it can be seen that the mean velocity in the upper part of the screw disk is lower than in the lower part. Due to the presence of the ship's hull and probably due to flow separation, it is more difficult to suck water in the upper part than in the lower part of the screw disk. It is clear that this result is in accordance with the usually found thrust eccentricity and the results of cavitation observation tests. A more refined design of the non-axisymmetrical nozzle must therefore in future be based on the results of a wake survey with running propeller.

In addition, the determination of a wake survey with running propeller in the case of the application of a non-axisymmetrical ducted propeller will give the final answer how far this system has made the flow more uniform at the impeller disk.

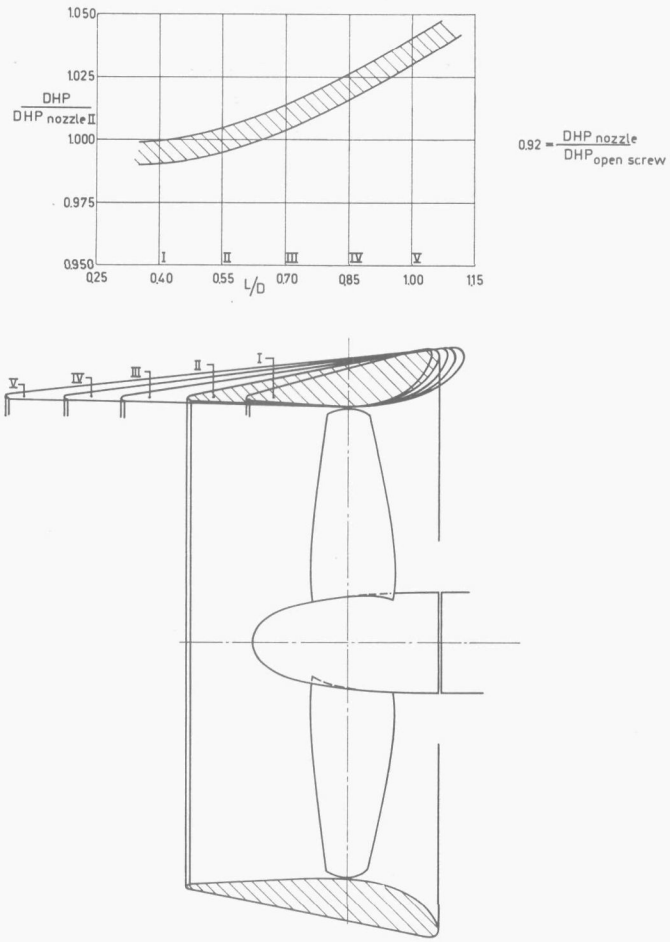

FIG. 81. Reduction in DHP due to application of ducted propeller systems with different length-diameter ratios L/D behind a tanker.

Finally a systematic series of tests with a tanker model (210.000 TDW) fitted with ducted propellers with different nozzle length-diameter ratios were performed. The considered nozzle profiles are given in Fig. 81. In this diagram, the results of the model self-propulsion tests are also given. These nozzles all have the same nozzle area ratio A_o/A_{EX} and yet the shortest nozzle ($L/D = 0.40$) is the best. However, the difference with the nozzle with $L/D = 0.55$ is small.

8.3. APPLICATION OF WAKE ADAPTED NOZZLES BEHIND TWIN-SCREW SHIPS

For naval ships it is of importance that the inception speed, or the lowest speed at which cavitation phenomena on the screw will occur, should be as high as possible. For tactical reasons a minimum sound radiation of propeller noise due to cavitation is necessary for these ships. Usually, fast naval ships (frigates, destroyers) are twin-screw vessels and typical B_P or C_T values for the screws of these ships were given in section 7. These values were $B_P \simeq 10$–20; $C_T \simeq 0.5$–1.0. From Fig. 13 it could be seen that the application of a decelerating ducted propeller may be attractive for fast naval ships, as this nozzle can attribute to a retardation of propeller cavitation.

In the case of twin-screw ships, the propellers operate in a varying inflow, due to the shaft inclination. This inclination is a consequence of the fact that the propeller has a sizeable inclination to both the horizon and the buttock lines in way of the propeller. Wake data indicate that the flow is probably following the buttock lines closely and should have a fairly uniform inclination over the disk. A view of the propeller and the hull in way of the propeller is given in Fig. 82. In addition the velocity

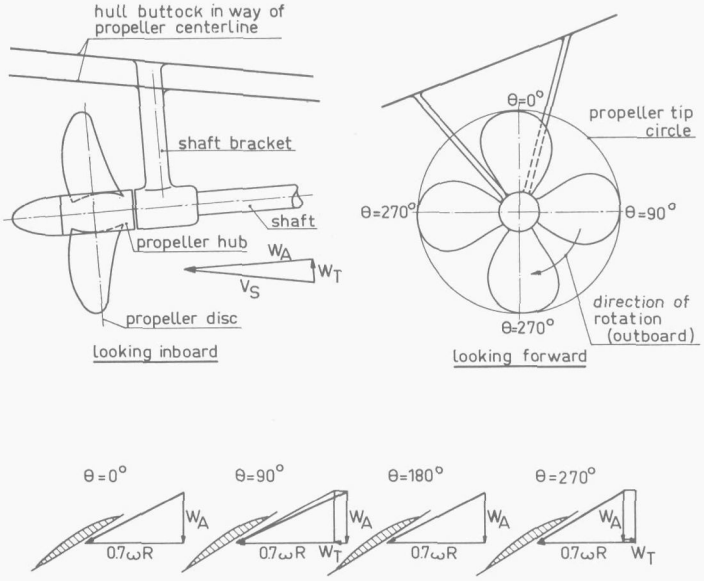

FIG. 82. View of propeller and hull of twin screw ship.

diagrams of a screw blade-element at a radius 0.7 R are given in this Figure for different positions of the blade during a revolution.

From the viewpoint of retardation of screw cavitation, the application of a non-axisymmetrical nozzle may be attractive here. This nozzle must be designed is such a way that the actual effective incidence changes of the blade sections of the impeller will be as low as possible during a revolution. A part of the stern of a twin-screw ship fitted with non-axisymmetrical nozzles is shown in Fig. 83. Particulars of the nozzle are given in Fig. 84. This nozzle (the starboard nozzle) accelerates the flow velocity with respect to the mean flow velocity at the starboard side ($\theta = 90°$) by increasing the exit area of the nozzle and decelerates the flow at the port side ($\theta = 270°$) by decreasing the exit area of the nozzle. The nozzle is still cylindrical at the trailing edge. The leading edge of the nozzle is adapted to the flow direction.

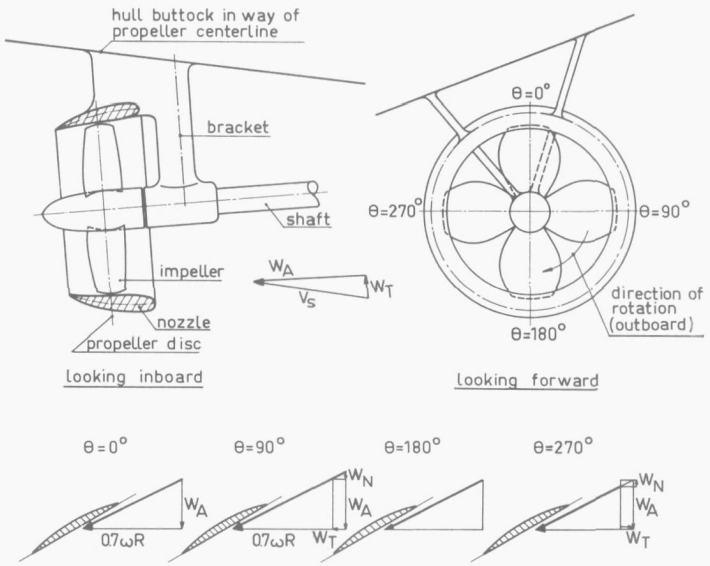

FIG. 83. Hull of twin-screw fitted with non-axisymmetrical nozzles.

The velocity diagrams of a screw blade-element at a radius 0.7 R are given in Fig. 83 for the different angular positions of the blade. These diagrams show that the angle of incidence of the flow with respect to the blade element will be constant during a revolution. However, the incidence velocity of the blade element will vary.

Preliminary results of tests performed with a non-axisymmetrical nozzle at different shaft inclinations in a cavitation tunnel of the NSMB have shown that an improvement in the cavitation characteristics of the impeller can be obtained. Further investigations will be performed to prove the reliability of this concept.

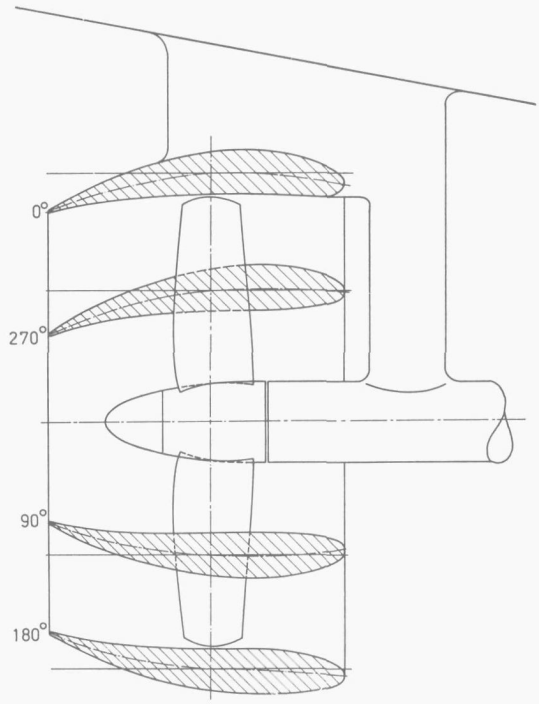

FIG. 84. Particulars of non-axisymmetrical nozzle.

8.4. DUCTED PROPELLER WITH CIRCULATION CONTROL

From tests performed with different ducted propeller systems it was found that the characteristics of the system strongly depend on the ratio between propeller disk area and the exit area of the nozzle. With an increase of the exit area of the nozzle, the circulation around the nozzle profile increases, the nozzle acts more accelerating and gives a larger contribution to the thrust of the ducted propeller system. In addition, the efficiency of the system increases. The loading of the nozzle, however, is restricted by the danger of flow-separation on the nozzle.

The circulation around the nozzle profile and the velocity at the impeller are strongly influenced by the exit area of the nozzle. If it is possible to make the exit area of the nozzle adjustable, for instance by means of a large number of flaps, then such a ducted propeller may operate favourably at different operating conditions, as with a controllable pitch propeller. In addition, it must be possible to deflect the propeller jet and generate transverse forces by an eccentric adjustment of the exit area of the nozzle.

From a practical point of view such a flap mechanism at the trailing edge of the nozzle can hardly be realized. The circulation around the nozzle profile can, however, also be effected by (a combined suction and) injection of water at the trailing edge of the nozzle. Such a concept is shown in the Figs. 85 and 86.

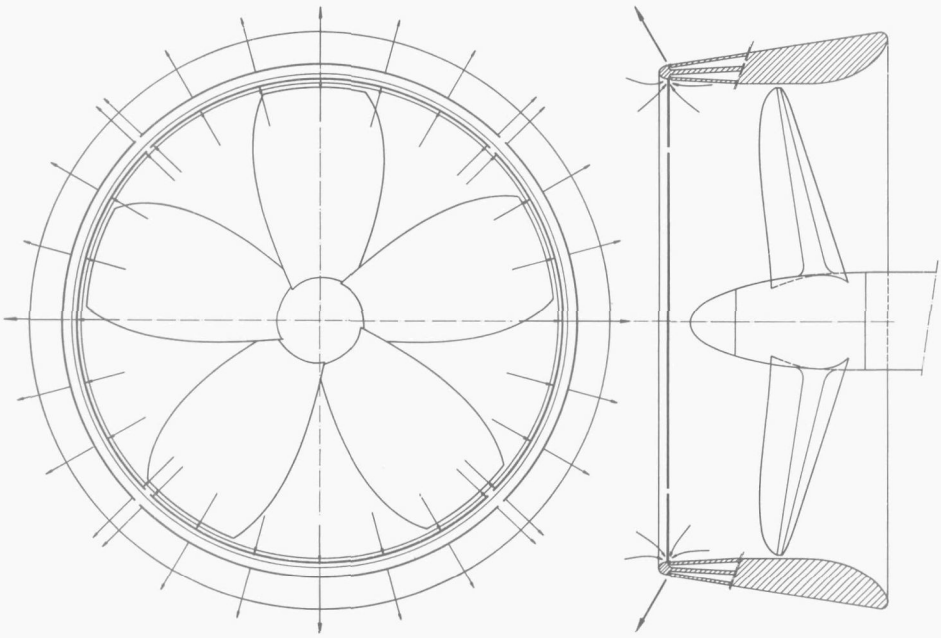

FIG. 85. Nozzle with combined suction and injection of water at the trailing edge of the nozzle.

By a combined suction and injection of water at the trailing edge of the nozzle the following objects can be pursued:

- by injection of water at the exterior surface of the nozzle (eventually combined with water suction at the interior surface) as indicated in Fig. 85, the circulation around the nozzle will be increased. The nozzle acts more accelerating, the thrust of the nozzle increases and the efficiency of the system becomes probably higher.
- the suction and injection of water along the trailing edge of the nozzle at the interior or exterior surface offers a means to accelerate or decelerate the inflow velocity to the impeller. By a proper choice of the flow rate through the slit at the trailing edge the inflow velocity of the impeller can be kept constant at different speeds of the ship.

  Thus the screw can absorb the full power at constant rpm at different ship speeds. This is attractive for tugs and trawlers (towing and free running condition) but also for cargo ships (loaded and ballast condition, added resistance in waves).
- non-axisymmetrical suction and injection of water along the trailing edge of the nozzle, as shown in Fig. 86, offers a means of deflecting the propeller jet. Consequently a transverse force will act on the nozzle.

  In this way the nozzle can be used for the steering of the ship.

In the near future the qualities of this concept will be determined by performing tests with a ship model fitted with a ducted propeller with circulation control.

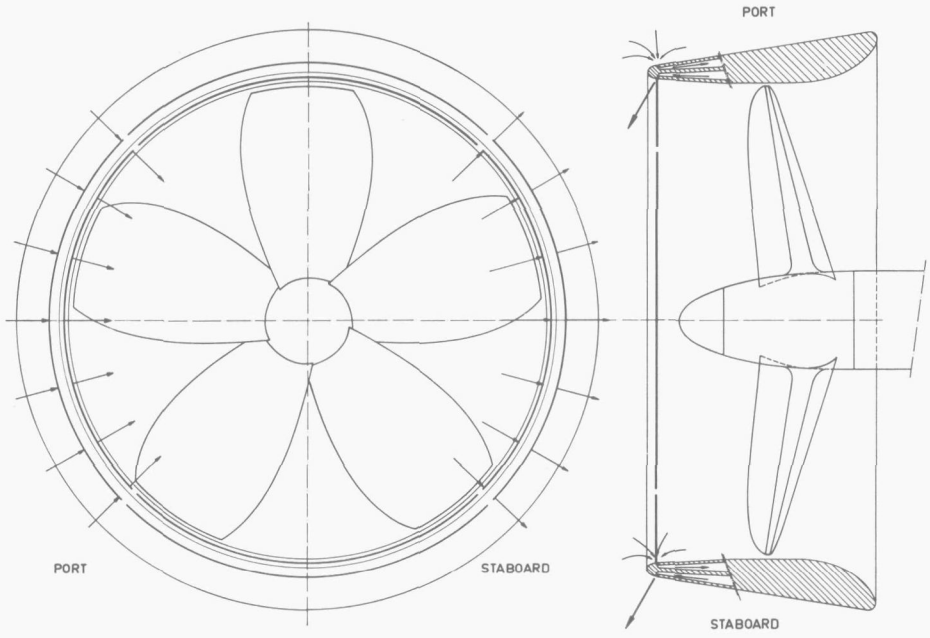

FIG. 86. Nozzle with non-axisymmetrical suction and injection of water at the trailing edge for steering.

9. RINGPROPELLERS

A ringpropeller is a propeller with a ring fitted to the blade tips. This ring rotates with the propeller. The ring may be countersinked in a conventional nozzle or may have a profile similar to the profile of the nozzle of a ducted propeller. These two configurations are shown in Fig. 87.

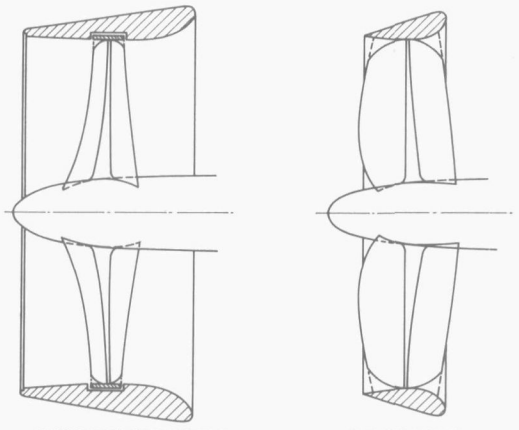

FIG. 87. Particulars of ringpropellers.

It was concluded in section 4 that the use of a nozzle only leads to an increase of the efficiency at higher screw loads, where the gain in ideal efficiency exceeds the loss in efficiency due to the frictional nozzle drag. It is clear that in the case of the ringpropeller a substantial additional drag acts in circumferential direction on the rotating nozzle. This extra torque will decrease the efficiency of the ringpropeller in comparison with a conventional ducted propeller system.

In order to investigate the effect of the additional drag of the rotating ring on the overall efficiency, calculations have been carried out for a series of ringpropellers in nozzle no. 19A. If we neglect the tangential induced velocities due to the impeller then the following relations hold for the axial and tangential flow velocities with respect to the nozzle ring:

$$\frac{V_P}{V_A} = \frac{C_T}{2\,[-1 + \sqrt{1 + \tau C_T}]}$$

and

$$\frac{V_t}{V_A} = \frac{\pi}{J}$$

and the decrease in thrust and increase in torque due to the rotating ring may be written as:

$$\Delta C_T = 4\, C_f \frac{b}{D} \left(\frac{V_P}{V_A}\right)^2$$

and

$$\Delta C_Q = 2\, C_f \frac{b}{D} \left(\frac{V_t}{V_A}\right)^2$$

where C_f is the turbulent skin-friction drag coefficient.

For a Ka 4-70 ring propeller screw in nozzle no. 19A, for instance, we can derive the relationship between B_P and η_o from the test results with the corresponding Ka 4-70 series screw in nozzle no. 19A by taking into account the additional drag of the rotating ring with:

$$\left[B_P\right]_{ring\ propeller} = \sqrt{1 + \frac{\Delta C_Q}{C_Q}}\, B_P$$

$$\left[\eta_o\right]_{ring\ propeller} = \frac{1 - \Delta C_T/C_T}{1 + \Delta C_Q/C_Q}\, \eta_o$$

where C_T, C_Q, J, B_P and η_o correspond with the considered Ka 4-70 series screw.

Calculations of the relationship between B_P and η_o of the ring propeller series have been made and the result is given in Fig. 88. From this diagram it can be seen that over the whole range of operating conditions the efficiency losses due to the additional drag of the rotating ring are substantial. Consequently, the rotating ring must be made as short as possible.

Model tests have been performed with a systematic series of ring propellers in combination with nozzle no. 19A. Propeller models of the existing Ka 4-70 series (pitch ratios $P/D = 0.6$; 0.8; 1.0; 1.2 and 1.4) were used for these tests. Each model was provided with a ring attached to the blade tips. Particulars of the Ka 4-70 ring propeller series in nozzle no. 19A are given in Fig. 89.

The tests were carried out with the usual tank apparatus for open-water tests with ducted propellers. The usual routine of open-water tests was followed; the rpm of the screw was kept constant and by varying the speed of advance the desired value of the advance coefficient J was obtained. The open-water test results were faired and plotted in the conventional way with the coefficients K_T K_{TN}, K_Q and η_o as functions of the advance coefficient J. The diagram is given in Fig. 90.

In addition, open-water tests have been conducted with a series of ringpropellers where the ring did have a profile similar to the shape of the nozzle of a ducted pro-

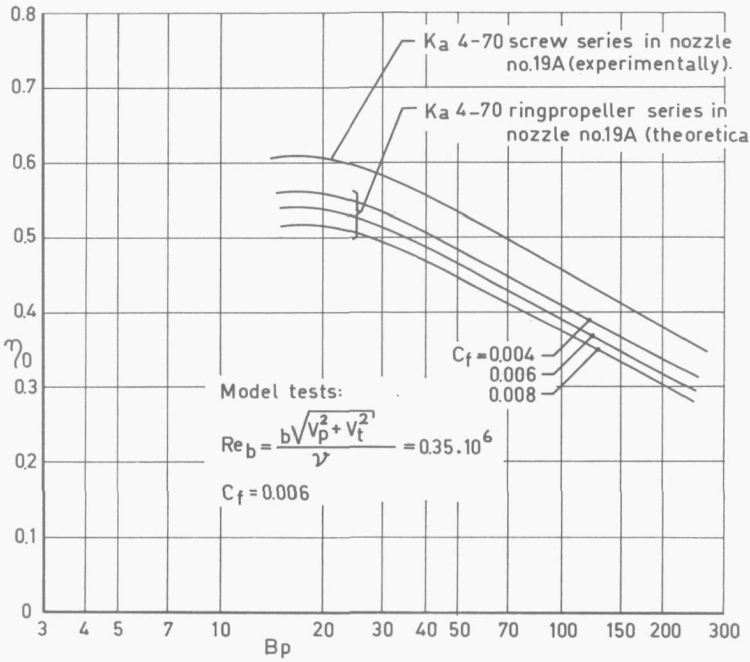

FIG. 88. Efficiency of ringpropeller series in nozzle taking into account the additional drag of the rotating ring.

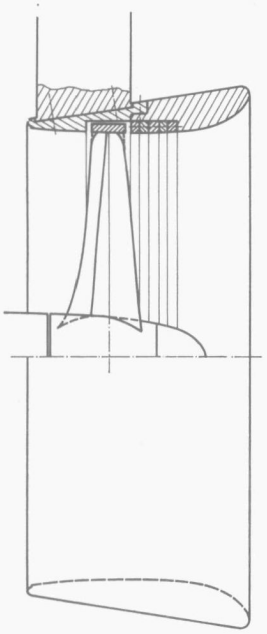

FIG. 89. Particulars of Ka 4–70 ringpropeller series in nozzle no. 19A

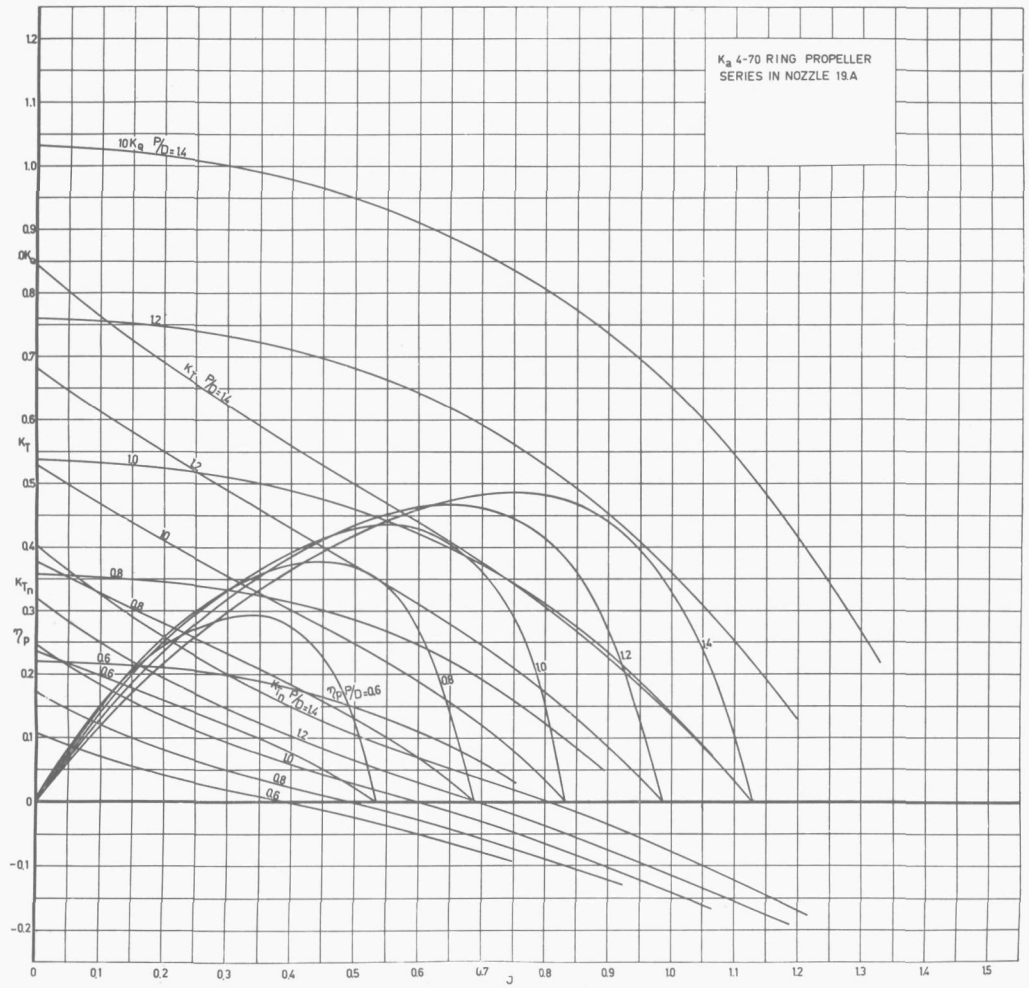

FIG. 90. Open-water test results of Ka 4–70 ringpropeller series in nozzle no. 19A.

peller. The particulars of the ring and of the four bladed propellers with a blade-area ratio of 0.55 are given in Fig. 91. This ringpropeller series was called the R 4-55 series. The results of these investigations were already given by VAN GUNSTEREN (28) and KELLER (29). The open-water test results of this series were faired and plotted in the conventional way with the coefficients K_T, K_Q and η_o as functions of J. The diagram is given in Fig. 92.

Finally, open-water tests have been carried out with a multiple nozzle arrangement with ringpropeller and ringstator proposed by VAN GUNSTEREN. The forward part of the nozzle ring is fixed and is fitted to a stator. This stator has 7 adjustable vanes. The aft part of the nozzle ring is fitted to the blade tips of a screw propeller. This ring is rotating with the propeller. This ducted propeller system is shown in Fig. 93.

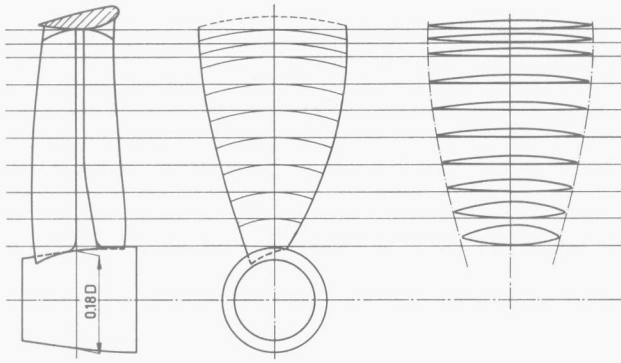

	P_r/D				
r/R	$P/D=1.0$	$P/D=1.2$	$P/D=1.4$	$P/D=1.6$	$P/D=1.8$
1.0	1.45	1.47	1.49	1.51	1.54
0.95	1.31	1.39	1.36	1.54	1.62
0.9	1.20	1.32	1.44	1.56	1.68
0.8	1.03	1.22	1.40	1.58	1.76
0.7	0.99	1.15	1.37	1.60	1.82
0.6	0.86	1.11	1.36	1.62	1.87
0.5	0.82	1.09	1.37	1.64	1.91
0.4	0.79	1.08	1.38	1.66	1.95
0.3	0.78	1.08	1.39	1.69	1.99
0.2	0.78	1.09	1.40	1.72	1.99

FIG. 91. Particulars of R 4–55 ringpropeller series.

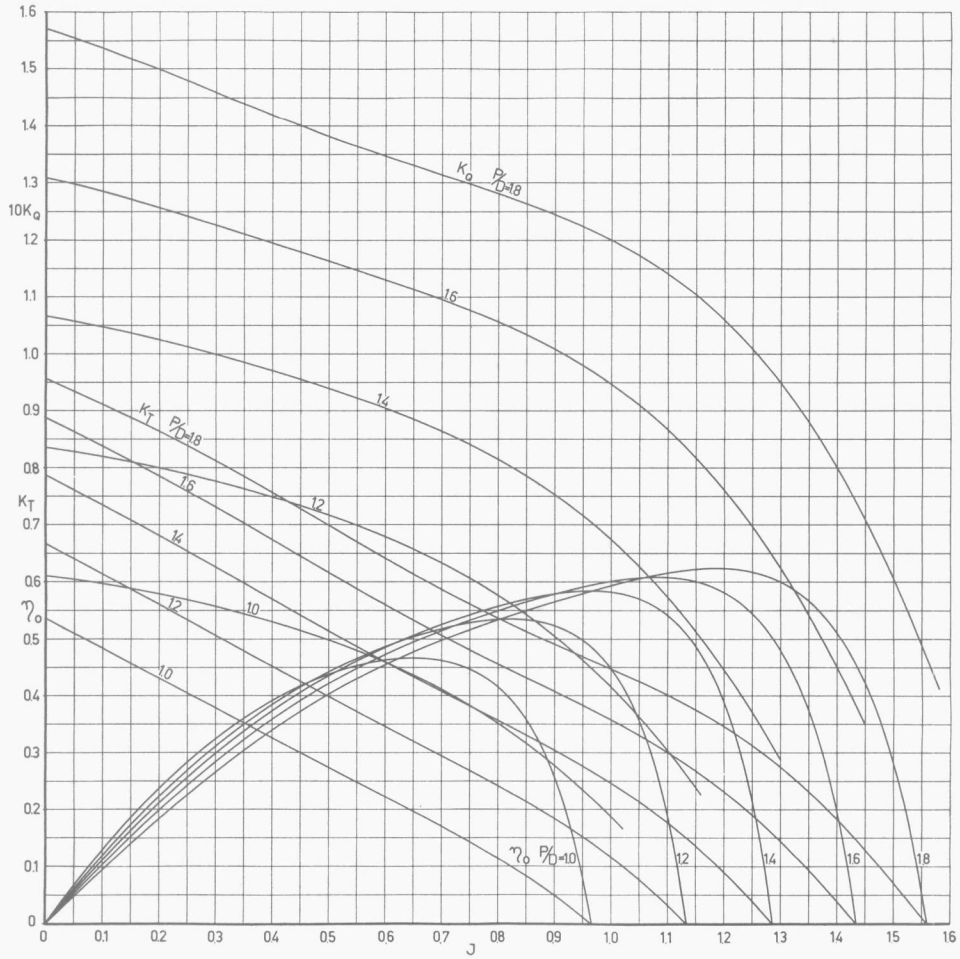

FIG. 92. Open-water test results of R 4–55 ringpropeller series.

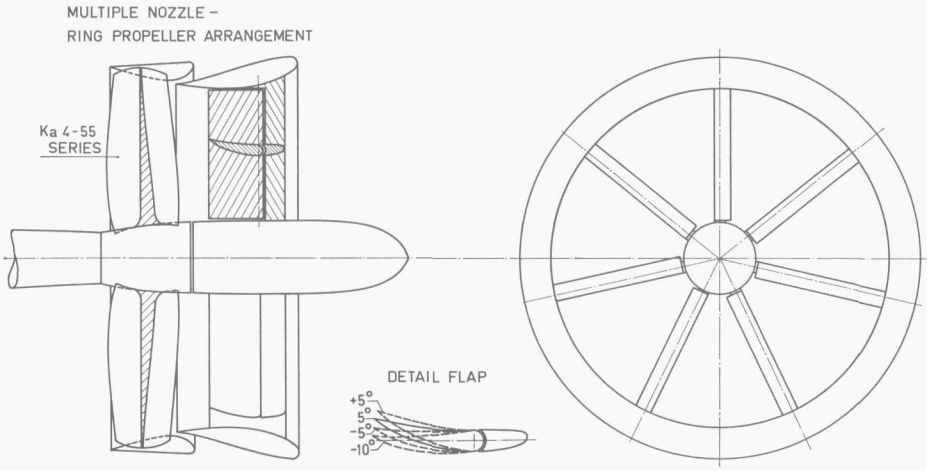

FIG. 93. Particulars of multiple nozzle-ringpropeller system.

Due to the fact that the nozzle profile has a slot, the nozzle may be very heavily loaded. Therefore, a strongly flow accelerating type of nozzle profile was chosen with a relatively large nozzle exit area. By giving different angles to the vanes of the stator, the system acts more or less like a controllable pitch propeller. So the system may operate satisfactorily at different loading conditions.

Tests were conducted with this system with screws of the Ka 4-55 series with pitch ratios of $P/D = 1.2$; 1.4 and 1.6 fitted to the aft rotating part of the nozzle. The vanes were designed such that at zero angle setting all the rotation was taken out of the flow by the screw with $P/D = 1.4$ and for the advance coefficient $J = 0.35$. In addition, tests were carried out with the screw with $P/D = 1.4$ and with the vanes at different angle settings. The test results are given in the Figs. 94 and 95.

As a comparison the optimum curves for open-water efficiency η_o and diameter coefficient δ of the B 4-70 screw series, the Ka 4-70 screw series in nozzle no. 19A, the Ka 4-70 ring propeller series in nozzle no. 19A, the R 4-55 ringpropeller series and the multiple nozzle-ring propeller system are presented on a base of the power coefficient B_P in Fig. 96.

It can be seen from the diagram that all ducted propeller systems with a part or the total nozzle ring attached to the propeller tips have a lower open-water efficiency than the conventional ducted propeller and the conventional screw series. The decrease in efficiency can be explained by the increase of the frictional drag of the system due to the drag of the ring attached to the propeller tips. The efficiency losses due to the increase in frictional drag pointed out to be more important than the gain in efficiency due to the reduced tip clearance losses over the range of screw loads considered. It can also be seen from Fig. 96 that the ducted propeller systems with a ring attached to the blade tips have a lower optimum diameter than the conventional ducted propeller and conventional screw series.

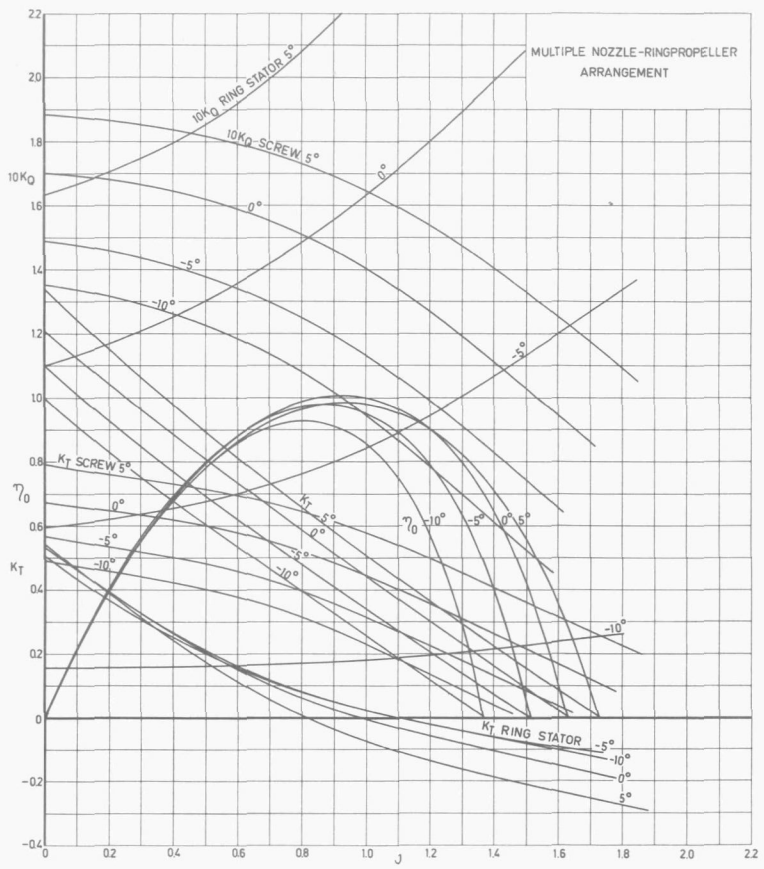

FIG. 95. Open-water test results of multiple nozzle-ringpropeller system.

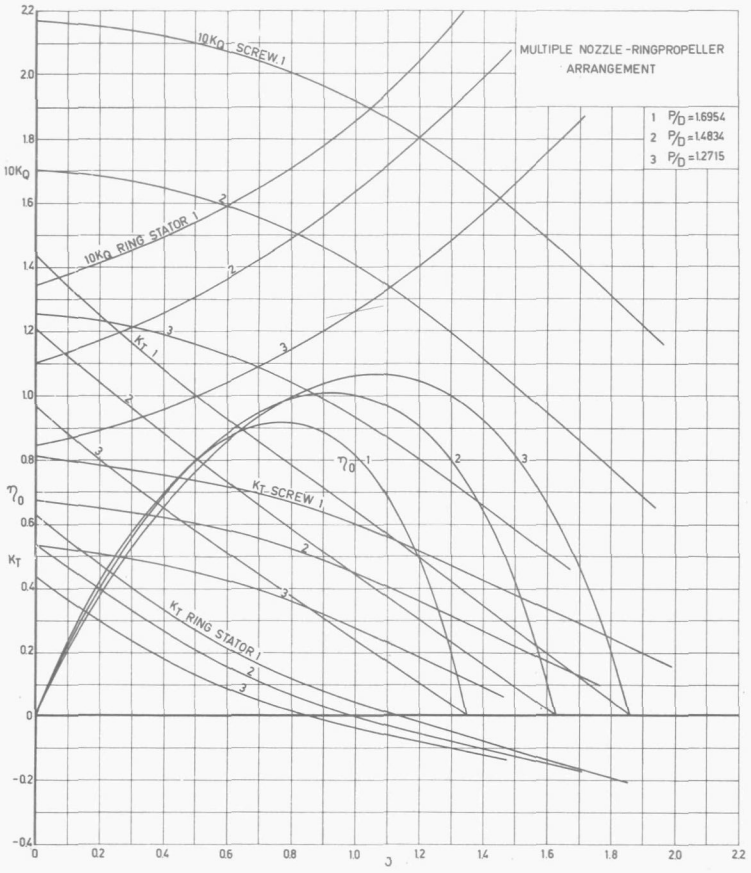

FIG. 94. Open-water test results of multiple nozzle-ringpropeller system.

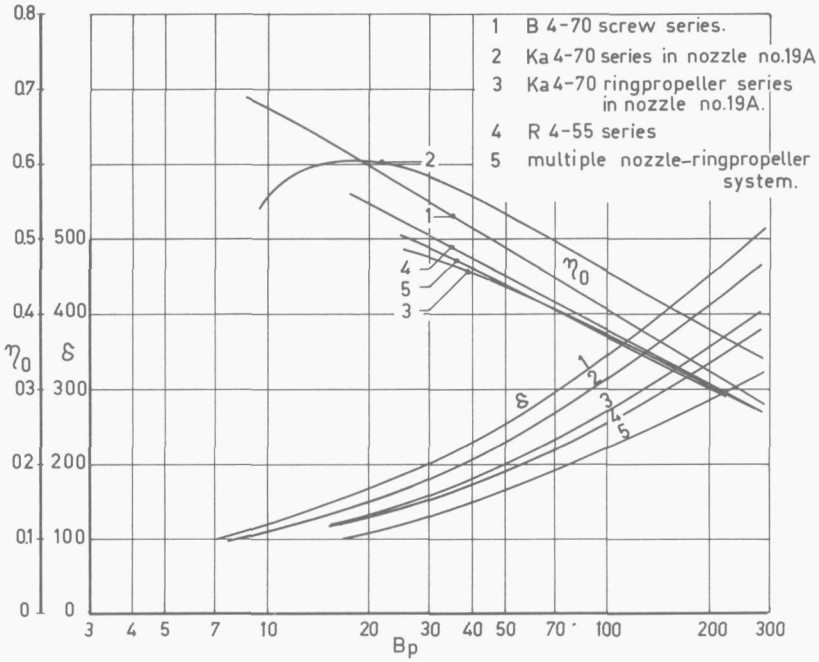

FIG. 96. Optimum relationship between η_o, δ and B_P of B 4–70 screw series, Ka 4–70 screw series in nozzle no. 19 A, the Ka 4–70 *ring*propeller series in nozzle no. 19 A, the R 4–55 series and the multiple nozzle-ringpropeller system.

Finally, the thrust which can be developed at bollard pull condition with the impeller running ahead was calculated for all these ducted propeller configurations. The calculations were carried out for a power absorption of 5000 HP and a maximum diameter of the system of 4 meters. For each system the pitch ratio of the impeller was so chosen that the thrust-power ratio at bollard pull condition was the greatest. The results are given in Table 12.

From this table it can be seen that for the bollard pull condition, the Ka 4-70 series screw in nozzle no. 19A and the multiple nozzle ring propeller system have the largest thrust-power ratios. However, also the Ka 4-70 ring propeller series in nozzle no. 19A

TABLE 12. Thrust at bollard pull condition for different ducted propeller configurations

$D = 4$ m $P = 5000$ HP	P/D	T (kg)	T/HP
B 4-70 screw series	0.70	52400	10.5
Ka 4-70 series in nozzle no. 19A	1.10	68000	13.6
Ka 4-70 ringpropeller series in nozzle no. 19A	1.20	57400	11.5
R 4-55 ringpropeller series	1.25	56600	11.3
Multiple nozzle with ring stator and screw	1.70	65500	13.1

and the R 4-55 series have larger thrust-power ratios than the conventional B 4-70 screw series.

In a recent publication by VAN GUNSTEREN (28) the advantages and disadvantages of ringpropellers were discussed. Advantages of the ringpropeller in comparison with the conventional screw propeller are:

- superior in off-design condition
- good efficiency if the conventional propeller operates at restricted diameter.
- protection of the propeller by the ring (manoeuvring in ice).

However, a disadvantage is, a relatively low efficiency. In comparison with the conventional ducted propeller it can be stated that the ringpropeller has a lower price, there are no problems of fitting a nozzle to the hull and there are no tip clearance problems (cavitation, centering and so on). For coasters and trawlers, for instance, the application of ringpropellers may be attractive.

Recently, a special type of ring propeller system has been proposed by SPARENBERG (39). This system has a ring around the blades of which the profile varies circumferentially. The basic idea is that in this way the strong trailing vortices of the blades can be evenly spread, resulting in a gain in efficiency. In other words, due to the finite number of screw blades there will be a variation in the velocities in circumferential direction in the wake of a screw. This variation will lead to additional kinetic energy losses. By designing the nozzle in such a way that the flow between the blades will be more accelerated than at the blades the flow in the slipstream will be more uniform. Probably a small increase in efficiency can be obtained by application of such a ring nozzle. However, the production of this nozzle ring seems quite difficult and expensive.

10. CONCLUSIONS

As a result of the investigations the following conclusions can be made:

1. The accelerating nozzle offers a means of improving the efficiency of a propulsion system at heavier screw loads ($C_T >$ 2-3). The nozzle which accelerates the flow as much as possible is the best from the viewpoint of efficiency. This nozzle has the lowest impeller thrust-total thrust ratio τ. The loading of the nozzle and consequently the acceleration of the flow is limited, however, by the risk of flow separation on the nozzle.
2. Application of a decelerating nozzle improves the cavitation properties of a propulsion system if the gain in static pressure compensates the unfavourable effect of the increased screw loading. This is the case for lightly loaded screws with normal blade area ratios and number of blades.
3. Ducted propellers have a fixed relation between the thrust coefficient C_T, the thrust ratio τ and the impeller area-nozzle exit area ratio, which is approximately independent of the particulars (for instance pitch ratio) of the impeller considered. This relation determines the range of application of the nozzle.
4. The ducted propeller system with a nozzle ring which is partly or completely fitted to the impeller blades has a relatively low efficiency due to the additional drag of the rotating nozzle ring. The system has, however, a reasonable thrust-horsepower ratio at bollard pull condition. For some types of ships (coasters, trawlers) the application of a ring propeller has attractive features.
5. The application of a wake adapted or non-axisymmetrical nozzle behind a full single screw ship (tanker, bulkcarrier) offers a means of making the inflow velocity of the propeller more constant over the screw disk. Consequently, this nozzle should minimize problems concerning propeller induced vibrations and cavitation. In addition, the applications of such a nozzle leads to a reduction in DHP.
6. In the case of twin-screw ships, a non-axisymmetrical nozzle offers a means of minimizing the actual effective incidence changes of a blade section during a revolution. Consequently, the non-axisymmetrical nozzle improves the cavitation properties of the screw. This is of particular importance for fast naval ships.
7. For the design of ducted propeller systems it is attractive to have a calculation method available supported by systematic experiments. Tests on ducted propellers were scarce. The results of the systematic tests presented here may help to fill up the lack of experimental data on ducted propellers.

Appendix

THEORETICAL ANALYSIS OF DUCTED PROPELLERS

1. Representation of ducted propellers by vortex distributions

The calculations of the ducted propellers were based on the following assumptions. The forward velocity was assumed to be sufficiently large, the nozzle loading sufficiently low to permit the application of the linearized theory. The effect of the hub shape on the flow field was neglected. The ducted propeller system considered consists of an annular airfoil of finite length and of an impeller having an infinite number of blades.

The mathematical model of the ducted propeller configuration can be composed by means of vortex distributions and sink and source distributions. The impeller was regarded as a uniformly loaded actuator disk set normal to the free stream. It was driven to rotate with an angular velocity ω. Free trailing vortices started from the propeller disk at hub and tip radius. The flow around the nozzle was represented by a sinusoidal bound ring vortex distribution with zero strength at the leading and trailing edges and by a ring vortex distribution with zero strength at the leading edge and equal to the strength of the circumferential component of the helical trailing vortices at the impeller disk.

The resulting mathematical model is summarized in Fig. 8.

Assume the vortex strength per unit impeller disk area at the impeller tip to be equal to $\gamma(R_1)$, the strength of the different vortex distributions then becomes:

- vortex strength per unit impeller disk area:

$$\gamma(r) = \frac{R_1}{r}\gamma(R_1)$$

- strength per unit area of the trailing vortex sheet starting from the impeller disk at the tip radius:

$$\sqrt{1+\mu^2}\cdot\gamma(R_1)$$

- strength per unit area of the trailing vortex sheet starting from the impeller disk at the hub radius:

$$\sqrt{1+\mu^2\lambda^2}\cdot\frac{1}{\lambda}\gamma(R_1)$$

- strength per unit area of the bound ring vortex distribution along the nozzle:

$$\mu\gamma(R_1)\frac{\sin\theta}{2\sqrt{a(1-a)}} \qquad (\text{for } -aL < \times < 0)$$

and

$$\gamma_1 (R_1) \sin \theta \qquad \text{(for } -aL < \times < (1-a)\, L\text{)}$$

where,

$$\mu = \frac{\omega R_1}{V_A};\ \lambda = \frac{R_0}{R_1};\ x + (a - 0.5)\, L = 0.5\, L \cos \theta$$

and the definitions of R_0, R_1, r, x, L, a and so on are given in Fig. 8.

The thickness effect of the nozzle profile on the flow field can be taken into account in the linearized theory by representing the nozzle by a distribution of ring sources and sinks along a cylinder with radius R_1 (see Fig. 8).

In the case of very thin nozzle profiles, as considered here, the strength of the sink and source distributions representing the nozzle profile can be calculated by considering the flow around the profile as two-dimensional.

Then the local source strength is equal to the derivative of the profile thickness:

$$g (\xi) = \frac{dh (\xi)}{d\xi}$$

where $h (\xi)$ denotes the local thickness of the nozzle profile.

2. Calculations of the flow field

The total induced velocities can be calculated according to the law of Biot-Savart if the main dimensions of the ducted propeller system (R_0, R_1, L and a), the thickness distribution of the nozzle ($h (\xi)$), the loading of duct and impeller ($\gamma (R_1)$) and ($\gamma_1 (R_1)$), the rotational velocity of the impeller (ω) and the undisturbed stream velocity (V_A) are given. In the following, we will give the induced velocities in the point (x, r) of the flow field due to the various vortex distributions and the source and sink distributions.

The relations are made non-dimensional in the following way:

$$\bar{x} = \frac{x}{R_1} \qquad \bar{\xi} = \frac{\xi}{R_1} \qquad \bar{r} = \frac{r}{R_1} \qquad \lambda = \frac{R_0}{R_1} \qquad \eta = \frac{L}{R_1}$$

$$\bar{\gamma} = \frac{\gamma (R_1)}{V_A} \qquad \bar{\gamma}_1 = \frac{\gamma_1 (R_1)}{V_A} \qquad \bar{g} (\bar{\xi}) = \frac{g (\xi)}{V_A} \qquad \bar{h} (\xi) = \frac{h (\xi)}{R_1}$$

$$\overline{W}_{a,t \text{ or } r} = \frac{W_{a,t \text{ or } r}}{V_A}$$

where a, t and r denote the axial, tangential and radial induced velocities respectively.

(1) Induced velocities due to the vortices representing the impeller disk

$$\overline{W}_a^{(1)}(\bar{x},\bar{r}) = 0$$

$$\overline{W}_t^{(1)}(\bar{x},\bar{r}) = \bar{\gamma} A_{1,1}(\bar{x},\bar{r})$$

$$\overline{W}_r^{(1)}(\bar{x},\bar{r}) = 0$$

$$A_{1,1}(\bar{x},\bar{r}) = \frac{1}{\pi}\int_{\lambda}^{1} d\bar{r}_1 \int_0^{\pi/2} d\psi \, \frac{\bar{x}\cos 2\psi}{[\bar{x}^2 + (\bar{r}_1 + \bar{r})^2 - 4\bar{r}_1\bar{r}\sin^2\psi]^{3/2}}$$

(2) Induced velocities due to the trailing vortex sheet starting from the impeller disk at the tip radius

$$\overline{W}_a^{(2)}(\bar{x},\bar{r}) = \mu\bar{\gamma} A_{2,1}(\bar{x},\bar{r})$$

$$\overline{W}_t^{(2)}(\bar{x},\bar{r}) = \bar{\gamma} A_{2,2}(\bar{x},\bar{r})$$

$$\overline{W}_r^{(2)}(\bar{x},\bar{r}) = \mu\bar{\gamma} A_{2,3}(\bar{x},\bar{r})$$

$$A_{2,1}(\bar{x},\bar{r}) = \frac{1}{\pi}\int_0^{\infty} d\tau \int_0^{\pi/2} d\psi \, \frac{\mu^2(1 + \bar{r}\cos 2\psi)}{[\{\mu\bar{x} - \tau\}^2 + \mu^2\{(1 + \bar{r})^2 - 4\bar{r}\sin^2\psi\}]^{3/2}}$$

$$A_{2,2}(\bar{x},\bar{r}) = \frac{1}{\pi}\int_0^{\infty} d\tau \int_0^{\pi/2} d\psi \, \frac{\mu(\bar{r} + \cos 2\psi)}{[- - - - - - - - - - - - - - - -]^{3/2}}$$

$$A_{2,3}(\bar{x},\bar{r}) = -\frac{1}{\pi}\int_0^{\infty} d\tau \int_0^{\pi/2} d\psi \, \frac{\mu[\mu\bar{x} - \tau]\cos 2\psi}{[- - - - - - - - - - - - - - - -]^{3/2}}$$

(3) Induced velocities due to the trailing vortex sheet starting from the impeller disk at the hub radius:

$$\overline{W}_a^{(3)}(\bar{x},\bar{r}) = \mu\bar{\gamma} A_{3,1}(\bar{x},\bar{r})$$

$$\overline{W}_t^{(3)}(\bar{x},\bar{r}) = \bar{\gamma} A_{3,2}(\bar{x},\bar{r})$$

$$\overline{W}_r^{(3)}(\bar{x},\bar{r}) = \mu\bar{\gamma} A_{3,3}(\bar{x},\bar{r})$$

$$A_{3,1}(\bar{x},\bar{r}) = -\frac{1}{\pi}\int_0^{\infty} d\tau \int_0^{\pi/2} d\psi \, \frac{\lambda\mu^2(\lambda + \bar{r}\cos 2\psi)}{[\{\mu\bar{x} - \tau\}^2 + \mu^2\{(\lambda + \bar{r})^2 - 4\lambda\bar{r}\sin^2\psi\}]^{3/2}}$$

$$A_{3,2}(\bar{x},\bar{r}) = -\frac{1}{\pi}\int_0^{\infty} d\tau \int_0^{\pi/2} d\psi \frac{\mu^2(\bar{r} + \lambda\cos 2\psi)}{[- - - - - - - - - - - - - - - -]^{3/2}}$$

$$A_{3,3}(\bar{x},\bar{r}) = \frac{1}{\pi}\int_0^{\infty} d\tau \int_0^{\pi/2} d\psi \frac{\lambda\mu[\mu\bar{x} - \tau]\cos 2\psi}{[- - - - - - - - - - - - - - - -]^{3/2}}$$

(4) Induced velocities due to the discontinuous ring vortex distributions along the nozzle:

$$\overline{W}_a^{(4)}(\bar{x},\bar{r}) = \mu\bar{\gamma}A_{4,1}(\bar{x},\bar{r})$$

$$\overline{W}_t^{(4)}(\bar{x},\bar{r}) = 0$$

$$\overline{W}_r^{(4)}(\bar{x},\bar{r}) = \mu\bar{\gamma}A_{4,3}(\bar{x},\bar{r})$$

$$A_{4,1}(\bar{x},\bar{r}) = \frac{1}{2\pi\sqrt{a(1-a)}}\int_{-a\eta}^{0} d\bar{\xi}\int_0^{\pi/2} d\psi \frac{(1 + \bar{r}\cos 2\psi)\sin\theta}{[(\bar{x} - \bar{\xi})^2 + (1 + \bar{r})^2 - 4\bar{r}\sin^2\psi]^{3/2}}$$

$$A_{4,3}(\bar{x},\bar{r}) = \frac{-1}{2\pi\sqrt{a(1-a)}}\int_{-a\eta}^{0} d\bar{\xi}\int_0^{\pi/2} d\psi \frac{(\bar{x} - \bar{\xi})\cos 2\psi}{[- - - - - - - - - - - -]^{3/2}}$$

(5) Induced velocities due to the sinusoidal ring vortex distribution along the nozzle:

$$\overline{W}_a^{(5)}(\bar{x},\bar{r}) = \bar{\gamma}_1 A_{5,1}(\bar{x},\bar{r})$$

$$\overline{W}_t^{(5)}(\bar{x},\bar{r}) = 0$$

$$\overline{W}_r^{(5)}(\bar{x},\bar{r}) = \bar{\gamma}_1 A_{5,3}(\bar{x},\bar{r})$$

$$A_{5,1}(\bar{x},\bar{r}) = \frac{1}{\pi}\int_{-a\eta}^{(1-a)\eta} d\bar{\xi}\int_0^{\pi/2} d\psi \frac{(1 + \bar{r}\cos 2\psi)\sin\theta}{[(\bar{x} - \bar{\xi})^2 + (1 + \bar{r})^2 - 4\bar{r}\sin^2\psi]^{3/2}}$$

$$A_{5,3}(\bar{x},\bar{r}) = -\frac{1}{\pi}\int_{-a\eta}^{(1-a)\eta} d\bar{\xi}\int_0^{\pi/2} d\psi \frac{(\bar{x} - \bar{\xi})\cos 2\psi\sin\theta}{[- - - - - - - - - - - -]^{3/2}}$$

(6) Induced velocities due to the ring sources and sinks along the nozzle representing the thickness of the nozzle:

$$\overline{W}_a^{(6)}(\bar{x},\bar{r}) = \frac{1}{\pi}\int_{-a\eta}^{(1-a)\eta} d\bar{\xi} \int_0^{\pi/2} d\psi\, \bar{g}(\bar{\xi}) \frac{(\bar{x}-\bar{\xi})}{[(\bar{x}-\bar{\xi})^2 + (1+\bar{r})^2 - 4\bar{r}\sin^2\psi]^{3/2}} = A_{6,1}(\bar{x},\bar{r})$$

$$\overline{W}_t^{(6)}(\bar{x},\bar{r}) = 0$$

$$\overline{W}_r^{(6)}(\bar{x},\bar{r}) = \frac{1}{\pi}\int_{-a\eta}^{(1-a)\eta} d\bar{\xi} \int_0^{\pi/2} d\psi\, \bar{g}(\bar{\xi}) \frac{(\bar{r}+\cos 2\psi)}{[(\bar{x}-\bar{\xi})^2 + (1+\bar{r})^2 - 4\bar{r}\sin^2\psi]^{3/2}} = A_{6,3}(\bar{x},\bar{r})$$

The total induced velocities may be written as:

$$\overline{W}_a(\bar{x},\bar{r}) = \mu\bar{\gamma}A_1(\bar{x},\bar{r}) + \bar{\gamma}_1 A_2(\bar{x},r) + A_6(\bar{x},\bar{r})$$
$$A_1(\bar{x},\bar{r}) = A_{2,1}(\bar{x},\bar{r}) + A_{3,1}(\bar{x},\bar{r}) + A_{4,1}(\bar{x},\bar{r})$$
$$A_2(\bar{x},\bar{r}) = A_{5,1}(\bar{x},\bar{r})$$
$$A_6(\bar{x},\bar{r}) = A_{6,1}(\bar{x},\bar{r})$$

$$\overline{W}_t(\bar{x},\bar{r}) = \bar{\gamma}A_3(\bar{x},\bar{r})$$
$$A_3(\bar{x},\bar{r}) = A_{1,2}(\bar{x},\bar{r}) + A_{2,2}(\bar{x},\bar{r}) + A_{3,2}(\bar{x},\bar{r})$$

$$\overline{W}_r(\bar{x},\bar{r}) = \mu\bar{\gamma}A_4(\bar{x},\bar{r}) + \bar{\gamma}_1 A_5(\bar{x},\bar{r}) + A_7(\bar{x},\bar{r})$$
$$A_4(\bar{x},\bar{r}) = A_{2,3}(\bar{x},\bar{r}) + A_{3,3}(\bar{x},\bar{r}) + A_{4,3}(\bar{x},\bar{r})$$
$$A_5(\bar{x},\bar{r}) = A_{5,3}(\bar{x},\bar{r})$$
$$A_7(\bar{x},\bar{r}) = A_{6,3}(\bar{x},\bar{r})$$

where the coefficients A are functions of $\bar{x}$, $\bar{r}$, the main dimensions of the ducted propeller system (thus R_0, R_1, L and a) and the thickness distributions ($h(\xi)$) of the nozzle only. These coefficients are independent of the vortex densities $\gamma(R_1)$ and $\gamma_1(R_1)$ and the advance coefficient μ.

3. Calculation of the camberline of the nozzle profile

The shape of the camberline of the nozzle profile can be obtained from the relation:

$$\frac{ds(x)}{dx} = \frac{W_r(x,R_1)}{V_A + W_a(x,R_1)} \quad \text{or} \quad s(x) = \int_0^x \frac{W_r(\xi,R_1)}{V_A + W_a(\xi,R_1)}\, d\xi \tag{1}$$

where the definition of $s(x)$ is given in Fig. 8.

4. Pressure distribution along the nozzle

With the aid of Bernoulli's theorem the pressure distribution along the nozzle can be calculated. The static pressure coefficients $C_P{}^+(x)$ and $C_P{}^-(x)$ are defined by:

$$C_p^+(x) = \frac{P_{(x)}^+ - P_\infty}{\frac{1}{2}\rho V_A^2}$$

$$C_p^-(x) = \frac{P_{(x)}^- - P_\infty}{\frac{1}{2}\rho V_A^2}$$

P_∞ and V_A are the static pressure and the velocity of the undisturbed flow, $P^+(x)$ and $P^-(x)$ are the static pressure at respectively the inner and outer side of the nozzle as a function of the location.

Calculation of the pressure distribution along the nozzle gives:

$$C_p^+(x) = \mu\bar{\gamma}\left[\frac{R_1 \sin\theta}{2\sqrt{a(1-a)}} + R_2 - 2A_1(\bar{x},1)\right] + \bar{\gamma}_1[\sin\theta - 2A_2(\bar{x},1)] - 2A_6(\bar{x},1) \tag{2}$$

$$C_p^-(\bar{x}) = \mu\bar{\gamma}\left[-\frac{R_1 \sin\theta}{2\sqrt{a(1-a)}} - R_2 - 2A_1(\bar{x},1)\right] + \bar{\gamma}_1[-\sin\theta - 2A_2(\bar{x},1)] - 2A_6(\bar{x},1) \tag{3}$$

where,

$$R_1 = 1 \quad R_2 = 0 \quad \text{for} \quad -a\eta < \bar{x} < 0$$
$$R_1 = 0 \quad R_2 = 1 \quad \text{for} \quad 0 < \bar{x} < (1-a)\eta$$

5. Calculation of thrust, torque and efficiency

The non-dimensional thrust and torque coefficients are defined by

$$C_T = \frac{T}{\frac{1}{2}\rho V_A^2 \frac{\pi}{4} D^2} \qquad C_{TP\ or\ N} = \frac{T_{P\ or\ N}}{\frac{1}{2}\rho V_A^2 \frac{\pi}{4} D^2}$$

$$C_Q = \frac{Q}{\frac{1}{2}\rho V_A^2 \frac{\pi}{4} D^2 D} \qquad \tau = \frac{T_P}{T} = \frac{C_{TP}}{C_T}$$

where T, T_P, T_N and Q denote the total thrust, the impeller thrust, the nozzle thrust and the torque respectively.

The thrust and torque coefficients become:

$$C_{TP} = 2\mu\bar{\gamma}\,(1 - \lambda^2) + 4\bar{\gamma}^2 \int_{\lambda}^{1} A_3\,(\bar{o},\bar{r})\,d\bar{r} \tag{4}$$

$$\begin{aligned} C_{TN} = {} & \bar{\gamma}_1^2 \left[-4 \int_{-a\eta}^{(1-a)\eta} A_5\,(\bar{x},1) \sin\theta\, d\bar{x} \right] + \\ & \bar{\gamma}_1 \left[\mu\bar{\gamma} \left\{ -\frac{2}{\sqrt{a\,(1-a)}} \int_{-a\eta}^{0} A_5\,(\bar{x},1) \sin\theta\, d\bar{x} - 4 \int_{-a\eta}^{(1-a)\eta} A_4\,(\bar{x},1) \sin\theta\, d\bar{x} \right\} \right. \\ & \left. + \left\{ -4 \int_{-a\eta}^{(1-a)\eta} A_7\,(\bar{x},1) \sin\theta\, d\bar{x} + 8 \int_{-a\eta}^{(1-a)\eta} A_2\,(\bar{x},1) \frac{dh(\bar{x})}{d\bar{x}}\, d\bar{x} \right\} \right] + \\ & 1. \left[(\mu\gamma)^2 \left\{ -\frac{2}{\sqrt{a\,(1-a)}} \int_{-a\eta}^{0} A_4\,(\bar{x},1) \sin\theta\, d\bar{x} \right\} + \right. \\ & \mu\bar{\gamma} \left\{ -\frac{2}{\sqrt{a(1-a)}} \int_{-a\eta}^{o} A_7\,(\bar{x},1) \sin\theta\, d\bar{x} + 4\bar{h}(0) + \right. \\ & \left. \left. 8 \int_{-a\eta}^{(1-a)\eta} A_1\,(\bar{x},1) \frac{d\bar{h}(\bar{x})}{d\bar{x}}\, d\bar{x} \right\} + \right. \\ & \left. 1. \left\{ 8 \int_{-a\eta}^{(1-a)\eta} A_6\,(\bar{x},1) \frac{d\bar{h}(\bar{x})}{d\bar{x}}\, d\bar{x} \right\} \right] \end{aligned} \tag{5}$$

$$C_T = C_{TP} + C_{TN} \tag{6}$$

$$C_Q = \frac{1}{\mu} \{(1 - \lambda^2)\,\mu\bar{\gamma} + 2 \int_{\lambda}^{1} \mu\bar{\gamma}\,[\mu\bar{\gamma} A_1\,(0,\bar{r}) + \bar{\gamma}_1 A_2\,(0,\bar{r}) + A_6\,(0,\bar{r})]\,\bar{r}\,d\bar{r} \tag{7}$$

The efficiency of the ducted propeller system is defined by

$$\eta_i = \frac{1}{2\mu} \cdot \frac{C_T}{C_Q} \tag{8}$$

6. Presentation of the computation results

The shape of the camberline of the nozzle profile $s(x)$, the pressure distribution along the nozzle $C_P{}^+(x)$ and $C_P{}^-(x)$, the thrust and torque coefficients C_{TP}, C_{TN}, C_T and C_Q and the ideal efficiency η_i of the ducted propeller system were given in the relations (1) through (8). From these relations it can be seen that $s(x)$, $C_P{}^+(x)$, $C_P{}^-(x)$, C_{TN} and μC_Q are completely determined by:

- The main dimensions of the ducted propeller system given by R_0, R_1, L and a, and thickness distribution $h(\xi)$ of the nozzle profile.
  the vortex density γ_1,
  the product of the vortex density γ and the advance ratio μ.

The thrust coefficient C_{TP} and consequently the total thrust coefficient C_T and the ideal efficiency η_i depend not only on the product $\mu\bar{\gamma}$ but also on $\bar{\gamma}$.

The impeller is represented by an actuator disk rotating with an *infinite* angular velocity if the undisturbed stream velocity V_A and the product $\mu\bar{\gamma}$ are kept constant and the advance coefficient μ becomes infinite. Then the vortex density $\bar{\gamma}$ goes to zero. Besides, the tangentially induced velocities and consequently the losses due to the rotation of the fluid become zero. The case that the actuator disk rotates with an infinite angular velocity coincides with the case that the actuator disk or the impeller rotates with finite angular velocity while a stator is used to eliminate the rotational losses. The total thrust coefficient C_T, the thrust ratio τ and the ideal efficiency η_i in that case are denoted by C_{T0}, τ_0 and η_{i0}.

The shape of the camberline of the nozzle profile is also completely determined by the values of C_{T0}, τ_0 the main dimensions of the ducted propeller system and the thickness distribution of the nozzle profile. Calculations of the thrust coefficient, C_T the thrust ratio τ and the ideal efficiency η_i at various advance coefficients μ were made for a number of nozzle shapes given by C_{T0}, τ_0 the main dimensions of the ducted propeller system, λ, η, a and the thickness distribution of the nozzle profile. In addition, the shapes of the camberlines of the nozzle profiles and the pressure distributions along the nozzle surfaces were calculated. The data used for the computations and the results are given in the tables I, II and III respectively.

Table I presents the thrust coefficients C_{T0}, the thrust ratio τ_0 the main dimensions of the ducted propeller system and the thickness ratio of the nozzle profile for which computations were carried out. All the considered nozzle shapes had a NACA four-digit basic thickness form.

Table II gives the effect of the rotational velocity of the screw on the ideal efficiency η_i, the thrust coefficient C_T and the thrust ratio τ of the ducted propeller systems.

Finally, Table III presents the mean lines and the pressure distributions along the nozzles of the various ducted propellers. In addition, the ideal efficiency η_i for $J = 0$ (η_{i0}) is given in this table.

TABLE I. Thrust coefficient C_{T0}, thrust ratio τ_0 and main dimensions of nozzles for which computations were carried out.

nozzle number	C_{T0}	τ_0	L/D	a/L	S/L	d/D
A, 1	0.5	1.0	0.6	0.5	0	0.2
2	0.5	1.0	0.6	0.5	0.15	0.2
3	0.5	1.0	0.3	0.5	0	0.2
4	0.5	1.0	0.3	0.5	0.15	0.2
5	0.5	1.0	0.9	0.5	0	0.2
6	0.5	1.0	0.9	0.5	0.15	0.2
B, 1	0.5	1.2	0.6	0.5	0	0.2
2	0.5	1.2	0.6	0.5	0.15	0.2
3	0.5	1.2	0.3	0.5	0	0.2
4	0.5	1.2	0.3	0.5	0.15	0.2
5	0.5	1.2	0.9	0.5	0	0.2
6	0.5	1.2	0.9	0.5	0.15	0.2
C, 1	0.5	1.4	0.6	0.5	0	0.2
2	0.5	1.4	0.6	0.5	0.15	0.2
3	0.5	1.4	0.3	0.5	0	0.2
4	0.5	1.4	0.3	0.5	0.15	0.2
5	0.5	1.4	0.9	0.5	0	0.2
6	0.5	1.4	0.9	0.5	0.15	0.2
D, 1	1.0	1.0	0.6	0.5	0	0.2
2	1.0	1.0	0.6	0.5	0.15	0.2
3	1.0	1.0	0.3	0.5	0	0.2
4	1.0	1.0	0.3	0.5	0.15	0.2
5	1.0	1.0	0.9	0.5	0	0.2
6	1.0	1.0	0.9	0.5	0.15	0.2
E, 1	1.0	1.2	0.6	0.5	0	0.2
2	1.0	1.2	0.6	0.5	0.15	0.2
3	1.0	1.2	0.3	0.5	0	0.2
4	1.0	1.2	0.3	0.5	0.15	0.2
5	1.0	1.2	0.9	0.5	0	0.2
6	1.0	1.2	0.9	0.5	0.15	0.2
F, 1	1.0	1.4	0.6	0.5	0	0.2
2	1.0	1.4	0.6	0.5	0.15	0.2
3	1.0	1.4	0.3	0.5	0	0.2
4	1.0	1.4	0.3	0.5	0.15	0.2
5	1.0	1.4	0.9	0.5	0	0.2
6	1.0	1.4	0.9	0.5	0.15	0.2

TABLE II. Effect of the advance coefficient J on the thrust coefficient C_T and the thrust ratio τ of the considered nozzle shapes

	Nozzles Nr. A		Nozzles Nr. B		Nozzles Nr. C	
J	C_T/C_{T0}	τ/τ_0	C_T/C_{T0}	τ/τ_0	C_T/C_{T0}	τ/τ_0
0	1.000	1.000	1.000	1.000	1.000	1.000
0.25	0.999	1.000	0.996	1.001	0.995	1.002
0.50	0.989	1.000	0.985	1.003	0.979	1.006
0.75	0.976	1.000	0.966	1.006	0.954	1.013
1.00	0.958	1.000	0.939	1.012	0.917	1.026
1.25	0.935	1.000	0.905	1.017	0.870	1.043
1.50	0.905	1.000	0.862	1.027	0.814	1.066
1.75	0.871	1.000	0.815	1.038	0.748	1.097
2.00	0.831	1.000	0.756	1.054	0.669	1.142

	Nozzles Nr. D		Nozzles Nr. E		Nozzles Nr. F	
J	C_T/C_{T0}	τ/τ_0	C_T/C_{T0}	τ/τ_0	C_T/C_{T0}	τ/τ_0
0	1.000	1.000	1.000	1.000	1.000	1.000
0.25	0.995	1.000	0.992	1.002	0.990	1.003
0.50	0.979	1.000	0.970	1.005	0.959	1.012
0.75	0.953	1.000	0.932	1.013	0.907	1.029
1.00	0.915	1.000	0.878	1.023	0.834	1.057
1.25	0.868	1.000	0.810	1.039	0.741	1.100
1.50	0.809	1.000	0.725	1.063	0.626	1.171
1.75	0.743	1.000	0.630	1.098	0.496	1.291
2.00	0.662	1.000	0.513	1.158	0.337	1.563

TABLE III. Mean lines, pressure distributions along the nozzle profile and ideal efficiency of the considered ducted propeller systems

Nozzle number	η_{i0}	x/R	$s(x)/R$	$C_P{}^+(x)$	$C_P{}^-(x)$
A, 1	0.889	− 0.600	+ 0.030	− 0.072	− 0.072
		− 0.540	+ 0.026	− 0.024	− 0.133
		− 0.480	+ 0.022	− 0.009	− 0.150
		− 0.240	+ 0.010	+ 0.009	− 0.220
		− 0	+ 0	+ 0	— 0.250
		+ 0	+ 0	+ 0	+ 0.250
		+ 0.240	− 0.010	− 0.010	+ 0.220
		+ 0.480	− 0.022	+ 0.009	+ 0.159
		+ 0.600	− 0.030	+ 0.072	+ 0.072
A, 2	0.898	− 0.600	− 0.011	+ 1.977	+ 1.977
		− 0.540	− 0.007	− 0.378	− 0.321
		− 0.480	− 0.003	− 0.431	− 0.353
		− 0.240	+ 0.005	− 0.481	− 0.362
		− 0	+ 0	− 0.387	− 0.258
		+ 0	− 0	− 0.387	+ 0.243
		+ 0.240	− 0.017	− 0.248	+ 0.329
		+ 0.480	− 0.047	− 0.073	+ 0.305
		+ 0.600	− 0.066	+ 0.121	+ 0.121
A, 3	0.889	− 0.300	+ 0.022	− 0.090	− 0.090
		− 0.270	+ 0.020	− 0.039	− 0.148
		− 0.240	+ 0.017	− 0.022	− 0.172
		− 0.120	+ 0.008	+ 0.003	− 0.226
		− 0	+ 0	+ 0	− 0.250
		+ 0	− 0	− 0	+ 0.250
		+ 0.120	− 0.008	− 0.003	+ 0.227
		+ 0.240	− 0.017	+ 0.002	+ 0.0172
		+ 0.300	− 0.022	+ 0.089	+ 0.089
A, 4	0.899	− 0.300	− 0.006	+ 1.952	+ 1.952
		− 0.270	− 0.004	+ 1.871	+ 1.960
		− 0.240	− 0.003	+ 1.815	+ 1.937
		− 0.120	− 0	+ 1.592	+ 1.778
		− 0	− 0	+ 1.326	+ 1.529
		+ 0	− 0	+ 1.321	+ 2.023
		+ 0.120	− 0.008	+ 0.981	+ 1.625
		+ 0.240	− 0.024	+ 0.361	+ 0.783
		+ 0.300	− 0.034	+ 0.115	+ 0.115

TABLE III (continued)

Nozzle number	η_{i0}	x/R	$s(x)/R$	$C_P{}^+(x)$	$C_P{}^-(x)$
A, 5	0.890	− 0.900	+ 0.033	− 0.062	− 0.062
		− 0.855	+ 0.031	− 0.027	− 0.105
		− 0.810	+ 0.028	− 0.015	− 0.124
		− 0.720	+ 0.024	− 0.002	− 0.151
		− 0.360	+ 0.010	+ 0.012	− 0.216
		− 0	+ 0	+ 0	− 0.249
		+ 0	− 0	− 0	+ 0.251
		+ 0.360	− 0.010	− 0.013	+ 0.217
		+ 0.720	− 0.024	+ 0.001	+ 0.152
		+ 0.900	− 0.033	+ 0.062	+ 0.061
A, 6	0.901	− 0.900	− 0.032	+ 1.995	+ 1.995
		− 0.855	− 0.027	− 0.410	− 0.365
		− 0.810	− 0.023	− 0.449	− 0.386
		− 0.720	− 0.015	− 0.501	− 0.415
		− 0.360	+ 0.003	− 0.481	− 0.350
		− 0	+ 0	− 0.372	− 0.229
		+ 0	− 0	− 0.372	+ 0.272
		+ 0.360	− 0.024	− 0.241	+ 0.340
		+ 0.720	− 0.069	+ 0.037	+ 0.423
		+ 0.900	− 0.098	+ 0.398	+ 0.398
B, 1	0.850	− 0.600	− 0.008	− 0.009	− 0.009
		− 0.540	− 0.002	− 0.072	+ 0.058
		− 0.480	+ 0.001	− 0.097	+ 0.084
		− 0.240	+ 0.005	− 0.147	+ 0.130
		− 0	+ 0	− 0.175	+ 0.126
		+ 0	− 0	− 0.175	+ 0.726
		+ 0.240	− 0.018	− 0.169	+ 0.658
		+ 0.480	− 0.052	− 0.075	+ 0.466
		+ 0.600	− 0.076	+ 0.164	+ 0.164
B, 2	0.872	− 0.600	− 0.049	+ 2.046	+ 2.046
		− 0.540	− 0.037	− 0.431	− 0.113
		− 0.480	− 0.026	− 0.526	− 0.088
		− 0.240	− 0	− 0.649	+ 0.020
		− 0	+ 0	− 0.576	+ 0.153
		+ 0	− 0	− 0.576	+ 0.754
		+ 0.240	− 0.026	− 0.421	+ 0.798
		+ 0.480	− 0.079	− 0.164	+ 0.634
		+ 0.600	− 0.116	+ 0.219	+ 0.219

TABLE III (continued

Nozzle number	η_{i0}	x/R	$s(x)/R$	$C_P{}^+(x)$	$C_P{}^-(x)$
B, 3	0.849	− 0.300	− 0.005	− 0.027	− 0.027
		− 0.270	− 0.002	− 0.151	+ 0.100
		− 0.240	+ 0	− 0.196	+ 0.149
		− 0.120	+ 0.004	− 0.288	+ 0.240
		− 0	+ 0	− 0.323	+ 0.252
		+ 0	− 0	− 0.324	+ 0.852
		+ 0.120	− 0.014	− 0.295	+ 0.783
		+ 0.240	− 0.041	− 0.143	+ 0.562
		+ 0.300	− 0.058	+ 0.187	+ 0.187
B, 4	0.934	− 0.300	− 0.043	+ 2.040	+ 2.040
		− 0.270	− 0.034	+ 1.727	+ 2.295
		− 0.240	− 0.026	+ 1.588	+ 2.370
		− 0.120	− 0.004	+ 1.210	+ 2.404
		− 0	+ 0	+ 0.902	+ 2.204
		+ 0	− 0	+ 0.897	+ 2.799
		+ 0.120	− 0.016	+ 0.597	+ 2.341
		+ 0.240	− 0.054	+ 0.143	+ 1.284
		+ 0.300	− 0.080	+ 0.238	+ 0.238
B, 5	0.850	− 0.900	− 0.008	− 0.002	− 0.002
		− 0.855	− 0.006	− 0.032	+ 0.032
		− 0.810	− 0.005	− 0.043	+ 0.046
		− 0.720	− 0.002	− 0.058	− 0.064
		− 0.360	+ 0.004	− 0.092	+ 0.095
		− 0	+ 0	− 0.118	+ 0.086
		+ 0	− 0	− 0.118	+ 0.086
		+ 0.360	− 0.019	− 0.122	+ 0.615
		+ 0.720	− 0.059	− 0.055	+ 0.427
		+ 0.900	− 0.088	+ 0.147	+ 0.147
B, 6	0.877	− 0.900	− 0.077	+ 2.062	+ 2.062
		− 0.855	− 0.068	− 0.415	− 0.214
		− 0.810	− 0.059	− 0.479	− 0.199
		− 0.720	− 0.043	− 0.563	− 0.177
		− 0.360	− 0.003	− 0.596	− 0.007
		− 0	+ 0	− 0.501	+ 0.142
		+ 0	− 0	− 0.500	+ 0.742
		+ 0.360	− 0.034	− 0.361	+ 0.778
		+ 0.720	− 0.107	− 0.025	+ 0.721
		+ 0.900	− 0.157	+ 0.490	+ 0.490

TABLE III (continued)

Nozzle number	η_{i0}	x/R	$s(x)/R$	$C_P^+(x)$	$C_P^-(x)$
C, 1	0.807	− 0.600	− 0.028	+ 0.032	+ 0.032
		− 0.540	− 0.020	− 0.110	+ 0.187
		− 0.480	− 0.014	− 0.160	+ 0.249
		− 0.240	+ 0.002	− 0.258	+ 0.366
		− 0	+ 0	− 0.300	+ 0.381
		+ 0	− 0	− 0.300	+ 1.081
		+ 0.240	− 0.025	− 0.283	+ 0.983
		+ 0.480	− 0.075	− 0.135	+ 0.694
		+ 0.600	− 0.111	+ 0.234	+ 0.233
C, 2	0.836	− 0.600	− 0.073	+ 2.090	+ 2.090
		− 0.540	− 0.057	− 0.469	+ 0.024
		− 0.480	− 0.041	− 0.592	+ 0.086
		− 0.240	− 0.003	− 0.765	+ 0.270
		− 0	+ 0	− 0.707	+ 0.422
		+ 0	− 0	− 0.707	+ 1.123
		+ 0.240	− 0.033	− 0.540	+ 1.137
		+ 0.480	− 0.103	− 0.227	+ 0.871
		+ 0.600	− 0.153	+ 0.291	+ 0.291
C, 3	0.805	− 0.300	− 0.023	+ 0.013	+ 0.013
		− 0.270	− 0.017	− 0.232	+ 0.269
		− 0.240	− 0.011	− 0.322	+ 0.369
		− 0.120	+ 0.002	− 0.496	+ 0.559
		− 0	+ 0	− 0.554	+ 0.597
		+ 0	− 0	− 0.554	+ 1.297
		+ 0.120	− 0.020	− 0.504	+ 1.193
		+ 0.240	− 0.058	− 0.260	+ 0.851
		+ 0.300	− 0.085	+ 0.263	+ 0.263
C, 4	0.919	− 0.300	− 0.065	+ 2.089	+ 2.089
		− 0.270	− 0.052	+ 1.633	+ 2.497
		− 0.240	− 0.040	+ 1.442	+ 2.631
		− 0.120	− 0.006	+ 0.968	+ 2.783
		− 0	+ 0	+ 0.633	+ 2.614
		+ 0	− 0	+ 0.628	+ 3.309
		+ 0.120	− 0.022	+ 0.355	+ 2.811
		+ 0.240	− 0.074	+ 0.006	+ 1.614
		+ 0.300	− 0.111	+ 0.323	+ 0.323

TABLE III (continued)

Nozzle number	η_{i0}	x/R	$s(x)/R$	$C_P^+(x)$	$C_P^-(x)$
C, 5	0.808	− 0.900	− 0.036	+ 0.038	+ 0.038
		− 0.855	− 0.031	− 0.037	+ 0.124
		− 0.810	− 0.027	− 0.064	+ 0.160
		− 0.720	− 0.019	− 0.099	+ 0.209
		− 0.360	+ 0	− 0.166	+ 0.305
		− 0	+ 0	− 0.202	+ 0.312
		+ 0	− 0	− 0.202	+ 1.012
		+ 0.360	− 0.026	− 0.201	+ 0.911
		+ 0.720	− 0.085	− 0.095	+ 0.633
		+ 0.900	− 0.129	+ 0.211	+ 0.211
C, 6	0.842	− 0.900	− 0.107	+ 2.104	+ 2.104
		− 0.855	− 0.094	− 0.419	− 0.116
		− 0.810	− 0.082	− 0.500	− 0.077
		− 0.720	− 0.061	− 0.605	− 0.023
		− 0.360	− 0.007	− 0.674	+ 0.216
		− 0	+ 0	− 0.589	+ 0.381
		+ 0	− 0	− 0.589	+ 1.082
		+ 0.360	− 0.041	− 0.443	+ 1.088
		+ 0.720	− 0.134	− 0.067	+ 0.936
		+ 0.900	− 0.200	+ 0.557	+ 0.557
D, 1	0.801	− 0.600	+ 0.060	− 0.144	− 0.144
		− 0.540	+ 0.052	− 0.048	− 0.265
		− 0.480	+ 0.044	− 0.019	− 0.318
		− 0.240	+ 0.019	+ 0.018	− 0.439
		− 0	− 0	− 0	− 0.499
		+ 0	− 0	− 0	+ 0.500
		+ 0.240	− 0.019	− 0.019	+ 0.441
		+ 0.480	− 0.044	+ 0.017	+ 0.318
		+ 0.600	− 0.059	+ 0.014	+ 0.144
D, 2	0.804	− 0.600	+ 0.021	+ 1.902	+ 1.902
		− 0.540	+ 0.020	− 0.400	− 0.461
		− 0.480	+ 0.020	− 0.438	− 0.522
		− 0.240	+ 0.015	− 0.466	− 0.595
		− 0	+ 0	− 0.382	− 0.522
		+ 0	− 0	− 0.381	+ 0.479
		+ 0.240	− 0.026	− 0.252	+ 0.536
		+ 0.480	− 0.068	− 0.062	+ 0.454
		+ 0.600	− 0.095	+ 0.190	+ 0.190

TABLE III (continued)

Nozzle number	η_{i0}	x/R	$s(x)/R$	$C_P{}^+(x)$	$C_P{}^-(x)$
D, 3	0.801	− 0.300	+ 0.044	− 0.179	− 0.179
		− 0.270	+ 0.039	− 0.078	− 0.296
		− 0.240	+ 0.034	− 0.054	− 0.344
		− 0.120	+ 0.016	+ 0.006	− 0.452
		− 0	+ 0	− 0	− 0.500
		+ 0	− 0	− 0	+ 0.500
		+ 0.120	− 0.016	− 0.006	+ 0.453
		+ 0.240	− 0.034	+ 0.045	+ 0.345
		+ 0.300	− 0.044	+ 0.178	+ 0.178
D, 4	0.805	− 0.300	+ 0.020	+ 1.855	+ 1.855
		− 0.270	+ 0.018	+ 1.842	+ 1.785
		− 0.240	+ 0.016	+ 1.809	+ 1.731
		− 0.120	+ 0.010	+ 1.623	+ 1.503
		− 0	+ 0	+ 1.357	+ 1.226
		+ 0	− 0	+ 1.351	+ 2.221
		+ 0.120	− 0.015	+ 1.006	+ 1.802
		+ 0.240	− 0.039	+ 0.400	+ 0.921
		+ 0.300	− 0.053	+ 0.196	+ 0.196
D, 5	0.801	− 0.900	+ 0.067	− 0.124	− 0.124
		− 0.855	+ 0.061	− 0.054	− 0.209
		− 0.810	+ 0.057	− 0.030	− 0.247
		− 0.720	+ 0.048	− 0.003	− 0.302
		− 0.360	+ 0.019	+ 0.024	− 0.432
		− 0	+ 0	− 0	− 0.498
		+ 0	− 0	− 0	+ 0.501
		+ 0.360	− 0.019	− 0.026	+ 0.434
		+ 0.720	− 0.047	+ 0.002	+ 0.303
		+ 0.900	− 0.066	+ 0.123	+ 0.123
D, 6	0.805	− 0.900	+ 0.004	+ 1.929	+ 1.929
		− 0.855	+ 0.006	− 0.437	− 0.477
		− 0.810	+ 0.008	− 0.462	− 0.519
		− 0.720	+ 0.011	− 0.500	− 0.578
		− 0.360	+ 0.013	− 0.464	− 0.583
		− 0	+ 0	− 0.367	− 0.497
		+ 0	− 0	− 0.366	+ 0.504
		+ 0.360	− 0.033	− 0.249	+ 0.549
		+ 0.720	− 0.091	+ 0.040	+ 0.563
		+ 0.900	− 0.129	+ 0.456	+ 0.456

TABLE III (continued)

Nozzle number	η_{i0}	x/R	$s(x)/R$	$C_P^+(x)$	$C_P^-(x)$
E, 1	0.738	− 0.600	+ 0.031	− 0.096	− 0.096
		− 0.540	+ 0.029	− 0.102	− 0.101
		− 0.480	+ 0.027	− 0.108	− 0.107
		− 0.240	+ 0.017	− 0.137	− 0.134
		− 0	+ 0	− 0.176	− 0.173
		+ 0	− 0	− 0.176	+ 1.026
		+ 0.240	− 0.029	− 0.180	+ 0.922
		+ 0.480	− 0.079	− 0.065	+ 0.656
		+ 0.600	− 0.112	+ 0.250	+ 0.250
E, 2	0.746	− 0.600	− 0.010	+ 1.954	+ 1.954
		− 0.540	− 0.004	− 0.456	− 0.288
		− 0.480	+ 0.002	− 0.530	− 0.300
		− 0.240	+ 0.012	− 0.627	− 0.274
		− 0	+ 0	− 0.563	− 0.179
		+ 0	− 0	− 0.563	+ 1.022
		+ 0.240	− 0.037	− 0.420	+ 1.033
		+ 0.480	− 0.104	− 0.148	+ 0.803
		+ 0.600	− 0.149	+ 0.300	+ 0.299
E, 3	0.737	− 0.300	+ 0.022	− 0.134	− 0.134
		− 0.270	+ 0.021	− 0.197	− 0.077
		− 0.240	+ 0.020	− 0.223	− 0.058
		− 0.120	+ 0.014	− 0.284	− 0.031
		− 0	+ 0	− 0.324	− 0.048
		+ 0	− 0	− 0.324	+ 1.152
		+ 0.120	− 0.024	− 0.298	+ 1.055
		+ 0.240	− 0.061	− 0.116	+ 0.769
		+ 0.300	− 0.085	+ 0.294	+ 0.294
E, 4	0.747	− 0.300	− 0.008	+ 1.911	+ 1.911
		− 0.270	− 0.004	+ 1.709	+ 2.042
		− 0.240	− 0	+ 1.607	+ 2.066
		− 0.120	+ 0.007	+ 1.293	+ 1.993
		− 0	+ 0	+ 0.990	+ 1.754
		+ 0	− 0	+ 0.984	+ 2.948
		+ 0.120	− 0.024	+ 0.674	+ 2.474
		+ 0.240	− 0.068	+ 0.216	+ 1.394
		+ 0.300	− 0.098	+ 0.323	+ 0.323

TABLE III (continued)

Nozzle number	η_{i0}	x/R	$s(x)/R$	$C_P^+(x)$	$C_P^-(x)$
E, 5	0.738	− 0.900	+ 0.032	− 0.076	− 0.076
		− 0.855	+ 0.031	− 0.064	− 0.093
		− 0.810	+ 0.029	− 0.061	− 0.102
		− 0.720	+ 0.027	− 0.060	− 0.117
		− 0.360	+ 0.016	− 0.078	− 0.165
		− 0	+ 0	− 0.118	− 0.213
		+ 0	− 0	− 0.118	+ 0.987
		+ 0.360	− 0.030	− 0.138	+ 0.875
		+ 0.720	− 0.087	− 0.054	+ 0.609
		+ 0.900	− 0.127	+ 0.220	+ 0.220
E, 6	0.747	− 0.900	− 0.033	+ 1.981	+ 1.981
		− 0.855	− 0.027	− 0.447	− 0.355
		− 0.810	− 0.021	− 0.494	− 0.365
		− 0.720	− 0.012	− 0.559	− 0.382
		− 0.360	+ 0.009	− 0.571	− 0.300
		− 0	+ 0	− 0.490	− 0.194
		+ 0	− 0	− 0.498	+ 1.006
		+ 0.360	− 0.045	− 0.366	+ 1.005
		+ 0.720	− 0.132	− 0.018	+ 0.879
		+ 0.900	− 0.192	+ 0.557	+ 0.557
F, 1	0.674	− 0.600	+ 0.013	− 0.069	− 0.069
		− 0.540	+ 0.016	− 0.143	+ 0
		− 0.480	+ 0.017	− 0.173	+ 0.026
		− 0.240	+ 0.016	− 0.246	+ 0.059
		− 0	+ 0	− 0.301	+ 0.031
		+ 0	− 0	− 0.301	+ 1.431
		+ 0.240	− 0.038	− 0.296	+ 1.291
		+ 0.480	− 0.106	− 0.123	+ 0.916
		+ 0.600	− 0.153	+ 0.334	+ 0.334
F, 2	0.684	− 0.600	− 0.028	+ 1.981	+ 1.981
		− 0.540	− 0.017	− 0.498	− 0.182
		− 0.480	− 0.008	− 0.597	− 0.162
		− 0.240	+ 0.011	− 0.738	− 0.075
		− 0	+ 0	− 0.691	+ 0.033
		+ 0	− 0	− 0.691	+ 1.433
		+ 0.240	− 0.045	− 0.539	+ 1.408
		+ 0.480	− 0.132	− 0.207	+ 1.068
		+ 0.600	− 0.191	+ 0.385	+ 0.384

TABLE III (continued)

Nozzle number	η_{i0}	x/R	$s(x)/R$	$C_P{}^+(x)$	$C_P{}^-(x)$
F, 3	0.673	− 0.300	+ 0.008	− 0.113	− 0.113
		− 0.270	+ 0.011	− 0.287	+ 0.062
		− 0.240	+ 0.013	− 0.353	+ 0.128
		− 0.120	+ 0.013	− 0.491	+ 0.243
		− 0	+ 0	− 0.554	+ 0.247
		+ 0	− 0	− 0.555	+ 1.646
		+ 0.120	− 0.031	− 0.508	+ 1.510
		+ 0.240	− 0.082	− 0.229	+ 1.092
		+ 0.300	− 0.116	+ 0.387	+ 0.287
F, 4	0.685	− 0.300	− 0.023	+ 1.937	+ 1.937
		− 0.270	− 0.016	+ 1.613	+ 2.197
		− 0.240	− 0.009	+ 1.468	+ 2.271
		− 0.120	+ 0.006	+ 1.069	+ 2.297
		− 0	+ 0	+ 0.740	+ 2.080
		+ 0	− 0	+ 0.735	+ 3.474
		+ 0.120	− 0.031	+ 0.448	+ 2.958
		+ 0.240	− 0.091	+ 0.094	+ 1.737
		+ 0.300	− 0.131	+ 0.421	+ 0.421
F, 5	0.675	− 0.900	+ 0.011	− 0.049	− 0.049
		− 0.855	+ 0.012	− 0.074	− 0.023
		− 0.810	+ 0.013	− 0.085	− 0.013
		− 0.720	+ 0.015	− 0.101	− 0.002
		− 0.360	+ 0.014	− 0.149	+ 0.002
		− 0	+ 0	− 0.202	− 0.037
		+ 0	− 0	− 0.203	+ 1.363
		+ 0.360	− 0.040	− 0.219	+ 1.215
		+ 0.720	− 0.118	− 0.094	+ 0.845
		+ 0.900	− 0.175	+ 0.297	+ 0.297
F, 6	0.686	− 0.900	− 0.055	+ 2.009	+ 2.009
		− 0.855	− 0.046	− 0.457	− 0.281
		− 0.810	− 0.038	− 0.519	− 0.272
		− 0.720	− 0.024	− 0.601	− 0.276
		− 0.360	+ 0.007	− 0.644	− 0.122
		− 0	+ 0	− 0.576	− 0.012
		+ 0	− 0	− 0.576	+ 1.389
		+ 0.360	− 0.054	− 0.449	+ 1.351
		+ 0.720	− 0.164	− 0.059	+ 1.120
		+ 0.900	− 0.241	+ 0.635	+ 0.635

SUMMARY

For the application behind ships two different types of ducted propellers are considered; the ducted propeller where the nozzle accelerates the flow at the propeller and the ducted propeller where the nozzle decelerates the flow at the propeller. The first type of ducted propeller is now extensively used in cases where the ship screw is heavily loaded or where the screw is restricted in diameter. The accelerating nozzle offers a means of increasing the efficiency of heavily loaded propellers. The second type of ducted propeller is used to increase the static pressure at the impeller. This nozzle may be used if retardation of propeller cavitation is desired.

For the design of a ducted propeller it is attractive to have a theoretical calculation method available supported by experiments. Tests on ducted propellers are scarce and most of the tests are restricted to isolated applications. The work described here deals with systematic experiments on ducted propellers and may contribute to fill up the lack of experimental data.

The potentialities of ducted propellers both with nozzles of the accelerating and the decelerating flow type are discussed based on simplified theories.

The open-water test results of systematic series of flow accelerating and flow decelerating nozzles are given. These data are of importance for the design of optimum ducted propeller systems as well from the viewpoint of efficiency as from the viewpoint of cavitation.

In addition, the results of open-water tests with ringpropellers and ringpropellers in nozzles are given.

Finally, the design and the application of non-axisymmetrical nozzles which are adapted to the wake behind the ship, are discussed. In the case of single-screw ships (tankers and bulkcarriers) the nozzle is designed in such a way that the flow at the propeller plane becomes more uniform. Such a nozzle offers, next to a reduction in DHP, a means of minimizing propeller induced vibration and cavitation problems.

In the case of twin-screw ships (fast naval ships; frigates, destroyers), the propellers operate in a varying inflow, due to the shaft inclination. The non-axisymmetrical nozzle is designed here, from the viewpoint of retardation of screw cavitation, in such a way that the actual effective incidence changes of the blade sections of the impeller will be as low as possible during a revolution.

SAMENVATTING

Voor toepassing bij schepen komen twee typen schroef-straalbuissystemen in aanmerking; het type waarbij de straalbuis de stroming ter plaatse van de schroef versnelt en het type waarbij de stroomsnelheid ter plaatse van de schroef vertraagd wordt.

Schroef-straalbuissystemen van het eerste type worden veelvuldig gebruikt in gevallen waarbij de schroef zwaar belast en/of beperkt in diameter is. De versnellende straalbuis verhoogt het rendement van zwaar belaste schroeven.

Schroef-straalbuissystemen van het tweede type worden gebruikt wanneer het gewenst is de druk ter plaatse van de schroef te verhogen. Door de verhoging van de druk kan schroefcavitatie verminderd of voorkomen worden.

Het biedt voordelen, gezien het grote aantal variabelen, om het ontwerp van een schroef-straalbuissysteem te baseren op een combinatie van theorie en experiment. Weinig resultaten van proefnemingen met schroef-straalbuissystemen zijn beschikbaar en bovendien betreffen deze proefnemingen vaak slechts een incidentele toepassing. De resultaten van de proefnemingen met schroef-straalbuissystemen gegeven in dit proefschrift dragen bij om het gebrek aan experimentele gegevens aan te vullen.

De eigenschappen van schroef-straalbuissystemen, zowel met versnellende als vertragende straalbuizen, worden, gebaseerd op eenvoudige theoriëen, afgeleid.

De resultaten van proefnemingen met systematische series versnellende en vertragende straalbuizen worden gegeven. Deze gegevens zijn van belang voor het ontwerpen van optimale schroef-straalbuizen uit oogpunt van rendement of cavitatie. Daarnaast worden de resultaten van vrijvarende proeven met ringpropellers en met ringpropellers in straalbuizen gegeven.

Tenslotte wordt het ontwerp en de toepassing van asymmetrische straalbuizen die aangepast zijn aan de volgstroom achter schepen besproken. Voor volle enkelschroefschepen (tankers, bulkcarriers) wordt de straalbuis zodanig ontworpen dat het snelheidsveld ter plaatse van de schroef gelijkmatiger wordt. Een dergelijke straalbuis biedt, naast een vermogensbesparing, ook de mogelijkheid om het gevaar voor trillingshinder (opgewekt door de schroef) en voor erosie van de schroefbladen door cavitatie te verminderen.

Bij dubbelschroefschepen (en in het bijzonder snelle Marine-schepen, zoals jagers en fregatten) werken de schroeven in een niet gelijkmatige aanstroming door de schuine asliggingen. De asymmetrische straalbuizen worden hier zodanig ontworpen dat de invalshoekvariaties van een blad gedurende een omwenteling zo klein mogelijk zijn. Het gevaar voor het optreden van schroefcavitatie kan hierdoor verminderd worden.

REFERENCES

1. STIPA, L.; 'Experiments with Intubed Propellers'. L'Aerotechnica pp. 923–953, August, 1931. Translated by Dwight M. Miner, NACA. NACA TM 655, January, 1932.
2. KORT, L.; 'Der neue Düsenschrauben-Antrieb', Werft-Reederei-Hafen, Jahrgang 15, Heft **4**, February 15, 1934.
3. SACKS, A. H. and J. A. BURNELL; 'Ducted propellers – A critical review of the State of the Art'. *Progress in Aeronautical Sciences*, Vol. **2**, New York 1962.
4. WEISSINGER, J. and D. MAASS; 'Theory of the ducted propeller. A review'. 7th Symp. on Naval Hydrodynamics, Rome, August 1968.
5. HORN, F. and H. AMTSBERG' 'Entwurf von Schiffdüsen systemen' (Kortdüsen), Jahrbuch der Schiffbautechnischen Gesellschaft, vol. **44**, 1950.
6. KÜCHEMANN, D. and J. WEBER; 'Aerodynamics of Propulsion', Mc. Graw-Hill Book Co., Inc., New York, 1953.
7. DICKMANN, H. E. and J. WEISSINGER; 'Beitrag zur Theorie optimaler Düsenschrauben', (Kortdüsen), Jahrbuch der Schiffbautechnischen Gesellschaft, vol. **49**, 1955.
8. MORGAN, W. B. and E. B. CASTER; 'Comparison of theory and experiment on ducted propellers', 7th Symp. on Naval Hydrodynamics, Rome, August, 1968.
9. VAN MANEN, J. D.; 'Open-water test series with propellers in nozzles'. Int. Shipb. Progress, vol. 1, no. 3, 1954.
10. VAN MANEN, J. D.; 'Recent research on propellers in nozzles', Int. Shipb. Progress, vol. **4**. no. 36, 1957.
11. VAN MANEN, J. D. and A. SUPERINA; 'The design of screw propellers in nozzles', Int. Shipb, Progress, vol. **6**, no. 55, 1959.
12. VAN MANEN, J. D.; 'Effect of radial load distribution on the performance of shrouded propellers', Trans. RINA, 1962.
13. VAN MANEN, J. D. and M. W. C. OOSTERVELD; 'Analysis of ducted propeller design', Trans. SNAME, 1966.
14. OOSTERVELD, M. W. C.; 'Model tests with decelerating nozzles', ASME, Symp. on Pumping Machinery for Marine Propulsion, Philadelphia, May 1968.
15. HOERNER, S. F.; 'Fluid Dynamic Drag', published by the Author 1968.
16. KELLER, J. AUF'M; 'Enige aspecten bij het ontwerpen van scheepsschroeven', Schip en Werf, (December 1966).
17. 'Principles of Naval Architecture' Published by the SNAME, New York (1967).
18. VAN LAMMEREN, W. P. A.; J. D. VAN MANEN and M. W. C. OOSTERVELD; 'The Wageningen B-screw series'. Trans. SNAME, 1969.
19. MINIOVICH, I. YA.; 'Investigation of hydrodynamic characteristics of screw propellers under conditions of reversing and calculation methods for backing of ship'. Bushipss Translation 697, 1960.
20. BAKER, D. W. and C. L. PATTERSON; 'Representation of propeller thrust and torque characteristics for simulations' NSRDC, Technical Note, MEL 202/69, April 1968.
21. VAN MANEN, J. D.; 'The choice of the propeller'. Marine Technology, April 1966.
22. VAN MANEN, J. D. and J. KAMPS; 'The effect of the shape of afterbody on propulsion'. Trans. SNAME, 1959.
23. VAN MANEN, J. D.; M. W. C. OOSTERVELD and J. H. WITTE; 'Research on the manoeuvrability and propulsion of very large tankers'. 6th Symp. on Naval Hydrodynamics, Washington, 1966.
24. OOSTERVELD, M. W. C.; 'The application of non-cylindrical nozzles for large tankers and bulk carriers'. Shipbuilding and Shipping Record, November 1968.
25. OOSTERVELD, M. W. C.; 'Ducted Propellers'. Seminar of the Royal Institute of Engineers, Delft, The Netherlands, May 1969.

26. LINDGREN, H.; C. A. JOHNSON and G. DYNE; 'Studies of the application of ducted and contra-rotating propellers on merchant ships'. 7th Symp. on Naval Hydrodynamics, Rome, August 1968.
27. WERELDSMA, R; 'Some aspects of the research into propeller induced vibrations'. Int. Shipb. Progress, vol. **14**, no. 154, June 1967.
28. VAN GUNSTEREN, L. A.; 'Ringpropellers', Paper read before SNAME and Institute of Marine Engineers, Canada, September 1969.
29. KELLER, W. H. AUF'M; 'Comparative tests with B-series screws and ringpropellers', NSMB-report no. 66-047, DWT, 1966.
30. SPARENBERG, J. A.; 'On optimum propellers with a duct of finite length'. Mathematisch Instituut Universiteit Groningen, report TW-54, 1968.

NOMENCLATURE

a = axial distance between leading edge of nozzle and impeller plane.
A_E = expanded blade area of screw
A_{EX} = exit area of nozzle
A_o = disk area of screw
B_P = loading coefficient, $B_P = 33.07\ K_Q{}^{1/2} \cdot J^{-5/2}$

C_{DN} = drag coefficient of nozzle, $C_{DN} = \dfrac{D_N}{\frac{1}{2}\rho\ V_A^2\ \pi DL}$

C_f = skin-friction drag coefficient
C_L = lift coefficient

C_P = pressure coefficient, $C_P = \dfrac{P - P_\infty}{\frac{1}{2}\rho\ V_A^2}$

C_T = thrust coefficient, $C_T = \dfrac{T}{\frac{1}{2}\rho\ V_A^2\ \pi/4\ D^2}$

C_Q = torque coefficient, $C_Q = \dfrac{Q}{\frac{1}{2}\rho\ V_A^2\ \pi/4\ D^2 \cdot D}$

C_T^* = thrust coefficient, $C_T^* = \dfrac{T}{\frac{1}{2}\rho\ [V_A^2 + (0.7\ \pi nD)^2]\ \pi/4\ D^2}$

C_Q^* = torque coefficient, $C_Q^* = \dfrac{Q}{\frac{1}{2}\rho\ [V_A^2 + (0.7\ \pi nD)^2]\ \pi/4\ D^2 \cdot D}$

D = propeller diameter
D_N = drag of nozzle
E = kinetic energy loss in propeller slipstream
$h(x)$ = thickness distribution of nozzle

J = advance coefficient, $J = \dfrac{V_A}{nD}$

K_T = thrust coefficient, $K_T = \dfrac{T}{\rho n^2 D^4}$

K_Q = torque coefficient, $K_Q = \dfrac{Q}{\rho n^2 D^5}$

L = nozzle length
n, N = number of revolutions per second and per minute

P = pressure

P_∞ = static pressure of undisturbed stream

P = power

Q = torque

r = radius

R_1 = screw radius

R_0 = hub radius of screw

T = thrust

U_1, U_2 = increment of axial velocity at impeller and infinite far downstream of impeller

U_P, U_N = mean axial velocity at impeller plane induced by impeller and nozzle

V_A = undisturbed stream velocity

V_P = mean axial velocity at impeller plane

Z = number of screw blades

A_E/A_o = blade area ratio of screw

A_o/A_{EX} = ratio between impeller disk area and exit area of nozzle

f/L = camber ratio of nozzle

L/D = nozzle length-diameter ratio

P/D = pitch ratio of screw

S/L = maximum thickness ratio of nozzle

α_i = angle between nose-tail line of nozzle profile and propeller shaft

β = advance angle at 0.7 R, $\beta = \arctan \dfrac{V_A}{0.7\,\pi nD}$

γ = vortex density

Γ = vortex strength

δ = diameter coefficient or speed ratio, $\delta = \dfrac{101.27}{J}$

η_i = ideal efficiency

η_{fN} = efficiency factor due to nozzle drag

η_o = open-water efficiency, $\eta_0 = \dfrac{J}{2\pi} \cdot \dfrac{K_T}{K_Q}$

λ = hub-diameter ratio of propeller

ρ = specific mass of water

τ = impeller thrust-total thrust ratio, $\tau = \dfrac{T_P}{T}$

ν = kinematic viscosity of water

μ = advance coefficient, $\mu = \dfrac{\pi}{J} = \dfrac{\omega R_1}{V_A}$

ω = angular velocity

ACKNOWLEDGEMENT

To the board of Directors of the Netherlands Ship Model Basin I am grateful for the permission to publish this research in the form of a thesis.

A special word of thanks must be given to the following institutes and companies for their faith and financial support in different parts of this work and for their kind permission to publish the results:

Office of Naval Research, U.S. Navy
Contract No. N 62558-3999
Contract No. N 62558-4555
Royal Netherlands Navy
Mobil Oil Corporation, New York
Lips N.V., Drunen
Esso International, New York.

Appreciation is also expressed to many members of the Special Projects Department of the N.S.M.B. whose valuable assistance has contributed a great deal to the completion of this study. Especially the readily available help of Mr. H. Nijding and Mr. A. J. P. Huybens is thankfully acknowledged.